AD_____

Award Number: DAMD17-01-1-0689

TITLE: The BESCT Lung Cancer Program (Biology, Education, Screening, Chemoprevention, and Treatment)

PRINCIPAL INVESTIGATOR: Waun K. Hong, M.D.
Fadlo R. Khuri, M.D.

CONTRACTING ORGANIZATION: The University of Texas
M. D. Anderson Cancer Center
Houston, Texas 77030

REPORT DATE: March 2003

TYPE OF REPORT: Annual

PREPARED FOR: U.S. Army Medical Research and Materiel Command
Fort Detrick, Maryland 21702-5012

REPORT DOCUMENTATION PAGE

Form Approved
OMB No. 074-0188

1. AGENCY USE ONLY (Leave blank)	2. REPORT DATE	3. REPORT TYPE AND DATES COVERED
	March 2003	Annual (16 Feb 02 - 15 Feb 03)

4. TITLE AND SUBTITLE
The BESCT Lung Cancer Program (Biology, Education, Screening, Chemoprevention, and Treatment)

5. FUNDING NUMBERS
DAMD17-01-1-0689

6. AUTHOR(S):
Waun K. Hong, M.D.
Fadlo R. Khuri, M.D.

7. PERFORMING ORGANIZATION NAME(S) AND ADDRESS(ES)
The University of Texas
M. D. Anderson Cancer Center
Houston, Texas 77030
E-Mail: **whong@mdanderson.org**

8. PERFORMING ORGANIZATION REPORT NUMBER

9. SPONSORING / MONITORING AGENCY NAME(S) AND ADDRESS(ES)
U.S. Army Medical Research and Materiel Command
Fort Detrick, Maryland 21702-5012

10. SPONSORING / MONITORING AGENCY REPORT NUMBER

11. SUPPLEMENTARY NOTES
Original contains color plates: All DTIC reproductions will be in black and white.

12a. DISTRIBUTION / AVAILABILITY STATEMENT
Approved for Public Release; Distribution Unlimited

12b. DISTRIBUTION CODE

13. Abstract ***(Maximum 200 Words)*** *(abstract should contain no proprietary or confidential information)*

Our long-term objectives are to define the molecular processes contributing to lung cancer development and progression in order to recognize genetic and phenotypic changes early enough to be reversed with molecularly-targeted therapy and to develop innovative therapeutic approaches to lung cancer. Therefore, the specific goals of this program are to understand molecular alterations in lung cancer, develop lung cancer prevention strategies, and implement experimental molecular approaches to lung cancer. We report herein that enolase-α down-regulation is common in NSCLC and associated with a poor clinical outcome; IL-10 expression is lost in a subset of NSCLC and such loss predicts a poor clinical outcome in patients with stage I NSCLC; the combination of the COX-2 inhibitor Celecoxib and the retinoid 4HPR results in more effective growth inhibition than each agent alone; lack of PTEN expression in NSCLC may be related to promoter methylation and is of prognostic importance in stage I NSCLC; Farnesyl Transferase Inhibitors down-regulate phosphorylated RAF and AKT and induce the ubiquitination of AKT protein.

14. SUBJECT TERMS:	15. NUMBER OF PAGES
lung cancer, genetic alterations, chemoprevention, molecular therapy	64
	16. PRICE CODE

17. SECURITY CLASSIFICATION OF REPORT	18. SECURITY CLASSIFICATION OF THIS PAGE	19. SECURITY CLASSIFICATION OF ABSTRACT	20. LIMITATION OF ABSTRACT
Unclassified	Unclassified	Unclassified	Unlimited

TABLE OF CONTENTS

INTRODUCTION

Lung cancer is a devastating worldwide public health hazard, with a total of 1,500,000 new cases anticipated in the year 2000 (1). Advances in the surgery, radiation therapy, and chemotherapy of non-small cell lung cancer have led to an improvement in five-year survival from 7% in 1970 to 15.8% IN 1994 (2). To reduce lung cancer incidence and mortality, it is imperative to develop effective therapeutic and preventive strategies targeting smokers and lung cancer patients. Our long-term objectives are to define the molecular processes contributing to lung cancer development and progression in order to recognize genetic and phenotypic changes early enough to be reversed with molecularly-targeted therapy and to develop innovative therapeutic approaches to lung cancer. The objectives can be met only by understanding the biology of lung cancer through molecular studies and preclinical experimental molecular therapeutic research. Therefore, the specific goals of this program are to understand molecular alterations in lung cancer, develop lung cancer prevention strategies, and implement experimental molecular approaches to lung cancer.

PROGRESS REPORT

Project 1 Mechanisms of Molecular Alterations in Lung Cancer

Specific Aim 1.1 Determine the mRNA splicing complex responsible for CEACAM splicing and identify potential altered component(s) in lung cancer cells

Using two-dimensional gel electrophoresis, we analyzed nuclear proteins from four cancer cell lines; two cell lines express predominantly the L-form-CEACAM1 (H1944 and A549) and two express predominantly the S-form-CEACAM1 (H460 and 17B). Two patterns of expression were observed (Figure 1).

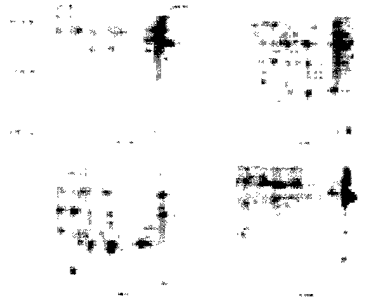

A group of proteins at pH 10 and molecular weight about 40kD was highly-expressed in H1944 and A549 but not in H460 and 17B. In contrast, several lower molecular weight proteins were expressed in the H460 and 17B cell lines. These proteins were purified and digested with proteinases for mass spectrometer based peptide mapping. These proteins are predominantly hnRNPs which are important in splicing regulation. Other proteins differentially expressed were also identified. An interesting feature is the presence of different splicing isoforms of hnRNPs in cell lines presenting distinct CEACAM1 splicing forms (Table 1). Our results suggest that hnRNPs and their alternatively spliced forms may play important roles in controlling CEACAM1 splicing patterns.

Table 1. Proteins identified from each of the four cell lines differentially expressed

Cell line	CAM form	Spot	I.D.	Accession #	pI	M.W.
A549	long >>>	A1	heterogeneous nuclear ribonucleoprotein	NP_002128	8.7	36.05

	short		(hnRNP) A2/B1			
		A2	hnRNP A2B1			
		A3	hnRNP A2/B1		8.7	36.05
		A4	hnRNP A2/B1		8.7	36.05
		A5	hnRNP A1	NP_002127		
		A6a-f	hnRNP A1		9.4	34.29
		A7	hnRNP A1			
		A8	hnRNP A1			
17B	short >> long	B1	ATPB_human ATP synthase beta chain, Mitochondrial precursor	P06576	5.3	56.54
		B2	outer mitochondrial membrane protein porin 2 (splicing variant?)	P45880	6.3	38.65
		B3	hnRNP A2/B1		8.7	36.05
		B4	hnRNP A2/B1			
		B5	Porin 31HM	AAB20246	8.8	30.74
		B6	hnRNP A1			
		B7	hnRNP A1			
		B8	alternative splicing factor ASF-2	B40040	5.6	32.32
		B11	hnRNP A2/B1			
		B12	hnRNP A2/B1			
		B13	hnRNP L (splicing variant)			
		B14	very-long-chain acyl-CoA dehydrogenase (splicing variant?)	D78298	9.2	70.87
		B15	hnRNP A2/B1			
		B16	hnRNP A2/B1			
		B17	hnRNP A1			
		B18	UP1 (hnRNP A1)			
		B20	peroxiredoxin 1; Proliferation-associated gene A; proliferation-associated gene A (natural killer-enhancing factor A)	NP_002565	8.7	22.32
		B23	hnRNP A2/B1			
460	short only	C1	actin, gamma 1 propeptide; cytoskeletal gamma-actin; actin, cytoplasmic 2	NP_001605	5.3	42.12
		C3	prohibitin	NP_002625	5.6	29.84
		C4	hnRNP L (splicing variant)	XP_008903	6.7	60.84
		C5	Porin 31HM	AAB20246	8.8	30.74
		C6	hnRNP A1 (splicing variant)			
		C7	hnRNP A1 (splicing variant)			
		C8	physical mixture or fusion protein of A1-A2/B1			
		C9	Similar to C8			
		C10	hnRNP L			
		C11	acyl-Coenzyme A dehydrogenase, very long chain precursor (splicing variant?)	NP_000009	9.2	70.77
		C14	peroxiredoxin 1; Proliferation-associated gene A; (same as B20)			
		C15	hnRNP A2/B1 - hnRNP A1			
		C16	hnRNP A2/B1			
		C19	hnRNP A2/B1			
		C20b	hnRNP A2/B1			
		C20a	voltage-dependent anion channel 2	NP_003366	7.7	32.09

		C21	voltage-dependent anion channel 2			
		C22	hnRNP A2/B1			
		C23	hnRNP A2/B1			
1944	long >>> short	D1	B23 nucleophosmin	CAA34809	4.7	31.09
		D4	hnRNP A2/B1			
		D5a-e	hnRNP A1		9.4	34.29

Specific Aim 1.2 ***Determine functions of the identified component(s) in pre-mRNA splicing control of CEACAM and potential alterations in lung cancers***

By serial deletion analysis, we found that the consensus-alternative splicing sequence of *CEACAM1* locates within exon 7 of CEACAM1. The 53 bp fragment contains two CACA Tra sites. Using the 53bp fragment, we performed sequence-specific affinity chromatography and found it binds two major proteins. We purified the proteins and analyzed their identity by peptide digestion and mass spectrometry. The two proteins turned out to be hnRNP-A1 and polypyrimidine tract-binding protein (PTB) both known to be important in splicing regulation. The binding specificity was verified by using gel shift analysis. The data further suggest that PTB can function as an exonic splicing enhancer to exclude the *CEACAM1* exon 7, which is a novel PTB function. To test the hypothesis, we co-transfected CEACAM1 mini-gene with three PTB isoforms and demonstrated that increased PTB levels can enhance the exclusion of exon 7 of CEACAM1.

Specific Aim 1.3 ***Determine the function of DNA methyltransferases and their roless in controlling methylation and the expression status of critical tumor supressor genes and tumor antigen genes***

We used multiple primers located at exon 4, exon 5 and exon 6 of DNMT3B to determine a potential starting site of the new transcript through primer extension assay and found the transcript stared at base pair (bp) 23990 and 23994 in the exon 5 of DNMT3B (GenBank AN: 15306493). This partial exon 5 is named as the first exon of the new transcript which contains only 28-bp or 24-bp respectively. The result was validated using nuclease S1 RNA mapping analysis. We designated the new transcript as DNMT3B6 following other previously published transcripts. To determine expression profile of the new transcript, we analyzed a panel of different tissues including peripheral lymphocytes, normal lung tissues, paired lung cancer tissues, lung cancer cell lines, and head and neck cancer cell lines and found that DNMT3B6 is a predominant expressing form of DNMT3B in these tissues.

To determine the existence of a promoter, we constructed a vector containing a 1080bp-DNA fragment including upstream 355bp from DNMT3B6 transcription starting site, the novel first exon, first intron and partial exon 2 (92bp). We performed a promoter activity assay and demonstrated a promoter activity of the DNA fragment. We further constructed serial vectors including both sense and reverse directions and various deletions. Using these constructs, we demonstrated that the core promoter of DNMT3B6 is in a 477-bp fragment containing one repressor element and three cis-acting elements. Interestingly, a common T-C transition polymorphism was found in the promoter region of DNMT3B6 located at –286bp from the DNMT3B6 transcriptional starting site, which may change a TFIID (CTcTATTCCA) binding site to GATA-1 (TCTAT**C**) binding site. We noticed a stronger promoter activity of the T form than the C form (18-fold vs. 12-fold compared to the control, respectively). In a case-control study,

we found that the CT heterozygote genotype had more than two-fold increased risk of lung cancer development .

We analyzed the mRNA expression profile of DNMT3B6s in normal lung cDNA library and lung cancer cell lines by RT-PCR. We found that the transcripts initiated from this novel promoter may generate at least 7 isoforms of DNMT3B6 through inclusion or exclusion of different combinations of exons 7, 8, 9, and 10 of DNMT3B1. We named these isoforms of DNMT3B6 as DNMT3B6-a, -b, -c, -d, –e, -f and –g. Detected by RT-PCR, these DNMT3B6 transcripts showed variable expression levels and patterns in different cancer cell lines and primary tumors. A comparative analysis of putative amino acid sequences shows that all variables are within the PWWP motif, which has recently been shown to have direct DNA binding capability.

Specific Aim 1.4 ***Determine expression profiles and abnormalities of DNMT3B isoforms in lung tumorigenesis and their association with de novo DNA methylation patterns, as well as potential clinical applications***

These studies are planned for Years 4 and 5 of the granting period.

Other research developments related to lung cancer biology supported in part by the fund

Activation of telomerase plays a critical role in unlimited cell proliferation and immortalization. To evaluate the significance of human telomerase reverse transcriptase catalytic subunit (hTERT) as a prognostic marker, we analyzed the expression of hTERT in a large population of 153 patients with stage I non-small cell lung cancer (NSCLC) by using the *in situ* hybridization (ISH) technique. We found that diffuse hTERT expression was present in 51 out of 153 patients (33%). Kaplan-Meier analysis showed that hTERT expression was strongly associated with shorter overall survival (P = 0.04), shorter disease-specific survival (P = 0.03) and shorter disease-free survival (P = 0.02). Multivariate analysis confirmed this independent prognostic value of hTERT expression. In conclusion, our results based on a large population of patients with stage I NSCLC indicate that hTERT mRNA expression is strongly associated with malignant tumor progression and poor outcome. hTERT may serve as a useful marker to identify patients with poor prognosis and select early-stage NSCLC patients that might be benefited from adjuvant treatment. (Clinical Cancer Research 8: 2883-2889, 2002)

The *PTEN* gene at chromosome 10q23.3 is a tumor-suppressor gene that is inactivated in several types of human tumors. Although mutation and homozygous deletion are the most common mechanisms of *PTEN* inactivation, promoter methylation and translational modification can also account for *PTEN* silencing. The aim of this study was to investigate the expression of PTEN protein in primary non-small cell lung cancer (NSCLC) samples and to investigate the promoter methylation status of the gene in a panel of NSCLC cell lines as well as primary tumors. We analyzed PTEN expression by immunohistochemistry in tissue samples from 125 patients with early-stage NSCLC. We also evaluated *PTEN* promoter methylation status by methylation-specific PCR in 20 microdissected PTEN-negative primary tumors from among the last specimens as well as in a panel of 16 NSCLC cell lines. Western and Northern blotting were performed in the same panel of NSCLC cell lines. Thirty (24%) of the 125 specimens showed lack of staining for PTEN. *PTEN* methylation was detected in seven (35%) of the 20 PTEN-negative NSCLC samples and in none of the 10 PTEN-positive NSCLC samples that were microdissected. Furthermore, *PTEN* methylation was observed in 11 (69%) of the 16 NSCLC cell lines tested. *PTEN* mRNA expression was increased in the NCI-H1299 cell line by *in vitro*

treatment with the demethylating agent 5-aza-2'-deoxycytidine. *PTEN* methylation was well correlated with PTEN expression in NSCLC cell lines by Western and Northern blot ($P = 0.025$). (Clinical Cancer Research 8: 1178-1184, 2002).

Enolase-α is a cytoplasmic glycolytic enzyme important in the formation of phosphoenolpyruvate. Enolase-α and *c-myc* binding protein (MBP-1) originate from a single gene through alternative use of translational starting sites. Both enolase-α and MBP-1 can bind to the P2 element in the *c-myc* promoter and compete with TATA-box binding protein (TBP) to suppress transcription of *c-myc*. Using a proteomic approach, we revealed that enolase-α is down-regulated in cell lines derived from metastases. To determine a potential role of enolase-α *in vivo*, we analyzed enolase-α expression in non-small cell lung cancer (NSCLC) tissues from 46 patients by Western blotting and immunohistochemical analysis. Twelve (26%) of the 46 tumors showed a significantly reduced enolase-α expression. Although no statistically significant association was observed between the down-regulation of enolase-α and pathologic stage, tumor histology, or differentiation, the patients whose tumors showed reduced endolase-α expression had a significantly poorer overall survival compared to those without down-regulation of this molecule ($P = 0.0398$). Our results indicate down-regulation of enolase-α is common in NSCLC and may play an important role in lung tumorigenesis. (Submitted, Clinical Cancer Research).

Chemoprevention has been widely explored as a promising strategy to control lung cancer which is the leading cause of cancer-related death in the United States. To maximize the benefit of chemoprevention, it is important to identify individuals with high risk for the disease. Besides tobacco smoking, individual's genetic background plays an important role in the person's susceptibility of developing lung cancer. We report here the identification of a polymorphic tandem repeats minisatellite (termed MNS16A) in the downstream region of human telomerase catalytic subunit (hTERT) gene. This minisatellite locates upstream of the antisense transcript of hTERT gene and has a promoter activity. The promoter activity is significantly lower in the construct containing a shorter repeats suggesting the polymorphism of MNS16A may have a role in biology. We analyzed genomic DNA from 107 individuals without cancer for genotypes of MNS16A and found four different alleles based on the length of the repeats which are classified as shorter repeats (S) and longer repeats (L). About 57% of the individuals carry LL genotype, 32% LS, and 11% SS. We further analyzed DNA from 53 patients with NSCLC and found 42% of these patients carry LL, 50% LS, and 8% SS. Patients with NSCLC carry a significantly higher LS/SS genotype(s) than individuals without cancer ($P = 0.032$ by χ^2 analysis), suggesting an important role of MNS16A in lung cancer susceptibility. (Submitted, Oncogene)

Interleukin-10 (IL-10) may play an important role in controlling tumor growth and metastasis. Some reports have shown that IL-10 can be a potent inhibitor of tumor growth, but others suggest that IL-10 expression by the tumor is an adverse prognostic factor. Since normal bronchial epithelial cells constitutively produce IL-10, we decided to test the prognostic value of IL-10 in a well-defined population of patients with stage I non-small cell lung cancer (NSCLC) treated in a single institution. Using immunohistochemical analysis, we retrospectively analyzed IL-10 expression in specimens from 138 patients with completely resected clinical/radiographic stage I NSCLC for whom clinical follow-up data were available. IL-10 expression was retained (IL-10 labeling index ≥ 10%) in 94 patients (68.1%) and lost in 44 patients (31.9%). The duration of overall survival, disease-specific survival and disease-free survival in the 44 patients lacking IL-10 expression was worse than in the 94 patients with IL-10 expression ($P = 0.08$; 0.02; and 0.05, respectively; log-rank test). Interestingly, IL-10 expression was observed more frequently in tumors with squamous cell histology than in tumors of other histological subtypes ($P = 0.04$;

chi-square test). Multivariate analysis confirmed the independent prognostic value of IL-10 expression for disease-specific survival (P = 0.04). Lack of IL-10 expression by the tumor was associated with a significantly worse outcome of early-stage NSCLC. The mechanisms underlying this clinically and biologically important finding need to be further explored. (in press, Clinical Cancer Research)

Project 2 Novel Strategies for Lung Cancer Chemoprevention

Specific Aim 2.1 *Evaluate the effects of aerosolized 13cRA delivered to former smokers by inhalation alone or in combination with Celecoxib*

This clinical trial is not scheduled to be initiated until Year 3 of the granting period.

Specific Aim 2.2 *Evaluate the effects of NSAIDS and 13cRA as single agents and in combinations on growth, apoptosis and carcinogenesis using an in vitro cell system and an animal model*

Tobacco-related cancers including those that develop in the head and neck and lungs are a major cause of cancer morbidity and mortality. Despite advances in chemotherapy, radiotherapy and surgery alone or in combination, the survival rates for lung cancer are still under 15% and those for head and neck cancers are under 50%. Therefore, there is an urgent need to develop new approaches to the prevention of cancers of the upper airways. The purpose of this specific aim is to evaluate effects of NSAIDs and retinoic acid as single agents and in combinations on lung cancer growth, apoptosis and carcinogenesis using an in vitro cell system and an animal model. In the first year of funding, we have determined the efficacy and mechanisms of action of arachidonic acid metabolizing enzymes including cyclooxygenase 2 (COX-2) and lipoxygenase (e.g., 5-LOX) inhibitors used as single agents and in combination with each other and with retinoic acid in suppression of cell growth and induction of apoptosis of normal, immortalized, premalignant, transformed and tumorigenic lung cells in vitro, and found that these effects were not related to the expression of the target enzymes. During the past year, we have investigated the expression of COX-2 and lipoxygenases and modulation of the growth and apoptosis in head and neck cancers by the COX-2 inhibitor celecoxib.

Expression of COX-2 and lipoxygenases in head and neck squamous cell carcinoma cells

We used five paired cell lines derived from primary Head and Neck squamous cell carcinoma (HNSCC) and metastases in the same patient. Three of the cell lines failed to express COX-2 by western blotting analysis whereas 7 were positive, albeit expressing different COX-2 levels. Interestingly, 3 of the pairs showed a greater expression of COX-2 in the primary cancer cell lines than in the cell lines derived from a metastasis.

Lipoxygenases 5 and 12 were detected in all HNSCC cell lines whether derived from primary or metastasis. However, 15-lipoxygenase was detected in only 3/6 cell lines.

Growth inhibitory effects of Celecoxib on HNSCC cell lines

Celecoxib inhibited the growth of all HNSCC cell lines tested with an IC50 of 40 to 60 μM in a 3-day assay. At concentrations of up to 50 μM, celecoxib induced growth inhibition but at higher doses apoptosis was observed. There was no correlation between the level of COX-2 or any of the lipoxygenases and the response to Celecoxib.

Effects of Celecoxib on the invasive potential of HNSCC cell lines

The invasive potential of HNSCC cell lines analyzed using a Matrigel-coated filter placed in a Boyden chamber was not correlated with the levels of COX-2 or any of the three lipoxygenases (5, 12, and 15). Celecoxib inhibited invasion of HNSCC cell lines only modestly. Furthermore, a dose-dependent increase in the levels of the vascular endothelial growth factor (VEGF) was observed after Celecoxib treatment of HNSCC 14A cells.

Increased expression of COX-2 in HNSCC cells treated with Celecoxib

Treatment of several HNSCC cell lines with celecoxib at concentrations as low as 0.1 μM increased the level of COX-2 within 3 hours. The level of COX-2 then declined by 48 hours. There was no correlation between the increase in COX-2 and growth inhibitory effect of Celecoxib because induction was observed at doses that had no effect on growth.

Effects of combinations of Celecoxib and the synthetic Retinoid 4HPR on HNSCC cells

4HPR inhibited the growth of all HNSCC cell lines tested with IC50 ranging from 6 to 13 μM. Combinations of 20 μM Celecoxib with different doses of 4HPR showed more than additive effects. 4HPR caused an increase in COX-2 level at 6 hours and then the level of COX-2 declined gradually reaching a lower level of untreated cells after 72 hours. When 1 μM 4HPR was combined with 20 μM Celecoxib, the overall increase in COX-2 protein levels was less pronounced than the maximal increase observed with each agent alone. 4HPR inhibited the invasion of HNSCC cells at low concentrations that had no effect on cell growth and also suppressed the levels of secreted vascular endothelial growth factor (VEGF). 4HPR also suppressed the increase in VEGF induced at high doses of Celecoxib.

Specific Aim 2.3 ***Investigate whether genetic approaches to inhibit PI3K activity decrease lung tumor size and number in K-ras mutant mice***

We have continued our efforts to inhibit PI3K pathway in the lungs of k-ras mice. Our progress has been slowed by 3 problems. First, the person in my lab who was carrying on this project, Dr. Ho-Young Lee, left the lab to start her own lab effort. We have solved this problem by recruiting a new graduate student, Dianren Xia, who has successfully expanded our adenoviral stocks that we will need for the proposed experiments. Second, 9 months ago, the mouse colony in the laboratory of Dr. Tyler Jacks developed an infection that caused him to have to sacrifice all of his animals and rederive his transgenics. This caused our mouse colony, which was totally dependent on mice shipments from Dr. Jacks, to be depleted. We have been unable to perform any experiments over the past 6 months because we have required that amount of time to grow our own mouse colony. We are almost to the point at which we will begin to perform the proposed experiments. Third, our aerosolized delivery method stopped effectively delivering adenovirus to lung tumors. We have used the few mice we have left to investigate the source of the problem and have determined it to be from the jet nebulizer. We have begun to find ways to solve this problem with new jet nebulizers and modifying the calcium phosphate precipitation to allow the virus to be delivered more effectively through the nebulizer. Despite these drawbacks, we have made progress in our publications. We have received a very favorable review from the *Journal of Biological Chemistry* of the preliminary data that went into this proposal and expect that our revised proposal has a good chance of being accepted for publication.

Project 3 **Experimental Molecular Therapeutic Approaches to Lung Cancer**

Specific Aim 3.1 ***Develop a relatively faithful murine model of lung cancer by crossing the k-ras mutant mouse (T. Jacks) with our p53 mutant missense mouse (G. Lozano) such that we can study the evolution of non-small cell lung cancer in primary lung tumor model with metastatic potential, as well as the effectiveness of these molecularly targeted strategies in that model.***

The initial experiments, to generate both mutations in an inbred background and to generate the cohort for tumor studies have been completed. The *p53R172H□g* mice and the Ras^{LA1} mice are now in the 129SV background. The following cohort has been established: Ras^{LA1}/+ *p53R172H□g/+* (50 mice); Ras^{LA1}/+ (50 mice); R172Hg/+ (50 mice); wild type (50 mice). These mice have begun to succumb to lung tumors. Figure 1 indicates the survival curves of the cohort thus far. The Ras^{LA1}/+ *p53R172H□g/+* are dying more quickly than the other cohorts due to the combined mutations in *ras* and *p53*. Samples have been collected for pathology.

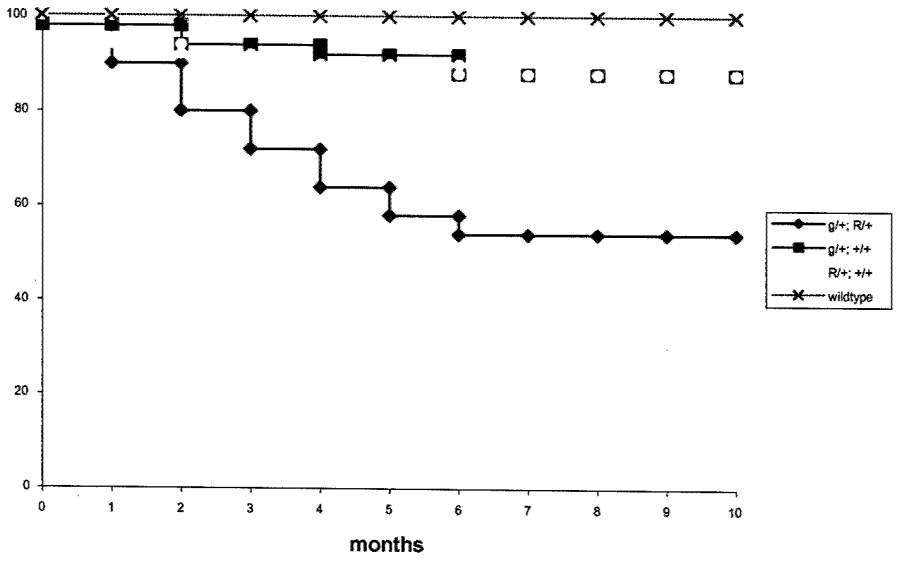

Figure 1. Survival curves for the ras and mutant p53 cohorts. R, Ras^{LA1}; g, *p53R172H□g/+*.

Matings have continued and the next cohort of mice will be treated with farnesyl transferase inhibitors to determine efficacy in an in vivo model.

Specific Aim 3.2 ***Evaluate novel signal transduction inhibitors, both alone and in combination with one another and with cytotoxic agents, in the treatment of these mouse lung cancer models and, ultimately, in the treatment of human lung cancers.***

Ras gene mutations are among the first described oncogenic changes in human cancer. Broadly, much work has been undertaken in the last two decades to better comprehend the functions of the various isoforms of *ras*, h-, n-, k-, and r-*ras*. A recent collaboration by the laboratories of Adrienne Cox (University of North Carolina) and Mark Phillips (New York University) has begun to elucidate the specific functions of various isotypes, by better defining their specific membrane localization. Added to the extensive work studying the *ras* gene mutations in the hematologic and oncologic malignancies, the functional significance of this crucial family of G-proteins/GTPases is becoming increasingly clear.

The major focus of our laboratory is on targeting post-translational modifications of the *ras* genes as a therapeutic target. Since Brown and Goldstein first elucidated the importance of isoprenylation of *ras* genes as a critical step in the maintenance oncogenic *ras* signaling, an academic and pharmaceutical race has been initiated to develop and license the first "*ras*-targeting" agents in man. Several clinical trials of farnesyl transferase inhibitors (FTIs), both alone and in combination with cytotoxic agents have shown promise, but not yet definitive efficacy in patients with hematological and solid tumor malignancies. To date, we have led or been involved in both single agent and combination trials of the three FTIs currently in phase II/III clinical trials, and have contributed to the understanding of how these agents down-regulate *ras*-dependent signaling in aerodigestive tract cancers. A major focus of our laboratory has been to understand how FTIs down-regulate phosphorylated raf and phosphorylated akt, and induce the degradation/ubiquitination of AKT/PKB proteins in lung cancers and head and neck squamous cell cancers (HNSCC).

We have studied the effects of FTIs on *raf* and *akt* activity in lung and head and neck cancers in preparation for combining them with Iressa. We have shown that in head and neck cancers and cell lines, the FTI lonafarnib induces downregulation of phosphorylated raf and phosphorylated akt, and induce the degradation/ubiquitination of AKT/PKB proteins. We have also continued our fruitful collaborations with Dr. Li Mao, PI of project 1, on the development of a molecular prognostic model of lung cancer, so that we can differentiate between those individuals with early stage(Stage I) Non-Small Cell Lung Cancer(NSCLC) who will do well postoperatively and those individuals whose prognosis is more guarded. Our collaborations have expanded to the study of the promoter methylation patterns in the PTEN/akt signaling pathway, whose downregulation we have shown to be vital to the effect of lonafarnib in NSCLC and HNSCC, and the prognostic expression of the vital telomeric regulatory component, hTERT, whose expression has been shown by Hahn and Weinberg to be necessary for ras dependent transformation of mammalian cell lines. Our continued prognostic understanding of these various critical signaling proteins in ras dependent transformation and progression, is the underpinning for our subsequent development of targeted, individualized therapies for high risk lung cancer patients.

Specific Aim 3.3 ***Produce and test a liposomal gene-therapeutic strategy targeted to a novel tumor suppressor gene located on chromosome 3p, both in the mouse model and in human patients with advanced non-small cell lung cancer***

The *FUS1* is a novel tumor suppressor gene (TSG) identified in the 120-kb homozygous deletion region at human chromosome 3p21.3. Previously, we found that *FUS1* was inactivated in primary lung cancer by either loss of genomic allele or deficiency of protein expression and that overexpression of the wild-type (wt)-FUS1 in FUS1-deficient NSCLC cells significantly inhibited tumor cell growth and induced apoptosis in vitro and in vivo. To understand further the molecular mechanism involved in *FUS1*-mediated tumor suppressing activity and cancer pathogenesis, we performed a computer-aided structural analysis of the Fus1 protein and characterized the biological properties of the predicted functional domains *in vitro* and *in vivo*. A motif-based profile scanning analysis of Fus1 protein sequence revealed a potential myristoylation site at the N-terminus of Fus1 protein sequence. We have identified the wild-type Fus1 protein as a myristoylated protein by a surface-enhanced laser desorption and ionization - Mass spectrometry (SELDI-MS) analysis on a Fus1-antibody-captured ProteinChip array (ACPA) and by Western-blot and immunoprecipitation analysis of the H^3-myristate-labeled Fus1 protein in the exogenous FUS1-expressing cells. We analyzed the subcellular localization of wt-Fus1 and the myristoylation-deficient mutant Fus1 proteins in plasmid-transfected H1299 cells. The mutant Fus1 had dramatically lost its characteristic intracellular membrane localization due to its depletion of myristoylation. To evaluate the biological function of myristoyl modification of Fus1 protein in vitro and in vivo, we compared the clonogenicity of the wt-FUS1 and mutant-FUS1 in plasmid vector-transfected H1299 cells on a soft-agar plate and the effect of enforced expression of wild-type FUS1 on the growth of s.c. H1299 tumor xenografts and on the development of A549 lung metastases in mice by intratumoral injection or systemic administration of lipoplexes of FUS1 DNA. Significant inhibition of clonogenicity and suppression of tumor growth and lung metastases were observed in myristoylated wt-FUS1-expressing H1299 tumor cells and tumor xenografts, but not in myristoylation-deficient mutant-Fus1-expressing cells, compared with the untransfected Fus1-non-expressing controls. We analyzed the apoptosis induced by systemic administration of FUS1-lipoplex in pulmonary metastatic tumors in vivo. Using in situ TUNEL staining, we found that only myristoylated wt-FUS1 could induce apoptosis, but not the myristoylation-deficient mutant FUS1 protein.

Furthermore, in a preliminary effort to evaluate Fus1 protein expression and posttranslational modifications in human lung tumors and non-involved tissues, we used Laser Capture Microdisection (LCM) to separate tumor cells from normal ones and applied the cell lysates to the ACPA with SELDI-TOF-MS. We found that only myristoylated protein species could be detected in normal cells, but both the unmyristoylated and myristoylated FUS1 protein were detected in tumor cells as indicated by the precise mass of FUS1 protein on the mass spectra. The mixed status of FUS1 protein in the tumor cells might be a reflection of the tumor cell molecular heterogeneity.

These results strongly suggest the biological role of posttranslational modification of FUS1 protein in FUS1-mediated tumor suppressing activity in vitro and in vivo. Our findings are expanding an essential role of protein posttranslational myristoylation in human cancer pathogenesis and warrant further studies of alternative mechanisms involved in inactivation of novel TSGs such as 3p21.3 FUS1 gene by posttranslational modification, loss of expression, and haploinsufficiency.

We have previously demonstrated the ability of a cationic liposome, DOTAP:Cholesterol, to efficiently deliver therapeutic genes to primary and disseminated lung tumors in a mouse xenograft model. Utilizing this approach, we tested the ability of a newly identified tumor suppressor gene, Fus1, to inhibit lung tumor growth following intratumoral and intravenous injections of DOTAP:Cholesterol-Fus1 (DOTAP:Chol-Fus1) complex. We used two human non-

small cell lung cancer cell lines, H1299 and A549, that are deficient for Fus1. Intratumoral injections of subcutaneous H1299 and A549 tumor bearing animals with DOTAP:Chol-Fus1 complex (50 μ/dose) daily for a total of six doses resulted in a significant inhibition (p=0.01) of tumor growth compared to control animals that were not treated, treated with Fus1 plasmid DNA, and treated with DOTAP:Chol-CAT complex. Similarly intravenous injection of DOTAP:Chol-Fus 1 complex (10 μ/dose) for a total of six doses via tail vein into animals bearing experimental A549 lung metastasis resulted in a significant inhibition (p=0.001) of lung metastasis compared to control animals. In addition, treatment of A549 lung metastasis bearing animals systemically with DOTAP:Chol-Fus1 complex (10 μ/dose) resulted in a prolonged survival (p= 0.01; mean- 80 days) compared to animals that were not treated (mean- 47.8 days), treated with plasmid DNA (mean – 51.6 days), treated with DOTAP:Chol. alone (mean- 47.2days), and treated with DOTAP:Chol-CAT (mean – 47.8 days). During the course of treatment, no significant toxicity was observed, indicating that the doses used are safe.

In conclusion, the results from the present study demonstrate that Fus1 is an effective tumor suppressor gene and can be used in the treatment of patients with primary and disseminated lung cancer. Based on these studies, a Phase I human clinical trial using systemic administration of FUS1-lipoplex has been initiated and approved by NIH RAC and FDA. The trial will start early this year.

In addition, we studied another potential apoptosis regulator, the CACNA2D2 gene, that has recently been identified in the homozygous deletion region of chromosome 3p21.3 in human lung and breast cancers. It is characterized structurally as a new a2d2 auxiliary subunit of the voltage-activated calcium channel (VACC) protein complex. The CACNA2D2 gene spans a ~140 kb genomic locus in the 3p21.3 region, consists of at least 40 exons, and is expressed as a 5.5-5.7 kb mRNA. The CACNA2D2 protein consists of 1146 amino acids with a predicted molecular mass of 130 kD (Gao et al., 2000). Three splicing variants of CACNA2D2 mRNA have been detected, which result in two protein isoforms with different N-terminals. The CACNA2D2 protein shows a 56% amino acid sequence homology to that of the a2d1 subunit of the VACC complexes and shares a similar secondary and tertiary structure the CACNA2D1, as suggested by the analysis of hydrophobicity, potential glycosylation sites, and bridge-forming cysteines of the primary sequence. The CACNA2D2 protein is highly expressed in normal lung tissue but either absent or underexpressed in more than 50% of lung cancers (Gao et al., 2000). Because cancer cells are deficient in CACNA2D2, it has been suggested that CACNA2D2 could be a tumor suppressor gene linking Ca2+ signaling with the pathogenesis of lung cancer and other cancers.

The CACNA2D2 gene, a new subunit of the Ca2+-channel complex, was identified in the homozygous deletion region of chromosome 3p21.3 in human lung and breast cancers. Expression deficiency of the CACNA2D2 in cancer cells suggests a possible link to the Ca2+-signaling in the pathogenesis of lung cancer and other cancers. We investigated the effects of overexpression of CACNA2D2 on intracellular Ca2+ contents, mitochondria homeostasis, cell proliferation, and apoptosis by adenoviral vector-mediated wild-type CACNA2D2 gene transfer in 3p21.3-deficient non-small cell lung cancer cell lines. Exogenous expression of CACNA2D2 significantly inhibited tumor cell growth compared with the controls. Overexpression of CACNA2D2 induced apoptosis in H1299 (12.5%), H358 (13.7%), H460 (22.3%), and A549 (50.1%) cell lines. Levels of intracellular free Ca2+ were elevated in AdCACNA2D2-transduced cells compared with the controls. Mitochondria membrane depolarization was observed prior to apoptosis in Ad-CACNA2D2 and Adp53-transduced H460 and A549 cells. Release of cyt C into the cytosol, caspase 3 activation, and PARP cleavage were also detected in these cells. Together, these results suggest that one of the pathways in CACNA2D2-induced apoptosis is

mediated through disruption of mitochondria membrane integrity, the release of cyt C, and the activation of caspases, a process that is associated with regulation of cytosolic free Ca2+ contents.

Specific Aim 3.4 ***Develop specific vascularly targeted strategies to the vascular epithelium of lung cancer cells in order to decrease the toxicity to normal cells and enhance the therapeutic index.***

Human MDP cDNA was amplified by PCR from normal lung cDNA library and cloned into a bacterial expression vector. A polyclonal antibody serum was then generated against this recombinant human MDP.

Immunohistochemistry in human tissues using this immune serum recapitulates the MDP tissue distribution seen in mice. Vascular distribution of MDP appears to be ubiquitous in the lung and absent in other organs and lung metastases, suggesting that MDP may play a role in human lung metastases as well.

KEY RESEARCH ACCOMPLISHMENTS

- Identified an association between hnRNPs/isoforms and CEACAM1 splicing patterns.
- Identified exon 7 of CEACAM1 contains a splicing controlling element and PTB plays an important role in CEACAM1 splicing through the element.
- Found enolase-α down-regulation is common in NSCLC and associated with a poor clinical outcome.
- Identified a novel minisatellite polymorphism in down-stream of hTERT gene (MNS16A) and demonstrated the size of MSN16A plays a role in lung cancer susceptibility.
- Demonstrated that IL-10 expression is lost in a subset of NSCLC and such loss predicts a poor clinical outcome in patients with stage I NSCLC.
- COX-2 expression is related to metastasis in 3/5 paired primary/metastasis cell lines. HNSCC cells that express COX-2 do not show greater sensitivity to COX-2 inhibitors than HNSCC cells that do not express COX-2.
- The combination of the COX-2 inhibitor Celecoxib and the retinoid 4HPR results in more effective growth inhibition than each agent alone.
- Demonstrated lack of PTEN expression in NSCLC may be related to promoter methylation and is of prognostic importance in stage I NSCLC.
- Farnesyl Transferase Inhibitors down-regulate phosphorylated RAF and AKT and induce the ubiquitination of AKT protein.

REPORTABLE OUTCOMES

Wang L, Soria JC, Kemp BL, Liu DD, Mao L, Khuri FR. hTERT expression is a prognostic factor of survival in patients with stage I non-small cell lung cancer. Clinical Cancer Research 8: 2883-2889, 2002.

Soria JC, Lee HY, Lee JI, Wang L, Issa JP, Kemp BL, Liu DD, Kurie JM, Mao L, Khuri FR. Lack of PTEN expression in non-small cell lung cancer could be related to promoter methylation. Clinical Cancer Research 8: 1178-1184, 2002.

Chang YS, Wu W, Walsh G, Hong WK, Mao L. Enolase-α is Frequently Down-Regulated in Non-Small Cell Lung Cancer and Produces Aggressive Biological Behavior. (submitted for publication, Clinical Cancer Research).

Wang L, Soria JC, Chang YS, Lee HY, Wei Q, Mao L. Association of a Functional Tandem Repeats in Downstream of Human Telomerase Gene and Lung Cancer. (submitted for publication, Oncogene).

Soria JC, Moon C, Kemp BL, Liu DD, Feng L, Tang X, Chang YS, Mao L, Khuri FR. Lack of Interleukin-10 Expression Predicts Poor Outcome in Patients with State I Non-Small Cell Lung Cancer. (submitted for publication, Clinical Cancer Research).

Sun SY, Yue P, Hong WK and Lotan R. Growth-inhibitory and Apoptosis-inducing Effects of the Combination of Low Doses of Celecoxib and *N*-(4-hydoxyphenyl)retinamide in Human Lung Cancer Cells. (submitted for publication, Clinical Cancer Research).

Lee HY, Srinivas H, Xia D, Lu Y, Superty R, LaPushin R, Gomez-Manzano C, Gal AM, Walsh GL, Force T, Ueki K, Mills GB, Kurie JM. Evidence that phosphatidylinositol 3-kinase-and mitogen-activated protein kinase kinase-4 / cJun N-terminal kinase-dependent pathways cooperate to maintain lung cancer cell survival. (submitted for publication, Journal of Biological Chemistry).

Ramesh R, Saeki T, Templeton NS, Ji L, Stephens LC, Ito I, Wilson DR, Wu Z, Branch CD, Minna JD, Roth JA. Successful treatment of primary and disseminated human lung cancers by systemic delivery of tumor suppressor genes using an improved liposome vector. Molecular Therapy 3: 337-350, 2001.

Ji L, Nishizaki M, Gao B. Burbee D, Kondo M, Kamibayashi G, Xu K, Yen N, Atkinson EN, Fang B, Lerman MI, Roth JA, and Minna JD. Expression of Several Genes in the Human Chromosome 3p21.3 Homozygous Deletion Region by an Adenovirus Vector Results in Tumor Suppressor Activities *in Vitro* and *in Vivo*, Cancer Research 62: 2715-2720, 2002.

Carboni GL, Gao B, Nishizaki M, Xu K, Minna JD, Roth JA, Ji L. CACNA2D2 mediated apoptosis in NSCLC cells is associated with alterations of the intracellular calcium signaling and disruption of mitochondria membrane integrity, Oncogene, 22: 615-626, 2003.

Patent:

Ji L, Roth JA, Minna JD, and Lerman MI. Chromosome 3p21.3 genes as tumor suppressors. U.S. Patent pending N0. 60/217, 112; International Patent Application No. PCT/US01/2178; European Patent Application Based on PCT/US01/21781.

CONCLUSIONS

Project 1 PTB is overexpressed in lung cancer and contributes to the splicing regulation of CEACAM1 through binding directly to exon 7 of the gene. Further investigation of the role of PTB in lung tumorigenesis may provide rationale of using PTB as a biomarker and/or therapeutic target. hnRNPs may also contribute to the regulation of CEACAM1 splicing and will be studied further. The identification of DNMT3B6 and its splicing isoforms as major expression

forms of DNMT3B in lung cancer is leading us to test their potential role in the important issue of differential promoter methylation in lung tumorigenesis.

Project 2 The mechanism of NSAIDs' action on normal premalignant and malignant lung epithelial cells may be independent of COX-2 inhibition. The combination of retinoic acid and either NS398 or MK886 does not appear to have advantage over single agent.

Project 3 Molecular prognostic models of Stage I NSCLC increasingly identify a group at heightened risk of recurrence. We are exploring various molecular therapeutic approaches in our novel mouse models of lung cancer, utilizing FUS1 gene therapy, vascular targeted approaches and small molecules to better understand their potential individualized therapeutic applications.

REFERENCES

1. Schottenfeld, D. Etiology and epidemiology of lung cancer. In: Lung Cancer Principles and Practice (2nd edition), Pass HI, Mitchell JB, Johnson DH, Turrisi AT, Minna JD (eds). Lippincott Williams and Wilkins, Philadelphia, 367-388, 2000.

2. Vaporciyan AA, Nesbitt JC, Lee JS, Stevens C, Komaki R, Roth JA. Cancer of the lung, Cancer Medicine (5th edition), Bast Jr., RC, Kufe DW, Pollock RE, Weichselbaum RR, Holland JF, Frei III E (eds). B. C. Decker, Inc., Hamilton, Ontario 1227-1292, 2000.

APPENDIX

doi:10.1006/mthe.2001.0266, available online at http://www.idealibrary.com on IDEAL

Successful Treatment of Primary and Disseminated Human Lung Cancers by Systemic Delivery of Tumor Suppressor Genes Using an Improved Liposome Vector

Rajagopal Ramesh,*,[1] Tomoyuki Saeki,* Nancy Smyth Templeton,[†] Lin Ji,* L. Clifton Stephens,[‡] Isao Ito,* Deborah R. Wilson,[§] Zheng Wu,[§] Cynthia D. Branch,* John D. Minna,[¶] and Jack A. Roth*

*Section of Thoracic Molecular Oncology, Department of Thoracic and Cardiovascular Surgery, and [‡]Department of Veterinary Medicine and Surgery, The University of Texas M. D. Anderson Cancer Center, Houston, Texas 77030
[†]Center for Cell and Gene Therapy, Baylor College of Medicine, Houston, Texas 77030
[§]Introgen Therapeutics Inc., Houston, Texas 77030
[¶]Department of Pathology, The University of Texas Southwestern Medical Center, Dallas, Texas 75390

Received for publication November 8, 2000; accepted in revised form January 10, 2001; published online March 9, 2001.

Delivery of therapeutic genes to disseminated tumor sites has been a major challenge in the field of cancer gene therapy due to lack of an efficient vector delivery system. Among the various vectors currently available, liposomes have shown promise for the systemic delivery of genes to distant sites with minimal toxicity. In this report, we describe an improved extruded DOTAP:cholesterol (DOTAP:Chol) cationic liposome that efficiently delivers therapeutic tumor suppressor genes *p53* and *FHIT*, which are frequently altered in lung cancer, to localized human primary lung cancers and to experimental disseminated metastases. Transgene expression was observed in 25% of tumor cells per tumor in primary tumors and 10% in disseminated tumors. When treated with DOTAP:Chol–*p53* and –*FHIT* complex, significant suppression was observed in both primary ($P < 0.02$) and metastatic lung tumor growth ($P < 0.007$). Furthermore, repeated multiple treatments revealed a 2.5-fold increase in gene expression and increased therapeutic efficacy compared to single treatment. Finally, animal survival experiments revealed prolonged survival (median survival time: 76 days, $P < 0.001$ for H1299; and 96 days, $P = 0.04$ for A549) when treated with liposome–*p53* DNA complex. Our findings may be of importance in the development of treatments for primary and disseminated human lung cancers.

Key Words: lung cancer; *p53; FHIT;* liposome; gene therapy; tumor suppressor; intratumoral; intravenous.

Introduction

Cancer of the lung is one of the leading causes of death worldwide (1). Patients often present with locally advanced or disseminated disease, and long-term survival rates have not improved appreciably over the past 20 years. Current treatments for lung cancer have shown little success, because they cannot eradicate disseminated tumors with an acceptable toxicity. One alternative strategy that has shown promise in the treatment of cancer is gene therapy. However, so far this approach has been shown in patients to mediate tumor regression only when delivered directly to solid tumors via intralesional or intraperitoneal injection (2–6). A gene therapy has yet to be developed that is effective for disseminated cancer. One reason for this has been the lack of a vector that is nontoxic and that can efficiently deliver genes when injected intravenously. However, Templeton *et al.* (7) recently reported development of extruded DOTAP:cholesterol (DOTAP:Chol) cationic liposomes that efficiently delivered the chloramphenicol acetyl transferase (*CAT*) gene to various organs and tissues with maximal gene delivery to the lung following intravenous administration. Indeed, in the same study DOTAP:Chol proved superior to previously reported liposome preparations, and it was the extrusion of the liposomes during synthesis that was impor-

[1] To whom correspondence and reprint requests should be addressed at Department of Thoracic and Cardiovascular Surgery, Box 109, The University of Texas M. D. Anderson Cancer Center, 1515 Holcombe Boulevard, Houston, TX 77030. Fax: (713) 794-4669. E-mail: rramesh@mdanderson.org.

1525-0016/01 $35.00

tant for mediating very high gene transfer to the lung. Although, effective gene delivery to the lung was previously demonstrated using DOTAP:Chol, the ability of these cationic liposomes to efficiently deliver and express therapeutic genes in primary or disseminated lung tumors has not been previously reported.

In this study, we therefore tested the ability of improved extruded DOTAP:Chol cationic liposomes to deliver the therapeutic tumor suppressor genes *p53* and fragile histidine triad (*FHIT*) to primary and disseminated experimental metastatic murine and human lung tumors and compared with conventional liposomes. We chose the *p53* gene because it is the most commonly mutated gene identified to date in human cancers (8) and the *FHIT* gene because its aberrant transcripts as well as the lack of detectable *Fhit* protein have been frequently observed in a variety of primary tumors and their derived cell lines, including cancers of the lung, stomach, breast, colon, cervix, and the head and neck (9, 10). The overall frequencies of *p53* and *FHIT* gene alterations in small cell lung cancer are 90 and 80%, respectively, and in non-small-cell lung cancer, approximately 55 and 40% (9–11). Furthermore, reintroduction and overexpression of the wild-type p53 or *Fhit* protein have demonstrated ability to suppress tumor cell growth *in vitro* and *in vivo* (12–15). As part of this study, we developed xenograft models of experimental metastases with human lung cancer cells that did not produce wild-type p53 or Fhit protein. We observed that extruded DOTAP:Chol cationic liposome-mediated gene delivery effectively transfected both primary and disseminated murine tumors and human lung tumor xenografts, and this was associated with suppressed tumor growth and prolonged animal survival with minimal toxicity.

Methods

Materials. All lipids (DOTAP, DOPE, cholesterol) were purchased from Avanti Polar Lipids (Albaster, AL). Lipofectamine (DOSPA:DOPE), RPMI 1640 medium, Ham's/F12 medium, and fetal bovine serum (FBS) were purchased from GIBCO-BRL-Life Technologies (New York, NY). DOTAP transfection reagent was purchased from Roche Molecular Biochemicals (Indianapolis, IN). Polyclonal rabbit antihuman FHIT antibody and mouse antihuman p53 monoclonal antibody (BP53.12) were obtained from Zymed Laboratories (San Francisco, CA) and Santa Cruz Biotechnology, Inc. (Palo Alto, CA), respectively.

Cell lines and animals. Human non-small cell lung carcinoma cell lines H1299 (*p53*^{null}/*FHIT*−) and A549 (*p53*$^{+}$/*FHIT*−) were obtained from American Type Culture Collection and maintained in RPMI 1640 and Ham's/F12 media supplemented with 10% FBS, 1% glutamate, and antibiotics. Murine fibrosarcoma cell line UV2337m, which has a mutant *p53* (16), was obtained from Dr. Isaiah J. Fidler, The University of Texas M. D. Anderson Cancer Center, and maintained in Dulbecco's modified Eagle's medium supplemented with 10% FBS. Cells were regularly passaged and tested for presence of mycoplasma. Four- to 6-week-old female immunocompetent C3H/HeNcr mice (National Cancer Institute, Frederick, MD), BALB/c nude (*nu/nu*) mice (Harlan-Sprague-Dawley Inc., Indianapolis, IN), and SCID/Beige mice (Charles River Laboratories, Wilmington, MA) used in the study were maintained in a pathogen-free environment and handled according to institutional guidelines established for animal care and use.

Purification of plasmids. The plasmids used in the study were either purchased (β-*gal*, Clontech Inc., Palo Alto, CA; *Luc*, Promega, Madison, WI) or cloned in an adenoviral shuttle vector (*p53*, *FHIT*, and *CAT*) and purified as described previously (7, 17). Briefly, plasmids carrying the bacterial β-galactosidase (*Lac-Z*), firefly luciferase (*Luc*), or *CAT* genes, or human *p53* or *FHIT* cDNA, under the control of cytomegalovirus (CMV) promotor, were grown under ampicillin or kanamycin selection in the *Escherichia coli* host strain DH5α. Endotoxin levels of purified plasmids were determined using the chromogenic limulus amebocyte lysate kinetic assay kit (Kinetic-QCL, Biowhittaker, Walkersville, MD). The concentration and purity of the purified plasmid DNAs were determined by $OD_{260/280}$ ratios.

Synthesis of liposomes and preparation of DNA:liposome mixtures. Liposomes (DOTAP:Chol and DOTAP:DOPE) were synthesized and extruded through Whatman filters (Kent, UK) of decreasing size (1.0, 0.45, 0.2, and 0.1 μm) as described previously (7). DNA:liposome complexes were prepared fresh 2 to 3 h before tail vein injection in mice. Briefly, DOTAP:Chol (20 mM) or DOTAP:DOPE (20 mM) stock solution and stock DNA solution diluted in 5% dextrose in water (D5W) were mixed in equal volumes to give a final concentration of 4 mM DOTAP:Chol–150 μg DNA in 300 μl final volume (ratio 1:2.6). All reagents were diluted and mixed at room temperature. Reagents were gently mixed in a 1.5-ml Eppendorf tube by pipetting. The DNA solution was added at the surface of the liposome and mixed rapidly up and down twice with the pipet tip. The DNA:liposome mixture thus prepared was precipitate free and used for all *in-vivo* experiments. The DOTAP–DNA liposome complex and lipofectamine–DNA liposome complex were prepared according to manufacturer's guidelines.

Particle size analysis. Freshly prepared DNA:liposome complexes were analyzed for mean particle size using the N4 particle size analyzer (Coulter, Miami, FL). The average mean particle size of the DNA:liposome complexes ranged between 300–325 nm.

In vivo transfection efficiency in normal lung, subcutaneous tumors, and tumor-bearing lungs. Before the start of the experiment, *nu/nu* mice were subjected to 3.5 Gy of total body irradiation to increase tumor uptake using a cesium source according to institutional guidelines. Mice were then injected with *p53* gene-null H1299 tumor cells [5×10^6/100 μl of phosphate-buffered saline (PBS)] subcutaneously on the right flank. When the tumors reached 4–5 mm^2 in size, a single dose of DOTAP:Chol–DNA complex (100 μg of *Lac-Z* DNA) was injected intratumorally. Forty-eight hours after injection, mice were euthanized by CO_2 inhalation, and tumors were removed and analyzed histochemically for β-galactosidase expression (18). Tumors were cut into 4-μm sections, stained for β-galactosidase, and evaluated by light microscopy.

Expression of the p53 and Fhit proteins in tumors was determined by Western blot analysis. Briefly, subcutaneous H1299 tumors injected intratumorally with DOTAP:Chol–DNA complex (100 μg of *Lac-Z, CAT, p53,* or *FHIT* DNA) were harvested 48 h after treatment and homogenized in Laemmli buffer. Protein concentrations were determined by using Bio-Rad protein assay reagent (Bio-Rad, Fremont, CA), and 50 μg of total protein was analyzed by sodium dodecyl sulfate (SDS)–polyacrylamide gel electrophoresis (PAGE). p53 and Fhit proteins were detected using mouse antihuman *p53* antibody (BP53.12) and rabbit antihuman *FHIT* antibody as described previously (15, 19, 20).

To determine the transfection efficiency of the liposome:DNA complexes in normal lungs, C3H mice were injected with DOTAP:Chol–*Lac-Z* or DOTAP:Chol–*p53* via tail vein. Forty-eight hours after injection, animals were euthanized by CO_2 inhalation; their lungs were harvested and either snap frozen for β-galactosidase analysis or formalin fixed for p53 analysis. Tissue sections were cut and analyzed histochemically (β-gal) or immunohistochemically (p53) as described previously (18, 19). To determine the transfection efficiency of the complexes in lung tumors *in vivo,* nude mice were injected with 1×10^6 A549 tumor cells suspended in 200 μl of PBS via tail vein. Two to 3 weeks later, a single dose of DOTAP:Chol–*Lac-Z* or DOTAP:Chol–*FHIT* complex (50 μg DNA) or naked plasmid DNA (50 μg) was injected via tail vein. Lungs were harvested 48 h later and analyzed for protein expression by histochemical (β-gal) or immunohistochemical (Fhit) analysis (18, 20).

Tumor growth and treatments in vivo. Before the start of all experiments involving subcutaneous tumor growth and treatments, *nu/nu* mice were irradiated (3.5 Gy) using a cesium source to enhance tumor uptake. In all the experiments, 5×10^6 tumor cells (H1299, A549) suspended in 100 μl sterile PBS were injected into the right dorsal flank. When the tumor had reached a size of 4–5 mm^2, the animals were randomized into groups and

treatment was initiated. Intratumoral injections were performed under anesthesia using methoxyflurane (Schering-Plough, Kenilworth, NJ) per institutional guidelines. Tumor measurements were recorded every other day without knowledge of the treatment groups, and tumor volumes were calculated by using the formula $V\ (mm^3) = a \times b^2/2$, where a is the largest dimension and b is the perpendicular diameter (21). Antitumor efficacy data are presented as cumulative tumor volumes for all animals in each group to account for both size and number of tumors.

For p53 experiments, subcutaneous H1299 tumor-bearing animals were divided into three groups of eight animals. Group 1 received no treatment, Group 2 received naked *p53* plasmid DNA (100 μg/dose), and Group 3 received extruded DOTAP:Chol-*p53* complex (100 μg/dose); treatments were given daily for a total of six doses. In a separate but parallel experiment, an additional control group was included that received a complex of extruded DOTAP:Chol with an irrelevant DNA plasmid (pAd). All other experimental conditions and treatment schedules were identical.

For FHIT experiments, H1299 and A549 subcutaneous tumors were established in nude mice. For each tumor type, four treatment groups were established comprising seven animals per group. Group 1 received no treatment, Group 2 received *FHIT* plasmid DNA (100 μg/dose), Group 3 received extruded DOTAP:Chol-*CAT* complex (100 μg/dose), and Group 4 received extruded DOTAP:Chol-*FHIT* complex (100 μg/dose). Animals were treated daily for a total of six doses. In all experiments, the statistical significance of changes in tumor size was determined by using the Student's *t* test.

Establishment of lung metastases and their treatments in vivo. To establish lung metastases, female SCID/Beige mice were injected via tail vein with 10^6 H1299 tumor cells suspended in 200 μl of sterile PBS. Three days later, the mice were divided into nine groups and treated as follows: no treatment (Group 1), naked *p53* plasmid DNA (Group 2), DOTAP-DOPE-*p53* complex (Group 3), extruded DOTAP:Chol-*CAT* complex (Group 4), nonextruded DOTAP:Chol-*p53* complex (Group 5), extruded DOTAP:Chol-*p53* complex (Group 6), empty liposome (Group 7), lipofectamine-*p53* complex (Group 8), and DOTAP:*p53* complex (Group 9). There were eight mice in each group. All treatments comprised 50 μg of plasmid DNA or 50 μg DNA:liposome complex and were administered via tail vein using a 27-gauge needle daily for a total of six doses. Two weeks following the last dose, animals were euthanized by CO_2 inhalation. Lungs from each of the mice from the nine groups were injected intratracheally with India ink and fixed in Feketes solution (22). The therapeutic effect of systemic *p53* gene treatment was determined by counting the number of metastatic tumors in each lung under a dissecting microscope without knowledge of the treatment groups. The data were analyzed, and differences among groups were interpreted as statistically significant if the P value was <0.05 by the Mann-Whitney rank-sum test.

To determine the therapeutic effect of the *p53* and *FHIT* tumor suppressor genes on lung tumor cells expressing wild-type p53, mice (*nu/nu*) were injected with A549 tumor cells (1×10^6) via tail vein. On day 6 after injection, mice were divided into groups ($n = 6$ or 8 animals per group) for treatment. Group 1 received no treatment; Group 2 received *p53* or *FHIT* plasmid DNA; Group 3 received extruded DOTAP:Chol-*CAT* complex; Group 4 received extruded DOTAP:Chol-*p53* complex or DOTAP:Chol-*FHIT* DNA:liposome complex; Group 5 received lipofectamine-*p53* DNA:liposome complex; Group 6 received empty liposome. Animals were treated daily for a total of six doses (50 μg/dose). Following the last dose, mice were euthanized, and the therapeutic effects of the *p53* and *FHIT* DNA:liposome complexes were determined as described above for the H1299/SCID/Beige model.

As a syngeneic lung tumor model, C3H mice were injected with murine UV2237m fibrosarcoma cells (1×10^6) and divided into nine groups ($n = 5$/group). Six days after injection, animals were treated as follows: no treatment, empty liposome, *p53* plasmid DNA, DOTAP-*p53* complex, lipofectamine-*p53* complex, DOTAP:DOPE-*p53* complex, nonextruded DOTAP:Chol-*p53* complex, extruded DOTAP:Chol-*CAT* complex, or extruded DOTAP:Chol-*p53* complex. Treatment schedule and analyses of therapeutic effect were the same as described above for the H1299 and A549 models.

Gene expression and therapeutic efficacy of single and multiple treatments in lung tumor-bearing animals. For evaluation of gene expression, UV2237m lung tumor-bearing C3H mice were divided into three groups. One group was not treated; the others were treated with one dose of extruded DOTAP:Chol-*Luc* complex or three daily doses of the same complex (50 μg DNA/dose). Lungs were harvested 48 h after injection, and the protein was extracted and analyzed for luciferase activity using the luciferase assay kit (Promega, Madison, WI). Luciferase activity was expressed as relative light units (RLU) per milligram of protein.

To determine the therapeutic efficacy of repeated treatments, UV2237m tumor-bearing animals were divided into groups ($n = 7$/group). Treatments comprised no treatment, one dose of extruded DOTAP:Chol-*p53* complex, or six daily doses of the same complex (50 μg DNA/dose). Lungs were harvested 2 weeks after the last treatment, and the number of tumor nodules counted as described earlier.

p53 effects on tumor cells. After subcutaneous H1299 tumors established in *nu/nu* mice, the mice were separated into groups; one group was not treated; a second was treated with *p53* plasmid DNA, and a third with *p53* DNA:liposome complex. The tumors were then harvested and fixed in 4% buffered formalin, paraffin embedded, and cut in 4-μm sections. Tissue sections were stained for *p53* gene expression as previously described (13, 23). The tumor cells staining positive for *p53* were analyzed under bright field microscopy and quantitated without knowledge of the treatment groups. At least five fields per specimen were analyzed. To determine the fate of tumor cells following treatment, sections of subcutaneous tumors and tumor-bearing lungs were stained for apoptotic cell death with terminal deoxynucleotide transferase (Tdt) (Boehringer Mannheim) and counterstained with methylene blue or methyl green as described previously (13, 23). In all the staining procedures, appropriate negative controls were included.

Tumor characteristics after treatment. To determine the therapeutic effect of the *p53* gene on metastatic lung tumors, tumor-bearing lungs were harvested from *nu/nu* mice 21 days after treatment and evaluated histopathologically for tumor size, viability, and mitotic index. Analysis was done by a pathologist without knowledge of the treatment groups.

Animal survival after treatment. To determine the efficacy of systemic treatment, survival experiments were performed using the two metastatic lung tumor (H1299, A549) models. Briefly, female SCID/Beige mice were injected with 10^6 H1299 tumor cells via the tail vein. Six days later, mice were divided into four groups of six mice. Group 1 received no treatment, Group 2 received naked *p53* plasmid DNA, Group 3 received extruded DOTAP:Chol-*CAT* complex, and Group 4 received DOTAP:Chol-*p53* complex. In a separate set of experiments, two additional groups were tested, which received treatment with DOTAP:DOPE-*p53* complex or nonextruded DOTAP:Chol-*p53* complex. The treatment schedule consisted of six daily injections of naked plasmid DNA or DNA:liposome complex in 100 μl volumes (50 μg DNA/dose). Mice were monitored daily following the last injection. Moribund animals were euthanized by CO_2 inhalation. The lungs, heart, liver, spleen, brain, kidney, colon, ovaries, pancreas, and bone were removed from each animal and analyzed histopathologically for the presence of disseminated tumors and treatment-associated toxic effects. Statistical differences in actuarial survival curves were analyzed by using the Kaplan-Meier survival estimation and Wilcoxon signed-rank tests.

The A549 lung metastatic tumor model was used to evaluate the effect of the DOTAP:Chol-*p53* complex on tumors that have the wild-type *p53* gene. Briefly, *nu/nu* mice were injected with 10^6 A549 tumor cells via the tail vein. Six days later, mice were divided into four groups of seven mice each. The experimental conditions and treatment schedule were identical to those used for the H1299-SCID/Beige lung tumor model. The effect of DOTAP:Chol-*p53* DNA:liposome complex on survival was calculated by using the Kaplan-Meier survival estimation and the Wilcoxon signed-rank tests.

Statistical analysis. The statistical significance of the experimental results was calculated using Student's *t* test for tumor measurements, the Mann-Whitney rank-sum test for lung metastases, and the Wilcoxon log-rank test and Kaplan-Meier survival test for animal survival.

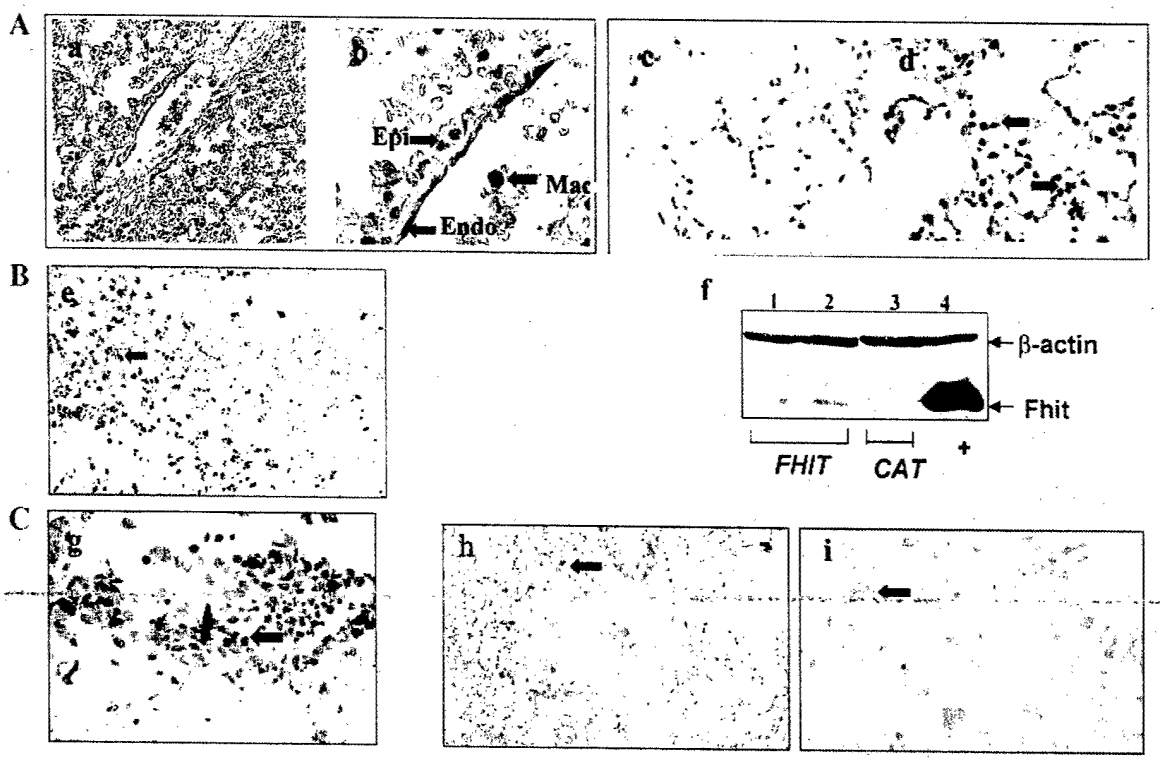

FIG. 1. *In vivo* transfection efficiency in normal lung, subcutaneous tumor, and metastatic lung tumors. (A) Female C3H mice were injected via the tail vein with either 50 μg of naked plasmid DNA (*Lac-Z* or *p53*) or 50 μg of plasmid DNA (*Lac-Z* or *p53*) complexed to liposomal DOTAP:Chol. Forty-eight hours after injection, lungs were harvested and analyzed for protein expression using histochemical (*Lac-Z*) and immunohistochemical (*p53*) methods. Alveolar epithelial (Epi) cells, endothelial (End) cells, and macrophages (Mac) of the lung from animals injected with DOTAP:Chol–DNA complexes showed gene expression, while those from animals injected with plasmid DNA showed no gene expression. This figure shows the production of β-galactosidase in lung tissue from an animal treated with DOTAP:Chol–*Lac-Z* complex at low (a) and high (b) magnification. Lung from a control animal treated with *p53* plasmid DNA is shown in c. Lung from an animal treated with DOTAP:Chol–*p53* produced p53 protein (d). (B) Subcutaneous H1299 tumors established in *nu/nu* mice given a single intratumoral injection of DOTAP:Chol liposome complexed to *Lac-Z, CAT,* or *FHIT* plasmid DNA (50 μg). Forty-eight hours later, tumors were removed and underwent either X-gal staining for β-galactosidase expression or Western blot analysis for Fhit protein production. A total of 25% of tumor cells treated with *Lac-Z* produced β-galactosidase (e). Fhit protein (f, lanes 1 and 2) production was demonstrated in tumors treated with *FHIT*. Lane 3 (f) represents tumors from animals treated with DOTAP:Chol–*CAT*. Lane 4 (f) represents the positive control for Fhit protein. (C) A549 lung tumor-bearing nude mice were injected with DOTAP:Chol liposome complexed to *Lac-Z* or *FHIT* DNA (50 μg) via the tail vein, and the lung tumors were analyzed for protein expression 48 h later. β-Galactosidase production (g) and Fhit production in lung tumors are shown at low (h) and high magnification (i). Arrows denote cells expressing transgene.

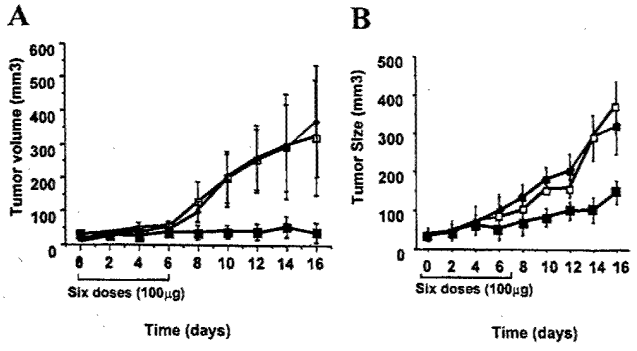

FIG. 2. DOTAP:Chol–*p53* complex suppress growth of subcutaneous human lung cancer xenografts. Subcutaneous H1299 tumor-bearing mice were divided into three groups (8 animals/group) and treated daily for a total of six doses (100 μg/dose), as follows: no treatment (●), *p53* plasmid DNA (□) and DOTAP:Chol–*p53* DNA:liposome complex (■) (A); no treatment (●), DOTAP:Chol–*pAd* complex (□) and DOTAP:Chol–*p53* complex (■) (B). Tumors were measured by using calipers, and the statistical significance of size changes was calculated using Student's *t* test. Each time point represents the mean tumor volume for each group. Bars represent standard errors.

Results

In Vivo Transfection in Normal Lung, Primary Lung Tumor Xenografts, and Experimental Metastatic Lung Tumors

We determined the ability of extruded DOTAP:Chol liposomes to effectively transfect and deliver plasmid DNA into normal lung, subcutaneous lung tumor xenografts, and experimental metastatic lung tumors by using expression plasmids encoding the bacterial β-galactosidase (*Lac-Z* gene) or the human p53 or Fhit protein. Forty-eight hours following a single tail vein injection of DOTAP:Chol liposomes complexed with *Lac-Z* plasmid DNA or human *p53* plasmid DNA, alveolar epithelial cells (type II pneumocytes) and endothelial cells in the lung were observed to produce β-galactosidase (Figs. 1a and 1b) or p53 protein (Fig. 1d). Few alveolar macrophages expressed the transgene. In contrast, no gene expression was ob-

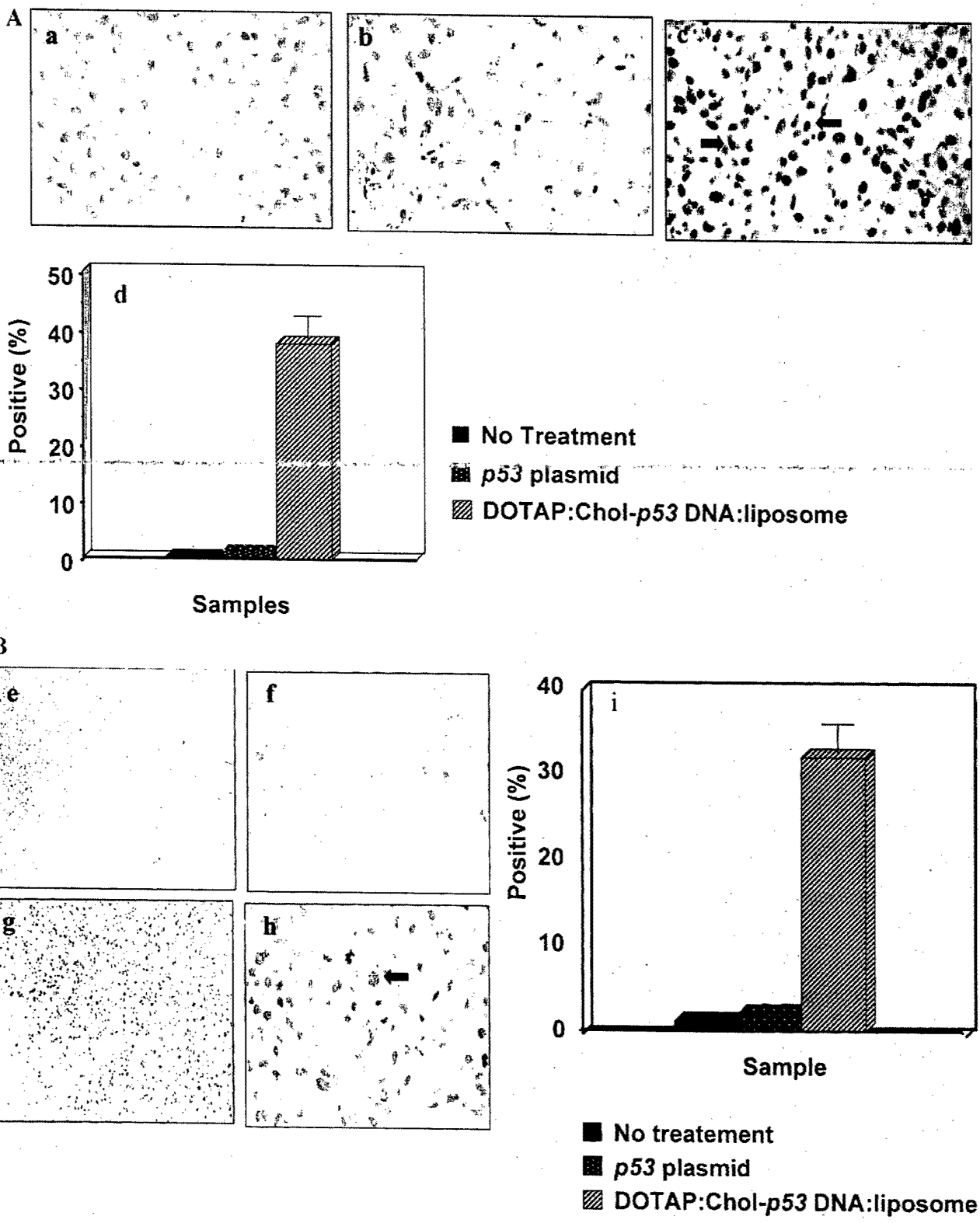

FIG. 3. *p53* gene expression and apoptotic cell death following treatment with the DOTAP:Chol–*p53* complex. Subcutaneous H1299 tumors from animals receiving no treatment (a), *p53* plasmid (b, e, f), or the DOTAP:Chol–*p53* complex (c, g, h) were harvested 48 h after treatment. p53 protein production was analyzed by (A) immunohistochemistry (a, b, c) and (B) apoptotic cell death by TUNEL staining (e, f, g, h). The percentages of cells producing the p53 protein (39%) (d) and undergoing apoptotic cell death (32%) (i) in tumors receiving the DOTAP:Chol–*p53* complex were significantly ($P = 0.001$) higher than the percentages of cells in the no treatment and p53 plasmid treatment groups.

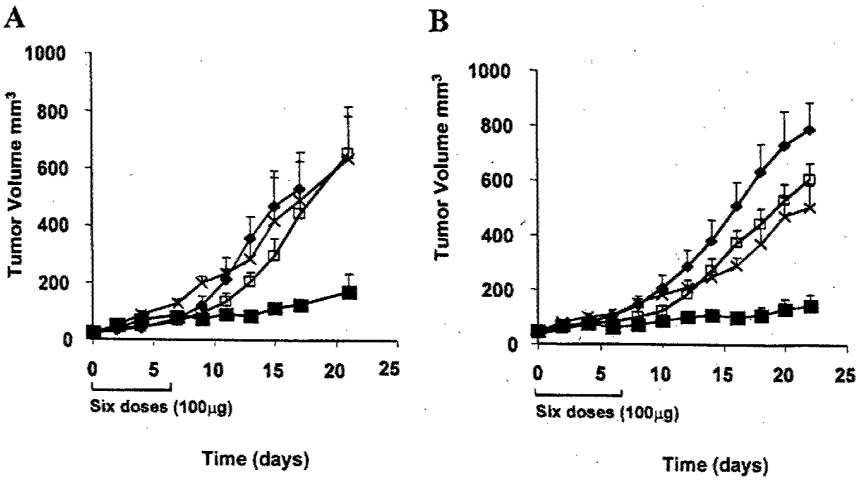

FIG. 4. Therapeutic effect of the DOTAP:Chol–*FHIT* complex on lung tumor xenografts. Subcutaneous H1299 and A549 tumor-bearing nude mice were divided into four groups (7 animals/group) and treated daily for a total of six doses (100 μg/dose), as follows: no treatment (◆), *FHIT* plasmid DNA, (□) DOTAP:Chol–*CAT* complex (X), and DOTAP:Chol–*FHIT* complex (■). The effects in H1299 tumors are shown in (A) and those in A549 tumors in (B). Tumor growth was significantly inhibited in both H1299 ($P = 0.02$) and A549 ($P = 0.001$) tumor-bearing animals treated with the DOTAP:Chol–*FHIT* complex. Bars denote standard errors.

served in animals injected with naked *p53* plasmid DNA (Fig. 1c).

To determine whether gene expression could also be achieved in solid primary tumors, human H1299 lung tumors were established subcutaneously in nude mice. Forty-eight hours following a single intratumoral injection of DOTAP:Chol–*LacZ* complex, 25% of the tumor cells produced β-galactosidase, as shown by histochemical staining (Fig. 1e). In contrast, no β-galactosidase production was observed in the untreated control tumors. Intratumoral injection of DOTAP:Chol–*FHIT* resulted in production of Fhit protein, as determined by Western blot analysis (Fig. 1f). Tumor-bearing animals injected with DOTAP:Chol -CAT (Fig. 1f) served as controls. Similarly, p53 protein expression was observed by Western blot analysis (data not shown).

The ability to transfect experimental human A549 lung metastatic tumors established in nude mice was also evaluated. A single tail vein injection of DOTAP:Chol–*Lac-Z* or DOTAP:Chol–*FHIT* into lung tumor-bearing mice resulted in 10% of the tumor cells producing β-galactosidase (Fig. 1g) or Fhit protein (Figs. 1h and 1i) at 48 h.

In Vivo Local Tumor Growth Suppression by p53 and FHIT

We assessed the ability of the DOTAP:Chol–*p53* complex to suppress the growth of *p53* gene-null H1299 human lung subcutaneous tumors in *nu/nu* mice. Treatment of tumor-bearing mice with the DOTAP:Chol–*p53* complex inhibited tumor growth significantly ($P = 0.001$) (Fig. 2A) compared with tumor growth in the control groups.

To further demonstrate the specific tumor-suppressive effects of the *p53* gene delivered by DOTAP:Chol liposomes, we performed a separate set of experiments in which subcutaneous H1299 tumor-bearing animals were divided into three groups, one receiving no treatment, one treatment with DOTAP:Chol liposome complexed to irrelevant plasmid DNA (*pAd*), and one treatment with the DOTAP:Chol–*p53* complex. No significant inhibition of tumor growth was observed in animals that were either not treated or treated with the DOTAP:Chol–pAd complex (Fig. 2B). In contrast, animals treated with the DOTAP:Chol–*p53* complex showed significant tumor growth inhibition ($P = 0.01$).

Further evidence that the observed therapeutic effect was due to *p53* gene expression was obtained by removing subcutaneous tumors 48 h after injection and analyzing them for *p53* gene expression by immunohistochemistry. *p53* gene expression was seen in 39% of tumor cells in animals receiving the DOTAP:Chol–*p53* complex (Figs. 3c and 3d) ($P = 0.001$), a significantly higher number than in the animals that were either not treated (Fig. 3a) or treated with *p53* plasmid DNA (Fig. 3b). Analysis of apoptotic tumor cell death by TUNEL studies showed that 32% of the tumor cells in mice receiving the DOTAP:Chol–*p53* complex were positive ($P = 0.001$) (Figs. 3g–3i), whereas tumors from control mice showed minimal apoptotic cell death (Figs. 3e, 3f, and 3i).

The therapeutic effects of the *FHIT* tumor suppressor gene on H1299 and A549 subcutaneous tumors in nude mice were similarly evaluated. Mice bearing tumors of each cell type were divided into four groups, one receiving no treatment, a second treatment with naked *FHIT* plasmid DNA, a third treatment with the DOTAP:Chol–*CAT* complex, and a fourth treatment with the DOTAP:Chol–*FHIT* complex. A significant growth inhibition of both H1299 tumors ($P = 0.02$; Fig. 4A) and A549 tumors ($P = 0.001$; Fig. 4B) was observed in mice treated with the DOTAP:Chol–*FHIT* complex when compared with the tumor growth in the three control groups for each tumor type.

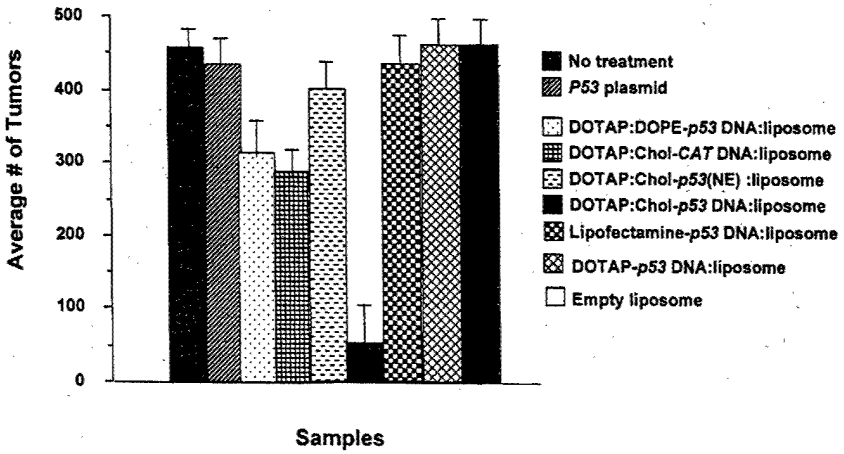

FIG. 5. Inhibition of H1299 lung metastases following treatment with the extruded DOTAP:Chol–*p53* complex. H1299 lung tumor-bearing SCID/Beige mice were either not treated or treated daily for a total of six doses (50 μg/dose) with *p53* plasmid DNA, empty liposome, lipofectamine–*p53* complex, DOTAP–*p53* complex, DOTAP:DOPE–*p53* DNA:liposome complex, nonextruded DOTAP:Chol–*p53* complex, extruded DOTAP:Chol–*CAT* complex, or extruded DOTAP:Chol–*p53* complex. Each group comprised eight animals. Metastatic tumor growth ($P = 0.001$) was significantly inhibited in mice treated with extruded DOTAP:Chol–*p53* complex when compared with growth in the other groups.

In Vivo Efficacy of p53 and FHIT Liposome:DNA Complexes for Treatment of Experimental Lung Metastases

The effectiveness of extruded DOTAP:Chol liposomes was compared to those of nonextruded DOTAP:Chol liposomes and other conventional liposome formulations [DOTAP, lipofectamine (DOSPA:DOPE), and DOTAP:DOPE] in a therapeutic xenograft model of human lung metastases using H1299 *p53*-null human lung cancer cells in SCID/Beige mice. There was a significantly ($P < 0.001$) lower number of lung metastases in mice receiving the extruded DOTAP:Chol–*p53* complex (Fig. 5) than in mice receiving no treatment, *p53* plasmid DNA, empty DOTAP:Chol liposome, DOTAP–*p53* complex, lipofectamine–*p53* complex, extruded DOTAP:Chol–*CAT* complex, DOTAP:DOPE–*p53* complex, or nonextruded DOTAP:Chol–*p53* complex. Metastatic tumor growth was also significantly ($P = 0.02$) inhibited in animals treated with the extruded DOTAP:Chol–*CAT* complex when compared with tumor growth in mice receiving no treatment, *p53* plasmid DNA, empty liposome, lipofectamine–*p53* DNA:liposome complex, or the DOTAP:*p53* complex.

To determine if the observed *p53* gene-mediated tumor inhibitory effects were restricted to *p53* gene-mutated or -null tumors, we studied the effects of the DOTAP:Chol–*p53* complex in A549 tumor cells, which are homozygous for the wild-type *p53* gene and form lung metastases following tail vein injection in *nu/nu* mice. A significantly lower ($P = 0.001$) number of metastases was observed in mice treated with the extruded DOTAP:Chol–*p53* complex (Fig. 6) than in control mice that were either not treated or were treated with *p53* plasmid DNA, empty DOTAP:Chol liposome, lipofectamine–*p53* complex, or DOTAP:Chol–*CAT* complex, thus eliminating the possibility that the *p53* gene-mediated inhibition was limited to *p53* gene-mutated or null tumors. No significant differences were observed in the number of metastases among the control groups.

The ability of the *FHIT* tumor suppressor gene to inhibit lung metastases formed by A549 tumor cells in nude mice was also evaluated. A significantly lower ($P = 0.007$) number of tumor metastases was observed in animals treated with the DOTAP:Chol–*FHIT* complex (Fig. 7) than in control animals that were not treated or were treated with *FHIT* plasmid DNA, empty DOTAP:Chol liposome, lipofectamine–*FHIT* complex or DOTAP:Chol–*CAT* complex. None of the control groups showed significant reductions in the number of tumor metastases.

Repeated Intravenous Injections of DOTAP:Chol–DNA Complex Increase Gene Expression and Therapeutic Efficacy

To determine whether repeated intravenous injections of DOTAP:Chol complex yield greater gene expression and thus therapeutic efficacy than single injections, UV2237m lung tumor-bearing immunocompetent C3H mice were divided into three groups; one group was not treated, another was treated with one dose of DOTAP:Chol–*luc* complex and the third was treated daily for a total of three doses of DOTAP:Chol–*luc* complex. Analysis of the animal's lungs 48 h after the last injection demonstrated a 2.5-fold greater ($P = 0.0004$) luciferase activity in the animals treated with three doses than in those treated with a single dose (Fig. 8). In addition, UV2237m lung tumor-bearing C3H mice that received repeated daily treatment with DOTAP:Chol–*p53* complex for a total of six doses demonstrated a significantly lower ($P = 0.0006$) number of tumors than those treated with only a single dose of DOTAP:Chol–*p53* complex or no treatment (Fig. 9).

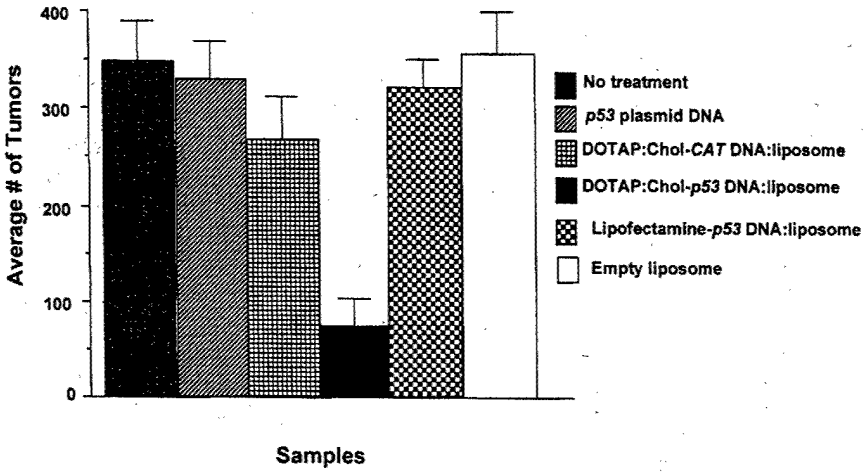

FIG. 6. Inhibition of A549 lung metastases following treatment with the extruded DOTAP:Chol–*p53* complex. A549 lung tumor-bearing *nu/nu* mice were either not treated or treated daily for a total of six doses (50 μg/dose) with *p53* plasmid DNA, empty liposome, lipofectamine–*p53* complex, extruded DOTAP:Chol–*CAT* complex, or extruded DOTAP:Chol–*p53* complex. Each group comprised eight animals. Metastatic tumor growth ($P = 0.001$) was significantly inhibited in mice treated with extruded DOTAP:Chol–*p53* complex compared with growth in the two control groups.

Apoptotic Cell Death in Lung Tumors Treated with DOTAP:Chol–p53 Complex

To determine the fate of tumor cells after treatment with the DOTAP:Chol–*p53* complex, A549 lung tumors from *nu/nu* mice were analyzed histologically, and apoptotic cell death was assessed by TUNEL staining. Histopathologic examination of lung sections from mice treated with the DOTAP:Chol–*p53* complex showed the presence of very few metastases; those that were present were small and contained only a few viable tumor cells (Figs. 10C and 10D). In addition, the number of tumor metastases in the lungs of these animals was significantly less than in control animals (data not shown). Furthermore, apoptotic cell death had occurred in these tumors (Fig. 11B). In contrast, lungs from control mice that received no treatment showed several large tumors with numerous mitoses (Figs. 10A and 10B) and no evidence of apoptotic cell death (Fig. 11A).

Inhibition of Murine UV2237m Lung Metastases in C3H Immunocompetent Mice Following Treatment with DOTAP:Chol–p53 Complex

To evaluate the efficacy of repeated treatments with DOTAP:Chol–p53 complex in an immunocompetent host, groups of UV2237m lung tumor-bearing C3H mice were either not treated or treated with *p53* plasmid DNA, empty DOTAP:Chol liposome, lipofectamine–*p53* com-

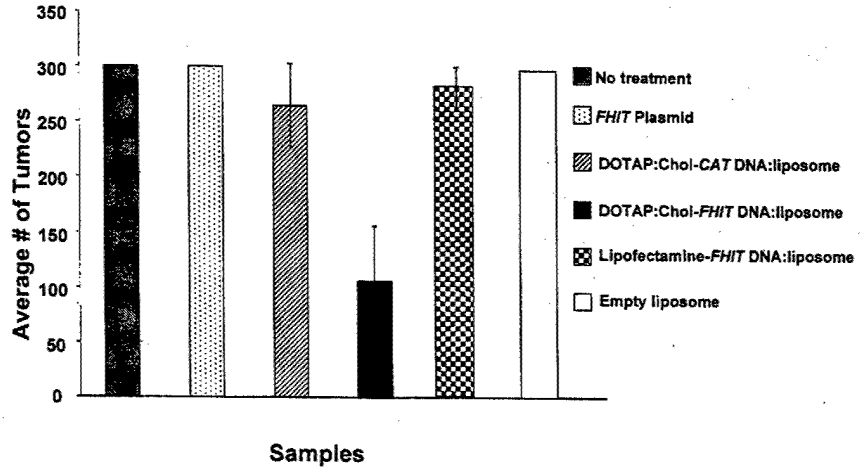

FIG. 7. Inhibition of A549 lung metastases following treatment with DOTAP:Chol–*FHIT* complex. A549 lung tumor-bearing *nu/nu* mice were divided into six groups and treated as follows: no treatment or treatment with *FHIT* plasmid DNA, empty liposome, lipofectamine–*FHIT* complex, extruded DOTAP:Chol–*CAT* complex, or extruded DOTAP:Chol–*FHIT* complex. Treatments were given daily for a total of six doses (50 μg/dose). Each group comprised six animals. There were significantly fewer lung tumors ($P = 0.007$) in mice treated with DOTAP:Chol–*FHIT* complex. In all the experiments, lungs were harvested 2 weeks after the last treatment, and metastases were counted without knowledge of the treatment group. Bars denote standard errors.

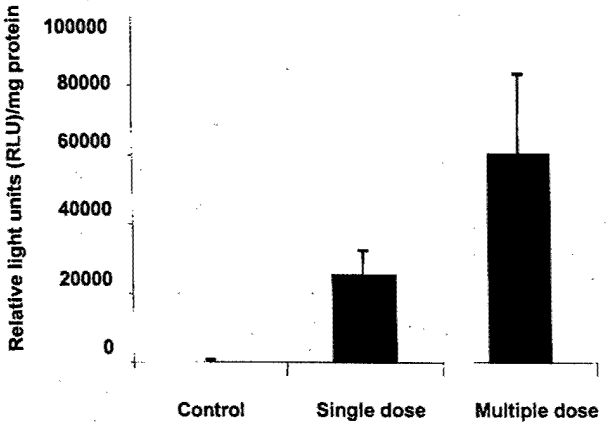

FIG. 8. Repeated intravenous injections of DOTAP:Chol–DNA complex increases gene expression. UV2237m lung tumor-bearing C3H animals were divided into three groups; one group was not treated, one was treated, with one dose of DOTAP:Chol–*luc* complex (50 μg DNA), and one was treated with three doses of DOTAP:Chol–*luc* complex (50 μg DNA/dose). Lungs were harvested 48 h after the last treatment and analyzed for luciferase activity. A 2.5-fold greater level of gene expression ($P = 0.0004$) was observed in animals treated with three doses than in animals treated with a single dose. Luciferase activity is expressed as relative light units (RLU) per milligram of protein.

plex, DOTAP–*p53* complex, the DOTAP:DOPE–*p53* complex, nonextruded DOTAP:Chol–*p53* complex, extruded DOTAP:Chol–*CAT* complex, or extruded DOTAP:Chol–*p53* complex. Each group comprised five animals. Analysis of the number of tumor nodules in each mouse 2 weeks after the last treatment demonstrated statistically significant tumor inhibition ($P = 0.01$) in mice treated with six doses of extruded DOTAP:Chol–*p53* complex when compared with any of the other groups (Fig. 12). Significant inhibition ($P = 0.03$) was also observed in animals treated with nonextruded DOTAP:Chol–*p53* complex when compared with animals receiving no treatment, empty liposome, or lipofectamine–*p53* complex. However, tumor inhibition was significantly less in the group treated with the nonextruded liposome:DNA complex than in the group treated with the extruded DNA:liposome complex.

DOTAP:Chol–p53 Prolongs Survival in a Mouse Model of Disseminated Human Lung Cancer

To determine the efficacy of the systemically administered extruded liposomal tumor suppressor gene complex, survival experiments were performed in the H1299 and A549 lung metastasis tumor models. H1299 lung tumor-bearing SCID/Beige mice were divided into four groups of six mice, as follows: no treatment (Group 1), *p53 plasmid DNA* (Group 2), DOTAP:Chol–*CAT* complex (Group 3), or DOTAP:Chol–*p53* complex (Group 4). Animals were monitored daily following the last treatment to assess morbidity and mortality. Mice from Groups 1, 2, and 3 died from the tumor burden between 30 and 60 days after tumor cell injection (median survival times: 38 days in Group 1, 40 days in Group 2, and 41 days in Group 3). In contrast, mice treated with the DOTAP:Chol–*p53* complex (Group 4) survived for a significantly longer period (median survival time: 76 days; $P = 0.001$). Moreover, 33% of mice from Group 4 were still alive on day 150 at the end of the experiment (Fig. 13A). In a separate set of experiments, additional control groups were tested that included DOTAP:DOPE–*p53* complex and nonextruded DOTAP:Chol–*p53* complex, but neither of these treatments significantly ($P = 0.35$) prolonged survival (median survival times: 44.8 days and 43.7 days, respectively, when compared with animals that were either not treated or treated with plasmid DNA. Again, in these experiments, treatment with extruded DOTAP:Chol–*p53* complex significantly prolonged ($P = 0.0002$) animal survival (median survival time: 81.3 days) (Fig. 13B). Histopathologic analysis of organs from animals in all the groups tested that died during the experiment showed no treatment-related toxic effects. However, all had dissemination of lung tumors to multiple organs and sites that included cervical lymph nodes, intestine, mesenteric lymph nodes, liver, kidney, spleen, pancreas, adrenal glands, ovaries, uterus, peritoneal cavity with ascites, and in all cases this was the cause of death (Figs. 13C–13F).

Survival in A549 lung tumor-bearing *nu/nu* mice was also evaluated. Following tumor cell injection, animals were divided into four groups, as follows: no treatment (Group 1), *p53* plasmid DNA (Group 2), DOTAP:Chol–*CAT* complex (Group 3), or DOTAP:Chol–*p53* complex (Group 4). The treatment schedule was identical to that followed in the H1299/SCID/Beige model. Mice in Group 4 had significantly longer survival (median survival time:, 96 days; $P = 0.04$) than mice in the three control groups (median survival times: 50 days in Group 1, 49 days in Group 2, and 52 days in Group 3) (Fig. 14). Histopathologic analysis of various organs revealed extensive tumor spread in the lungs of all four groups of animals, but

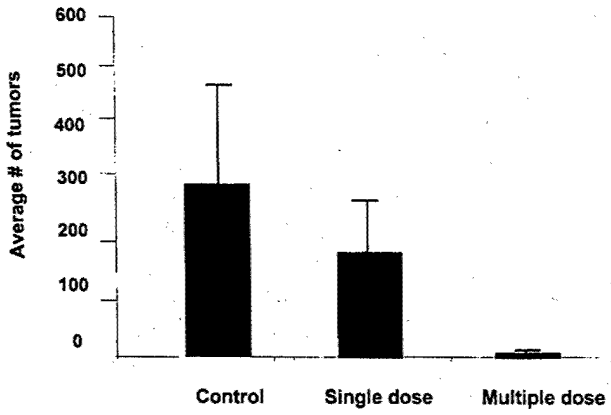

FIG. 9. Repeated intravenous injections of DOTAP:Chol–DNA complex increases therapeutic efficacy. UV2237m lung tumor-bearing C3H mice were divided into three groups ($n = 7$/group); one group was not treated, one received one dose of DOTAP:Chol–*p53* complex (50 μg DNA), and the third group received six daily doses of DOTAP:Chol–*p53* complex (50 μg DNA/dose). Lungs were harvested 2 weeks after the last treatment, and the tumor nodules were counted. Significantly ($P = 0.0006$) fewer tumors were observed in animals treated with six doses than in animals that were not treated or treated with one dose.

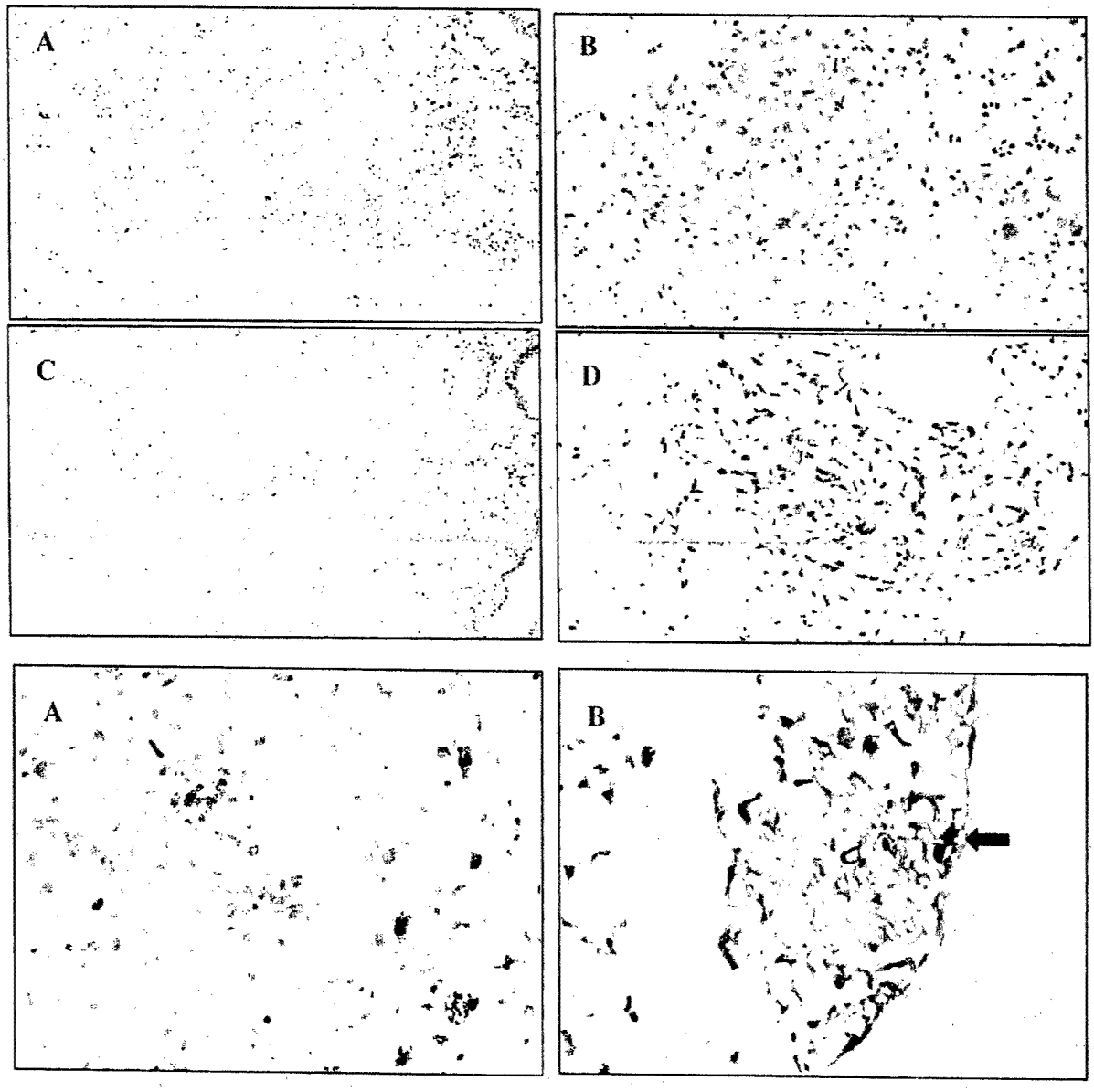

10

11

FIG. 10. Histopathologic analysis of A549 lung metastases treated with DOTAP:Chol–*p53* complex. Tumor viability, the mitotic index, and the number of tumors were analyzed histologically in tumor-bearing lungs from untreated control mice and from mice treated with DOTAP:Chol–*p53* complex. Many viable tumors with high mitotic indices were observed in untreated control mice (A, B), while few tumors with pyknotic nuclei were observed in animals treated with the DOTAP:Chol–*p53* complex (C, D) [magnification = ×100 (A, C) and ×250 (B, D)].

FIG. 11. Systemic treatment of A549 lung metastases with DOTAP:Chol–*p53* complex induces apoptosis. Apoptotic cell death in A549 lung tumors from mice untreated (A) or treated with the DOTAP:Chol–*p53* complex (B), as determined by TUNEL staining. Arrows indicate tumor cells undergoing apoptotic cell death (magnification ×250).

dissemination to other organs was not observed in animals in any of the four groups. In addition, treatment-associated toxic effects were not observed in animals in any of the four groups.

Discussion

Local-regional treatment of cancers by viral vector-mediated replacement with the *p53* tumor suppressor gene has shown success (2–4). However, the use of this strategy for the systemic treatment of disseminated diseases, such as cancers of the lung, breast, and colon, has been limited by the potential for vector-associated toxicity and the inability to efficiently deliver genes to the target. Recent studies demonstrated the ability of extruded DOTAP:Chol cationic liposomes to deliver genes efficiently to systemic sites with minimal vector-associated toxicity (7). In this study, we evaluated the ability of the extruded DOTAP:Chol liposome to deliver two tumor suppressor genes, *p53* and *FHIT*, and the efficacy of this treatment in primary

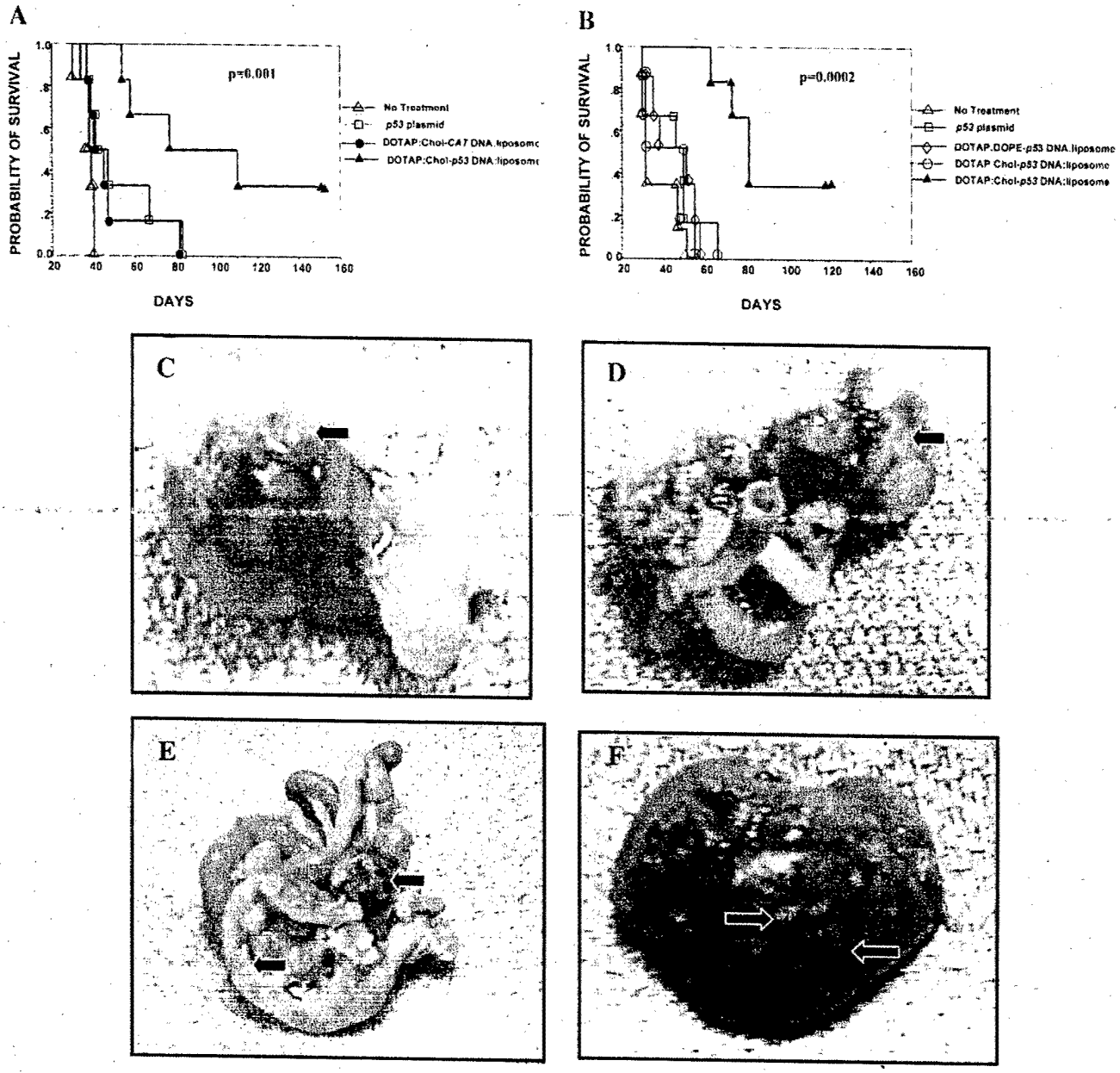

FIG. 13. Prolonged survival in H1299 lung tumor bearing mice treated with DOTAP:Chol–*p53* complex. Female SCID/Beige mice were injected with 10^6 H1299 tumor cells (six animals/group) via the tail vein. Groups were treated daily, as follows: no treatment (△), *p53* plasmid DNA (□), treatment with the DOTAP:Chol–*CAT* complex (●), DOTAP:DOPE–*p53* complex (◇), nonextruded DOTAP:Chol–*p53* complex (○), or DOTAP:Chol–*p53* complex (▲). Animals in each group received a total of six daily doses (50 μg/dose) and were monitored daily thereafter to assess morbidity and mortality. Animal survival was estimated by using the Kaplan–Meier and Wilcoxon signed-rank tests. Survival was significantly longer in H1299 lung tumor-bearing animals treated with the DOTAP:Chol–*p53* complex ($P = 0.001$) than in control animals that received either no treatment or treatment with *p53* plasmid DNA or DOTAP:Chol–*CAT* complex (A). It was also significantly longer ($P = 0.0002$) than in control animals treated with DOTAP:DOPE–*p53* complex or nonextruded DOTAP:Chol–*p53* complex (B). H1299 tumor-bearing animals receiving no treatment showed tumor dissemination to various organs and tissues, including the cervical lymph nodes (C), colon (D), mesentery (E), and liver (F). Arrows denote tumors.

and disseminated lung tumors of murine and human origin.

Before testing the therapeutic effect we determined the toxicity and transfection efficiency of the DOTAP:Chol–DNA complexes in subcutaneous tumors, normal lung, and experimental lung metastases. Liver enzyme profile and histopathologic analysis demonstrated no significant liposome–DNA complex mediated toxicity. A single intratumoral injection resulted in 25% of tumor cells expressing the transgene. The ability to deliver and mediate high levels of gene expression throughout solid tumors, albeit at lower levels than adenoviral vectors, following a single injection has not been previously demonstrated. Similarly the type of cells expressing the transgene in the lung has not been previously determined (7). Our study showed that the transgene was expressed primarily in the alveolar

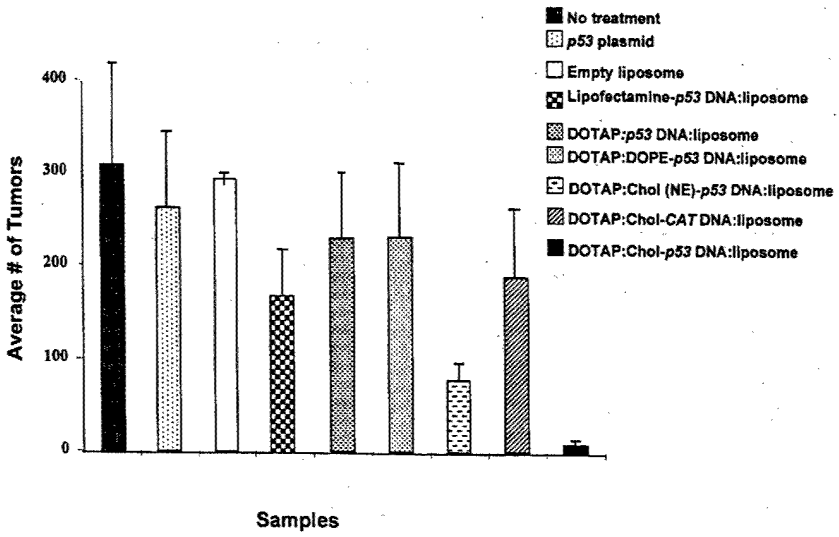

FIG. 12. Inhibition of murine UV2237m lung metastases following treatment with DOTAP:Chol–*p53* complex. UV2237m lung tumor-bearing C3H mice were either not treated or treated daily for a total of six doses (50 μg/dose) with *p53* plasmid DNA, empty liposome, lipofectamine–*p53* complex, DOTAP–*p53* complex, DOTAP:DOPE–*p53* complex, nonextruded DOTAP:Chol–*p53* complex, extruded DOTAP:Chol–*CAT* complex, or extruded DOTAP:Chol–*p53* complex. Each group comprised five animals. The number of tumor nodules was significantly lower ($P = 0.01$) in mice treated with six doses of extruded DOTAP:Chol–*p53* DNA:liposome complex than in the other groups. Bars denote standard errors.

epithelia of type II pneumocyte origin and endothelial cells. Few alveolar macrophages also expressed the transgene.

The ability of the injected DNA:liposome complexes to escape the reticuloendothelial system (RES) and be expressed in epithelial cells was surprising, since previous studies using a variety of formulations have demonstrated RES to be a major target for liposomes (24, 25). Therefore, we further assessed gene expression in alveolar macrophages of Balb/c mice (data not shown). The plasmid used in these experiments contained only a macrophage-specific promoter and enhancer to regulate *Lac-Z* expression. Intravenous tail vein injection of DOTAP:Chol–*Lac-Z* complex showed little or no *LacZ* expression in the lungs; low-level expression was detected infrequently and only at high doses (100 μg of DNA). Therefore, this formulation does not efficiently transfect macrophages in the lung (data not shown). The mechanism by which these DNA:liposome complexes escape the RES system is not well understood, and elucidation of the mechanism was beyond the scope of the present study.

Similarly, a single intravenous injection of a DNA:liposome complex into tumor bearing animals resulted in 10% of tumor cells per tumor expressing the transgene.

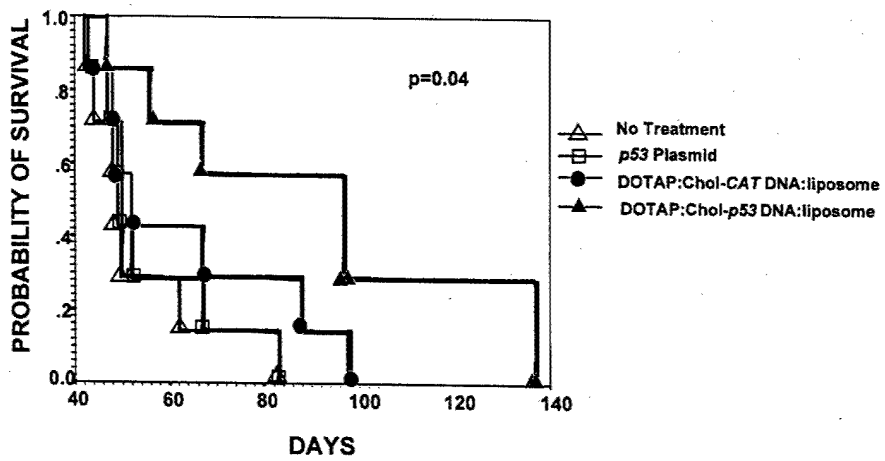

FIG. 14. Prolonged survival in A549 lung tumor bearing mice treated with DOTAP:Chol–*p53* complex. Female BALB/c *nu/nu* mice were injected with 10^6 A549 tumor cells (seven animals/group) via the tail vein. Groups were treated daily, as follows: no treatment (△), *p53* plasmid DNA (□), treatment with the DOTAP:Chol–*CAT* complex (●), or DOTAP:Chol–*p53* complex (▲). Animals in each group received a total of six daily doses (50 μg/dose) and were monitored daily thereafter to assess morbidity and mortality. Animal survival was estimated by using the Kaplan–Meier and Wilcoxon signed-rank tests. Survival was significantly longer ($P = 0.04$) in A549 lung tumor-bearing animals treated with the DOTAP:Chol–*p53* complex than in animals from control groups.

The reason for the discrepancy observed between the percent of tumor cells in the lung and in subcutaneous tumors expressing the transgene is not clear. It is possible that intratumoral injection leads to DNA uptake directly by the tumor cells while systemic delivery leads to DNA uptake through another mechanism, possibly leaky tumor vasculature. Whatever the underlying mechanism(s), the ability of the DNA:liposome complexes to escape the RES, extravasate through endothelial cell junctions, and be expressed in tumor cells is of clinical importance in the treatment of metastatic cancer.

We also determined the ability of these complexes to effectively deliver therapeutic genes and mediate tumoricidal effects in *vivo*. Treatment of subcutaneous tumors with DOTAP:Chol–*p53* or –*FHIT* DNA complexes resulted in tumor shrinkage and, in some cases, complete cures. The possibility that the observed tumoricidal effect was due simply to mechanical disruption or liposomal toxicity was eliminated by demonstrating transgene expression and induction of apoptosis in distinct regions of the tumors. Furthermore, treatment with empty liposomes and other conventional liposome:DNA complexes demonstrated no significant tumor inhibition (data not shown).

Although treatment of subcutaneous tumors with DOTAP:Chol–*FHIT* complex inhibited tumor growth in most cases, tumors in a few treated animals grew slowly but progressively. When treated with a second cycle of six doses, 3 weeks after the first cycle, however, tumors in 33% of these animals demonstrated complete regression, and have been tumor free for more than 9 months (data not shown). Despite the small sample number, these results indicate the feasibility of administering multiple treatments with no treatment resistance.

The ability of the extruded DOTAP:Chol DNA:liposome complexes to eliminate lung tumors when given intravenously was then compared with that of the nonextruded complexes. Repeated treatments with extruded DOTAP:Chol–*p53* complex significantly reduced the number of metastases, compared to nonextruded DOTAP:Chol–*p53*, suggesting that extrusion of DOTAP:Chol liposome is an important component for its function. The lack of resistance to repeated treatments observed in the present study was surprising, since resistance to repeated treatments and suppression of transgene expression has been documented previously (26, 27). One possibility is that experiments in the present study were primarily performed in immunodeficient animals. To further understand this, experiments were performed in syngeneic lung tumor-bearing C3H mice. Repeated multiple treatments resulted in a significantly greater gene expression than a single treatment. Furthermore, multiple treatments with DOTAP:Chol–*p53* yielded a significantly higher therapeutic efficacy in tumor-bearing animals than single treatment. The difference between the results observed in our study and those observed in other studies reflects the type of liposome used and its use in lung tumor bearing animal models. It is possible, as demonstrated by Lopez *et al.* (28), that the inflammatory response is suppressed in these tumor-bearing animals by tumor-derived factors that are not present in tumor-nonbearing animals, thereby allowing greater gene expression.

The ability of DOTAP:Chol–*CAT* complex and the conventional liposome: DNA complex (DOTAP:DOPE–*p53*) to show some tumor-inhibitory effects is not surprising and can be attributed to nonspecific antitumor activity as observed previously with the use of other cationic liposome:DNA complexes (29–31). To further differentiate the observed nonspecific antitumor activity from transgene-mediated specific antitumor activity, *in vivo* experiments were performed. Treatment of UV2237m lung tumors with DOTAP:Chol–*p53* complex resulted in a very significant tumor inhibition when compared to treatments with other cationic liposomes or nonextruded DOTAP:Chol liposomes. These results indicate that the observed tumor-inhibitory activity is mediated only in part by the transgene (*p53*, *FHIT*) and may be enhanced by the liposome: DNA mixture. Furthermore, histopathologic analysis revealed that DOTAP:Chol–*p53*-treated A549 tumors had been eliminated by apoptotic cell death in the few small tumors that had developed; this contrasts markedly with the relative lack of apoptotic cell death in the several large tumors showing numerous mitoses that developed in the lungs of control mice. Similar to previous observations (32, 33) the ability to eliminate A549 tumors *in vivo* demonstrates the efficiency of using exogenous wild-type *p*53 to suppress tumors with endogenous wild type *p*53. Similar reduction in the number of tumors when treated with DOTAP:Chol–*FHIT* complex, indicates that this effect is not restricted to a single tumor suppressor gene.

To further evaluate the effects of extruded liposomes on disseminated cancer, animal survival experiments were performed. Repeated treatments with DOTAP:Chol–*p53* complex significantly prolonged survival in H1299 or A549 lung tumor bearing mice. In particular 33% of the H1299 tumor-bearing animals were alive at the end of the experiment (150 days), suggesting that tumor cells at multiple metastatic sites were totally eliminated, since mice that died in these experiments all had widely disseminated metastases.

It is interesting that the degree of inhibition of tumor growth appeared to exceed the inhibition expected from the greater transfection efficiency of the improved liposomal vector. This effect has been attributed to p53 mediated bystander effects, and several mechanisms acting in concert are most likely responsible for the bystander effect (2, 3, 12, 34–40). The mechanism by which *FHIT* exerts its tumor suppressive effect is currently not known. Reintroduction of *FHIT* demonstrated upregulation of *p*53 and *p*27 in A549 cells and inhibition of tumor angiogenesis in both, 1299 and A549 lung tumors (unpublished observations). On the basis of these observations, we hypothesize that a bystander effect similar to that observed with *p53* might exist.

The most important observation from the study presented here is that extruded DOTAP:Chol liposome-mediated *p53* and *FHIT* gene delivery can suppress tumor

growth *in vivo* when administered locally and systemically and that this activity is associated with no toxic effects. Our studies further indicated that this extruded liposomal delivery system is restricted by neither gene nor tumor type. Of the greatest consequence are our data indicating that extruded DOTAP:Chol cationic liposome-based tumor gene therapy may be useful either alone or in combination with other therapeutic strategies in the treatment of human cancers *in vivo*.

ACKNOWLEDGMENTS

The authors thank Dr. Neely Atkinson (Department of Biomathematics, The University of Texas M. D. Anderson Cancer Center) and Kelly Willis Merriman for statistical analysis, Stacey Mott and Willie Virgil for technical assistance, and Monica Contreras for preparation of the manuscript. This work was supported in part by Public Health Service Grant P01CA78778-01A1 (J. A. Roth), by the Specialized Program of Research Excellence (SPORE) in Lung Cancer (P50-CA70907) (J. A. Roth), by the Texas Tobacco Settlement Fund, by The M. D. Anderson Cancer Center W. M. Keck Center for Cancer Gene Therapy, by Cancer Center Support (CORE) Grant CA 16672, and by a sponsored research agreement with Introgen Therapeutics, Inc.

REFERENCES

[1] Parker, S. L., Tong, T., Bolden, S., and Wingo, P. A. (1997) Cancer statistics, 1997. *CA Cancer J. Clin.* **47:** 5–27.

[2] Swisher, S. G., *et al.* (1999). Adenoviral-mediated *p53* gene transfer in advanced non-small cell lung cancer. *J. Natl. Cancer Inst.* **91:** 763–771.

[3] Roth, J. A., *et al.* (1996). Retrovirus-mediated wild-type *p53* gene transfer to tumors of patients with lung cancer. *Nat. Med.* **2:** 985–991.

[4] Clayman, G. L., *et al.* (1998). Adenovirus-mediated *p53* gene transfer in patients with advanced recurrent head and neck squamous cell carcinoma. *J. Clin. Oncol.* **16:** 2221–2232.

[5] Nabel, G. J., *et al.* (1993). Direct gene transfer with DNA–liposome complexes in melanoma—Expression, biologic activity, and lack of toxicity in humans. *Proc. Natl. Acad. Sci. USA* **90:** 11307–11311.

[6] Hung, M. C., Wang, S. C., and Hortobagyi, G. (1999). Targeting *HER-2/neu*-overexpressing cancer cells with transcriptional repressor genes delivered by cationic liposome. In *Non Viral Vectors for Gene Therapy* (L. Huang, M. C. Hung, and E. Wagner, Eds.), pp. 357–377. Academic Press, San Diego.

[7] Templeton, N. S., *et al.* (1997). Improved DNA:liposome complexes for increased systemic delivery and gene expression. *Nat. Biotechnol.* **15:** 647–652.

[8] Levine, A. J., Momand, J., and Finlay, C. A. (1991). The *p53* tumour suppressor gene. *Nature* **351:** 453–456.

[9] Mao, L. (1998). Tumor suppressor genes: Does *FHIT* fit? (Editorial Comment). *J. Natl. Cancer Inst.* **90:** 412–414.

[10] Lebeau, M. M., *et al.* (1998). A *FHIT* tumor suppressor gene. *Genes Chromosomes Cancer* **21:** 281–289.

[11] Minna, J. D., and Gazdar, A. F. (1996). Translational research comes of age [comment]. *Nat. Med.* **2:** 974–975.

[12] Cai, D. W., Mukhopadhyay, T., Liu, Y., Fujiwara, T., and Roth, J. A. (1993). Stable expression of the wild-type *p53* gene in human lung cancer cells after retrovirus-mediated gene transfer. *Hum. Gene Ther.* **4:** 617–624.

[13] Fujiwara, T., *et al.* (1993). A retroviral wild-type *p53* expression vector penetrates human lung cancer spheroids and inhibits growth by inducing apoptosis. *Cancer Res.* **53:** 4129–4133.

[14] Sard, L., *et al.* (1999). The tumor-suppressor gene *FHIT* is involved in the regulation of apoptosis and in cell cycle control. *Proc. Natl. Acad. Sci. USA* **96:** 8489–8492.

[15] Ji, L., *et al.* (1999). Induction of apoptosis and inhibition of tumorigenicity and tumor growth by adenovirus vector-mediated *FHIT* gene overexpression. *Cancer Res.* **59:** 3333–3339.

[16] Kanjilal, S., *et al.* (1993). High frequency of *p53* mutations in ultraviolet radiation-induced murine skin tumors: Evidence for strand bias and tumor heterogeneity. *Cancer Res.* **53:** 2961–2964.

[17] Gaensler, K. M. L., *et al.* (1999). Fetal gene transfer by transuterine injection of cationic liposome–DNA complexes. *Nat. Biotechnol.* **17:** 1188–1192.

[18] Couffinhal, T., *et al.* (1997). Histochemical staining following *LacZ* gene transfer underestimates transfection efficiency. *Hum. Gene Ther.* **8:** 929–934.

[19] Hamada, K., *et al.* (1996). Adenovirus-mediated transfer of a wild-type *p53* gene and induction of apoptosis in cervical cancer. *Cancer Res.* **56:** 3047–3054.

[20] Sozzi, G., *et al.* (1997). Absence of Fhit protein in primary lung tumors and cell lines with *FHIT* gene abnormalities. *Cancer Res.* **57:** 5207–5212.

[21] Georges, R. N., Mukhopadhyay, T., Zhang, Y., Yen, N., and Roth, J. A. (1993). Prevention of orthotopic human lung cancer growth by intratracheal instillation of a retroviral antisense K-*ras* construct. *Cancer Res.* **53:** 1743–1746.

[22] Kataoka, M., *et al.* (1998). An agent that increases tumor suppressor transgene product coupled with systemic transgene delivery inhibits growth of metastatic lung cancer *in vivo*. *Cancer Res.* **58:** 4761–4765.

[23] Fujiwara, T., *et al.* (1994) Induction of chemosensitivity in human lung cancer cells *in vivo* by adenoviral-mediated transfer of the wild-type *p53* gene. *Cancer Res.* **54:** 2287–2291.

[24] Liu, Y., *et al.* (1997). Factors influencing the efficiency of cationic liposome-mediated intravenous gene delivery. *Nat. Biotechnol.* **15:** 167–173.

[25] McLean, J. W., Thurston, G., and McDonald, D. M. (1999). Sites of uptake and expression of cationic liposome/DNA complexes injected intravenously. In *Non Viral Vectors for Gene Therapy* (L. Huang, M. C. Hung, and E. Wagner, Eds.), pp. 119–135. Academic Press, San Diego.

[26] Li, S., *et al.* (1999). Effect of immune response on gene transfer to the lung via systemic administration of cationic lipidic vectors. *Am. J. Physiol.* **276:** L796–L804.

[27] Song, Y. K., *et al.* (1997). Characterization of cationic liposome-mediated gene transfer *in vivo* by intravenous administration. *Hum. Gene Ther.* **8:** 1585–1594.

[28] Lopez, D. M., *et al.* (1996). Cytokine production by lymphoreticular cells from mammary tumor bearing mice: The role of tumor-derived factors. *Anticancer Res.* **16:** 3923–3930.

[29] Lesoonwood, L. A., Kim, W. H., Kleinman, H. K., Weintraub, B. D., and Mixson, A. J. (1995). Systemic gene therapy with *p53* reduces growth and metastases of a malignant human breast cancer in nude mice. *Hum. Gene Ther.* **6:** 395–405.

[30] Dow, S. W., *et al.* (1999). Lipid–DNA complexes induce potent activation of innate immune responses and antitumor activity when administered intravenously. *J. Immunol.* **163:** 1552–1561.

[31] Whitmore, M., *et al.* (1999). LPD lipopolyplex initiates a potent cytokine response and inhibits tumor growth. *Gene Ther.* **6:** 1867–1875.

[32] Cajot, J. F., *et al.* (1992). Growth suppression mediated by transfection of p53 in Hut292DM human lung cancer cells expressing endogenous wild-type *p53* protein. *Cancer Res.* **52:** 6956–6960.

[33] Hsiao, M., *et al.* (1997). Intracavitary liposome-mediated *p53* gene transfer into glioblastoma with endogenous wild-type *p53 in vivo* results in tumor suppression and long-term survival. *Biochem. Biophys. Res. Commun.* **233:** 359–364.

[34] Munshi, A., Ramesh, R., Marrogi, A., and Freeman, S. (1997). Evaluation of adenovirus *p53* mediated bystander effect *in vivo*. *Proc. Am. Assoc. Cancer Res.* **38:** 343. [abstract]

[35] Rizk, N., *et al.* (1996). Evaluation of the bystander effect in adeno virus mediated *p53* gene therapy. *Cancer Gene Ther.* **3:** 536. [abstract]

[36] Nishizaki, M., *et al.* (1999). Recombinant adenovirus expressing wild-type *p53* is antiangiogenic: A proposed mechanism for bystander effects. *Clin. Cancer Res.* **5:** 1015–1023.

[37] Dameron, K. M., Volpert, O. V., Tainsky, M. A., and Bouck, N. (1994). Control of angiogenesis in fibroblasts by p53 regulation of thrombospondin-1. *Science* **265:** 1582–1584.

[38] Bouvet, M., *et al.* (1998). Adenovirus-mediated wild-type *p53* gene transfer down-regulates vascular endothelial growth factor expression and inhibits angiogenesis in human colon cancer. *Cancer Res.* **58:** 2288–2292.

[39] Owen-Schaub, L. B., *et al.* (1995). Wild-type human *p53* and a temperature-sensitive mutant induce Fas/APO-1 expression. *Mol. Cell. Biol.* **15:** 3032–3040.

[40] Owen-Schaub, L. B., Cusack, J. C., Kruzel, E., Bucana, C. D., and Roth, J. A. (1998). Induction of Fas expression and sensitivity by adenoviral-mediated p53 gene transfer in a non-small cell lung carcinoma: Implications for gene therapy for lung cancer. *Proc. Am. Assoc. Cancer Res.* **39:** 78. [abstract]

[CANCER RESEARCH 62, 2715–2720, May 1, 2002]

Expression of Several Genes in the Human Chromosome 3p21.3 Homozygous Deletion Region by an Adenovirus Vector Results in Tumor Suppressor Activities *in Vitro* and *in Vivo*[1]

Lin Ji,[2] Masahiko Nishizaki, Boning Gao, David Burbee, Masashi Kondo, Craig Kamibayashi, Kai Xu, Nancy Yen, E. Neely Atkinson, Bingliang Fang, Michael I. Lerman, Jack A. Roth, and John D. Minna

Section of Thoracic Molecular Oncology, Departments of Thoracic and Cardiovascular Surgery [L. J., M. N., K. X., N. Y., B. F., J. A. R.] and Biomathematics [E. N. A.], The University of Texas M. D. Anderson Cancer Center, Houston, Texas 77030; Department of Internal Medicine and Pharmacology, Hamon Center for Therapeutic Oncology Research, University of Texas Southwestern Medical Center, Dallas, Texas 75390 [B. G., D. B., M. K., C. K., J. D. M.]; and Laboratory of Immunobiology, National Cancer Institute, Frederick Cancer Research and Development Center, Frederick, Maryland 21702 [M. I. L.]

ABSTRACT

A group of candidate tumor suppressor genes (designated *CACNA2D2, PL6, 101F6, NPRL2, BLU, RASSF1, FUS1, HYAL2,* and *HYAL1*) has been identified in a 120-kb critical tumor homozygous deletion region (found in lung and breast cancers) of human chromosome 3p21.3. We studied the effects of six of these 3p21.3 genes (*101F6, NPRL2, BLU, FUS1, HYAL2,* and *HYAL1*) on tumor cell proliferation and apoptosis in human lung cancer cells by recombinant adenovirus-mediated gene transfer *in vitro* and *in vivo*. We found that forced expression of wild-type *FUS1, 101F6,* and *NPRL2* genes significantly inhibited tumor cell growth by induction of apoptosis and alteration of cell cycle processes in 3p21.3 120-kb region-deficient (homozygous) H1299 and A549 cells but not in the 3p21.3 120-kb region-heterozygous H358 and the normal human bronchial epithelial cells. Intratumoral injection of Ad-101F6, Ad-FUS1, Ad-NPRL2, and Ad-HYAL2 vectors or systemic administration of protamine-complexed vectors significantly suppressed growth of H1299 and A549 tumor xenografts and inhibited A549 experimental lung metastases in *nu/nu* mice. Together, our results, coupled with other studies demonstrating a tumor suppressor role for the *RASSSF1A* isoform, suggest that multiple contiguous genes in the 3p21.3 120-kb chromosomal region may exhibit tumor suppressor activity *in vitro* and *in vivo*.

INTRODUCTION

Lung cancers develop after a multistage process involving a variety of genetic and epigenetic changes in dominant oncogenes and TSGs[3] (1, 2). Several of these changes can be found in smoking damaged respiratory epithelium in preneoplastic lesions, normal appearing epithelium, and in persons even before lung cancer develops (3–6). In these and related studies, allelic loss of chromosome region 3p (particularly 3p21.3) was found to be a frequent and early event in the development of several cancers, including lung and breast cancers (4–9). Several *3p* genes have been extensively studied and include *FHIT* at 3p14.2, *RARB* at 3p24, and *VHL* at 3p25 (summarize for lung cancer in Ref. 1). These results directed an intensive TSG search of the 3p21.3 region for one or more genes that could function as "gatekeepers" in the molecular pathogenesis of lung cancer, as well as several other human cancers.

Identification of nested 3p21.3 homozygous deletions in small cell lung cancers and a breast cancer line directed positional cloning efforts to a 630-kb region, which was narrowed subsequently to a 120-kb subregion by a breast cancer homozygous deletion (10, 11). This defined 3p21.3 region undergoes allele loss in ~80% of primary lung cancers and ~40% of preneoplastic or normal epithelial samples of smoking-damaged lung, marking it as one of the first sites to be involved (6). In addition, patients whose peripheral blood lymphocytes showed greater damage in this 3p21.3 region after *in vitro* treatment with the carcinogen benzo-a-pyrene diol epoxide had an increased risk of having lung cancer, suggesting the potential for genetic polymorphisms in this region predisposing to lung cancer development (12). The 630-kb region contains ≥25 genes, whereas 9 genes are located in or on the border of the 120-kb 3p21.3 region (10). This group of potential TSGs includes *CACNA2D2* (GenBank no. AF040709), *PL6* (U09584), *101F6* (AF040704), *NPRL2* (AF040707), *FUS1* (AF055479), *BLU* (U70880), *RASSF1* (AF040703, RASSF1C and AF102770, RASSF1A), *HYAL2* (U09577), and *HYAL1* (U03056). The *RASSF1A* isoform of the *RASSF1* gene has been studied extensively for promoter methylation in a variety of tumors, including lung and breast cancer, found to be frequently epigenetically inactivated in these tumors, and shows the ability to suppress lung cancer malignant growth (13, 14). The *FUS1* gene was also found to suppress the growth of NSCLCs *in vitro* (15). However, there have been no detailed tests comparing the activity of several of the genes in this small region or in testing their effect on lung cancer xenografts (local tumors or metastases) *in vivo*. At the start of the search for a 3p21.3 TSG, everyone expected that one gene would be found that frequently suffered mutations. However, from detailed studies of the genes in the region, that was not the case (10). In addition, the possibility of haploinsufficiency needed to be considered. Thus, it was important to further define the tumor suppressing capability of these genes both *in vitro* and *in vivo*. Such identification, which is the focus of the current report, would target the gene(s) for development as new tools for the early detection, monitoring of prevention efforts, prognosis, and therapy of lung and other cancers.

In this study, we used recombinant adenoviruses to introduce WT 3p21.3 genes into NSCLC tumor cell lines or tumor xenografts, where 3p21.3 120-kb region genes are either heterozygous or homozygous to characterize their potential tumor suppressing function *in vitro* and *in vivo*. We demonstrate that introduction of individual WT 3p21.3 genes by recombinant adenoviral vector-mediated transfer into lung cancer cells with loss of heterozygosity at the3p21.3 120-kb region inhibited tumor cell growth and induced apoptosis *in vitro*. Moreover, intratumoral injection of recombinant adenoviral vectors containing WT 3p21.3 genes significantly suppressed growth of human NSCLC xenografts, whereas systemic administration of protamine-complexed

Received 1/4/01; accepted 3/4/02.

The costs of publication of this article were defrayed in part by the payment of page charges. This article must therefore be hereby marked *advertisement* in accordance with 18 U.S.C. Section 1734 solely to indicate this fact.

[1] Supported in part by grants from the National Cancer Institute and the NIH SPORE (2P50-CA70970-04, to J. D. M. and J. A. R.; P01 CA78778-01A1, to J. A. R.; and CA71618, to J. D. M.), gifts to the Division of Surgery from Tenneco and Exxon for the Core Laboratory Facility, the UT M. D. Anderson Cancer Center Support Core Grant (CA 16672), a grant from the Tobacco Settlement Funds as appropriated by the Texas State Legislature (Project 8), a W. M. Keck Gene Therapy Career Development Grant (L. J.), and a sponsored research agreement with Introgen Therapeutics, Inc. (SR93-004-1).

[2] To whom requests for reprints should be addressed, at Department of Thoracic and Cardiovascular Surgery, Box 445, The University of Texas M. D. Anderson Cancer Center, 1515 Holcombe Boulevard, Houston, TX 77030. Phone: (713) 745-4530; Fax: (713) 794-4901; E-mail: lji@mail.mdanderson.org.

[3] The abbreviations used are: TSG, tumor suppressor gene; NSCLC, non-small cell lung cancer; TUNEL, terminal deoxynucleotidyl transferase-mediated nick end labeling; WT, wild type; HBEC, human bronchial epithelial cell; GFP, green fluorescence protein; pfu, plaque-forming unit(s); vp, viral particle; FACS, fluorescence-activated cell sorter; MOI, multiplicities of infection.

adenoviral vectors of 3p21.3 genes efficiently inhibited development of experimental metastases of lung cancer cells in xenograft mouse models. Together, our results strongly suggest that multiple contiguous genes in the 3p21.3 chromosomal region may function as TSGs *in vitro* and *in vivo*.

MATERIALS AND METHODS

Cell Lines and Cell Culture. Four human NSCLC cell lines with varied 3p21.3 and *p53* gene status, A549 (homozygous for multiple 3p21.3 region markers and WT *p53*), NCI-H1299 (homozygous for multiple 3p21.3 region markers and homozygous deletion of *p53*), NCI-H358 (retained heterozygosity of multiple 3p21.3 region markers and homozygous deletion of *p53*), and NCI-H460 (homozygous for multiple 3p21.3 region markers and WT *p53*), and a normal HBEC line, were used for *in vitro* and *in vivo* experiments. The multiple 3p21.3 polymorphic markers that were used for typing the lung cancer lines are located in the 630-kb homozygous deletion region in which the 120-kb region containing the six genes studied in this report reside and have been described previously (16). The homozygosity of multiple markers is consistent with loss of heterozygosity in this region. In this report, lung cancer cell lines with such homozygosity are referred to as "3p21.3-deficient" cells. The A549 line was maintained in Ham's F12 medium supplemented with 10% FCS. The H1299, H358, and H460 lines were maintained in RPMI 1640 supplemented with 10% FCS and 5% glutamine. Normal HBECs were obtained from Clonetics, Inc. (Walkersville, MD) and cultured in the medium supplied by the manufacturer according to the instructions provided.

Construction of Recombinant Ad-3p21.3 Gene Vectors. The recombinant Ad-3ps were constructed using our recently developed ligation-mediated plasmid adenovirus vector construction system, named herein pAd-RAP and pAd-RAP-Shuttle (detailed structures of plasmids will be provided on request). The 3p21.3 genes were assembled as a mammalian expression cassette that is driven by a cytomegalovirus promoter and tailed with Bovine Growth Hormone poly(A) signal sequence. The resulting Ad-3p vectors were named Ad-101F6, Ad-NPRL2, Ad-BLU, Ad-RASSF1C, Ad-FUS1, Ad-HYAL1, and Ad-HYAL2. Sequences of 3p21.3 genes in the viral vectors were confirmed by automated DNA sequencing. A vector expressing GFP gene (Ad-GFP), and a vector carrying the β-galactosidase gene *LacZ* (Ad-LacZ), were used to monitor efficiency of transduction by the viral vectors and as nonspecific transgene expression controls. Ad-EV, an E1-deleted empty vector, was used as a negative control. Ad-p53, a vector containing the WT *p53* gene, was used as a positive tumor suppressor control. Viral titers were determined by both absorbance measurement (*i.e.*, vp/ml) and plaque assay (*i.e.*, pfu/ml).

Cell Viability Assay. Inhibition of tumor cell growth by treatment with various Ad-3p vectors was analyzed by quantitatively determining cell viability using an improved 2,3-bis[2-methoxy-4-nitro-5-sulfophenyl]-2H-tetrazolium-5-carboxanilide inner salt (XTT) assay (Roche Molecular Biochemicals, Indianapolis, IN; Ref. 17) as described previously (18). Percentage of cell viability was calculated in terms of the absorbency of treated cells relative to the absorbency of untreated control cells. Experiments were repeated at least three times with quadruplicate samples for each treatment in each individual experiment.

Analysis of Apoptosis and Cell Cycle Kinetics. Induction of apoptosis in tumor cells treated by various Ad-3p vectors was analyzed by flow cytometry (FACS) using TUNEL reaction with FITC-labeled dUTP (Roche Molecular Biochemicals, Mannheim, Germany). Cells were processed for FACS analysis for apoptosis and cell cycle kinetics as described previously (19).

Animal Studies. All animals were maintained, and animal experiments were performed under NIH and institutional guidelines established for the Animal Core Facility at the University of Texas M. D. Anderson Cancer Center. Procedures for A549 and H1299 s.c. tumor inoculations in *nu/nu* mice were described previously (19). When average tumor size reaches ~0.5 cm in diameter, mice were injected intratumorally three times within a week with various Ad-3p and control vectors at a dose of 3×10^{10} pfu (3×10^{12} vp)/tumor in a volume of 0.2 ml. Differences in tumor volumes between treatment groups were analyzed with a mixed model ANOVA using the Statistica software (StatSoft, Inc., Tulsa, OK). A difference was considered to be statistically significant when $P < 0.05$.

An experimental A549 lung metastasis model was used to study the effects of 3p21.3 genes on development of metastases. Briefly, *nu/nu* mice were inoculated with A549 cells ($1–2 \times 10^6$) in 200 μl of PBS via tail vein injection. Pulmonary experimental metastatic tumor colonies were formed 7–10 days after inoculation. Then, protamine-complexed Ad-3p (P-Ad3p) vectors or control complexes were administered systemically to animals by i.v. injection for three times within a week at each a dose of $2–5 \times 10^{10}$ vp/200–500 μg of protamine in a total volume of 200 μl/animal. The P-Ad complexes are prepared by mixing an equal volume of the adenoviral vector (1×10^{10} vp) and the protamine sulfate (100 μg; Fujisawa USA, Inc., Deerfield, IL) in room temperature for 15 min and then bringing it to a total volume of 200 μl with PBS. Two weeks after the last injection, the animals were euthanized, and their lung metastatic tumors were stained with India ink. Tumor colonies on lung surfaces were counted under a dissecting microscope without knowledge of the treatment groups, and the lung tissues were sectioned for further pathologic and immunohistochemical analysis.

RESULTS

Effects of Forced Expression of 3p Genes on Tumor Cell Growth. To test the hypothesis that one or more of the 3p genes function as tumor suppressors *in vitro*, we performed a series of experiments to study the effects of expression of the 3p21.3 genes on cell proliferation in several types of Ad-3p-transduced human NSCLC and normal HBEC cells. Cells from each line were transduced *in vitro* by Ad-101F6, Ad-FUS1, Ad-NPRL2, Ad-BLU, Ad-RASSF1C, Ad-HYAL2, and Ad-HYAL1 vectors at various MOIs in units of vp/c; cells were also treated with PBS, Ad-EV, Ad-LacZ, or Ad-p53 as mock, negative, nonspecific, or positive controls, respectively. The ratio of vp/ml:pfu/ml in our adenoviral preparations is ~100:1. The transduction efficiency was determined by examining GFP-expressing cells in the Ad-GFP-transduced cell population under a fluorescence microscope and was found to be >80% at the highest MOI applied for each cell line.

Cell proliferation was analyzed by using the XTT assay to determine the number of viable cells at 1, 2, 3, and 5 days after transduction (only data for day 5 at various MOIs are shown; Fig. 1). In all cases, the viability of transduced cells was compared with that of untransduced (PBS treated) control cells (whose viability was set at 100%). As can be seen in Fig. 1, cell viability was reduced significantly in Ad-101F6-, Ad-Fus1-, and Ad-NPRL2-transduced A549 and H460 cells, which show homozygosity for multiple 3p21.3 markers and contain WT *p53*, and H1299 cells, which exhibit 3p21.3 homozygosity but also have a homozygous deletion of p53. A modest reduction of cell viability was shown in Ad-RASSF1C-transduced H1299 cells (data not shown). However, no significant effect on growth was observed in any of these cells transduced with Ad-HYAL1, Ad-HYAL2, Ad-BLU, Ad-EV, or Ad-LacZ. These results suggest that exogenous expression of some but not all WT 3p21.3 genes can inhibit 3p-deficient tumor cell growth *in vitro*.

To clarify the specificity of the observed inhibitory effects on tumor cell growth and examine the potential cytotoxicity of the exogenously expressed 3p21.3 genes on normal cells, we analyzed the effects of these 3p21.3 genes on cell proliferation in 3p21.3 heterozygous H358 cells and normal HBECs (Fig. 1). As shown in Fig. 1, HBECs transduced with all Ad-3p genes at MOIs that generated >80% transduction efficiency had reductions in cell number after 5 days of transduction of <10%, whereas H358 cells transduced with the same vectors had losses of <20% when compared with the untransduced control cells. Similar levels of losses of cell numbers were observed in H358 and HBEC cells transduced with control vectors Ad-EV and Ad-LacZ. As a positive control, H358 cells, which are homozygously deleted for *p53*, showed reduced cell numbers when transduced with the Ad-p53 vector. These results, coupled with the lack of effect with Ad-LacZ, Ad-HYAL2, Ad-HYAL1, Ad-RASSF1C, and Ad-BLU,

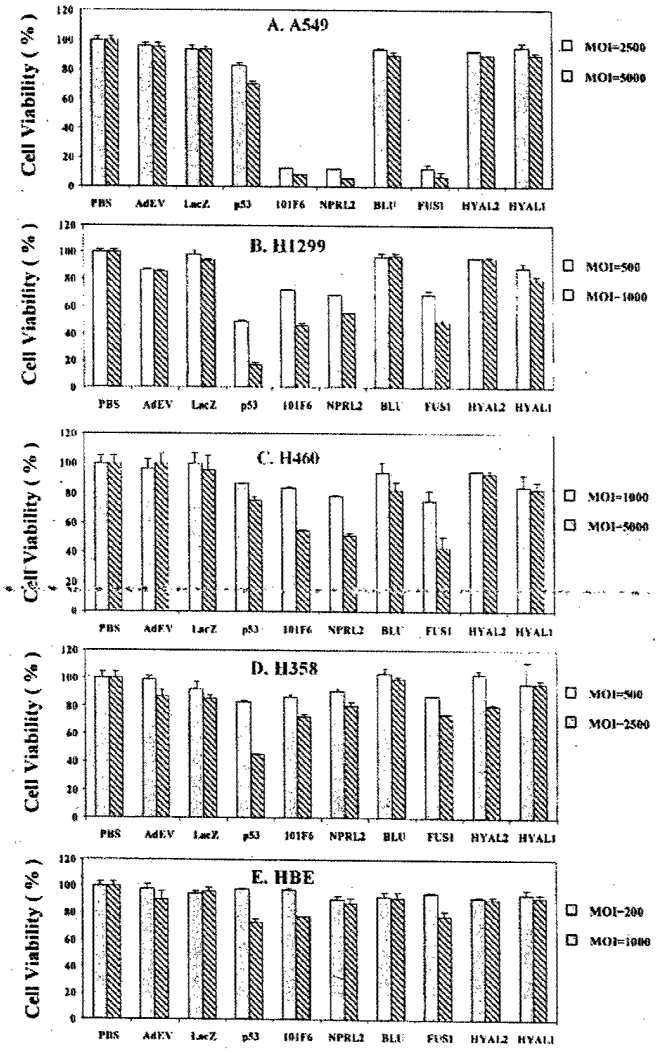

Fig. 1. Effects of exogenous expression of 3p21.3 genes on tumor cell growth in Ad-3p-transduced human lung cancer cells and normal bronchial epithelial cells. Cells were transduced with adenoviral vectors of 3p21.3 genes *101F6, NPRL2, BLU, FUS1, HAYL2,* and *HYAL1,* control genes *LacZ* and *p53,* and empty vector, Ad-EV, at various MOIs (vp/c) as indicated, and PBS alone was used as a mock control. The cell viability was expressed as the percentage of viable adenoviral vector-transduced cells in relation to PBS-treated control cells (100%). *Bars,* SDs of the mean in at least three individual experiments. Treatments were given in quadruplicate for each experiment. The significance of the difference in cell viability between vector-treated cells and the Ad-EV-, Ad-LacZ-, or PBS-treated controls was analyzed by two-sided Student's *t* test. $P < 0.05$ was taken as significant. The differences between the cell viability of the Ad-EV- and Ad-LacZ-transduced cells *versus* PBS-treated controls were not significant ($P = 0.25$–0.95 from different time points and cell lines). The differences between the cell viability of the Ad-101F6-, Ad-Fus1-, and Ad-NPRL2-transduced cells *versus* the Ad-EV- and Ad-LacZ-transduced or PBS-treated controls at the same MOI were significant in A549, H1299, and in H460 at both 3 and 5 days post-transduction ($P \leq 0.0001$–0.005) but not significant in H358 and HBEC cell lines at both 3 and 5 days post-transduction ($P \geq 0.10$–0.95, from different time points and cell lines), respectively. The effects of Ad-BLU, Ad-HYAL2, and Ad-HYAL1 on cell viability were not significant in all cell lines ($P > 0.45$), compared with those of Ad-EV and Ad-LacZ.

demonstrate the specificity of the tumor suppressing function of 3p21.3 genes *FUS1*, *NPRL2*, and *101F6* in 3p-deficient tumor cells and indicate that no generalized cytotoxicity was associated with exogenous expression of these WT 3p21.3 120-kb region genes.

Expression of 3p21.3 genes in Ad-3p-transduced H1299 and normal HBEC cells was verified by quantitative real-time reverse transcription-PCR. Known concentrations of human Raji total RNA and a TaqMan probe for *glyceraldehyde-3-phosphate dehydrogenase* cDNA were used to make a standard curve as an internal control. The increase in levels of transcripts of exogenously expressed 3p21.3 genes relative to those of endogenously expressed mRNAs in HBEC is ~10–15-, 30–50-, and 50–80-fold at an MOI of 100, 500, and 1000 vp/cell, respectively (data not shown). The levels of expression in transduced H1299 cells were similar to those in HBEC (data not shown). In addition, there was an association between increased levels of expression of these 3p21.3 genes and increased MOIs of the corresponding Ad-3p vectors transduced in both H1299 and HBEC cells. The expression of FUS1 and 101F6 proteins after transfection was detected by Western blot analysis using available polyclonal antibodies raised against the oligopeptides derived from their deduced amino acid sequences (data not shown).

Induction of Apoptosis by 3p Genes in Ad-3p-transduced Tumor Cells. The ability of exogenously expressed 3p21.3 genes to induce apoptosis in the Ad-3p-transduced H1299, A549, H460, H358, and HBEC cells was analyzed by FACS using the TUNEL reaction (Fig. 2). Induction of apoptosis was detected in Ad-101F6-, Ad-FUS1-, and Ad-NPRL2-transduced A549 (Fig. 2*A*), H1299 (Fig. 2*B*), and H460 (Fig. 2*C*) cells but not in H358 (Fig. 2*D*) and HBEC (Fig. 2*E*) cells. The apoptotic cell populations increased with increased duration of transduction; >15–20, 40–65, and 75% of cells were apoptotic 5 days after transduction with Ad-101F6, Ad-FUS1, and Ad-NPRL2 in the transduced H1299, A549, and H460 cells, respectively, whereas only ~7 and 10% of cells treated with PBS alone and transduced with Ad-EV vector, respectively, were TUNEL positive after the same time interval. The levels of apoptosis induction by Ad-101F6, Ad-FUS1, and Ad-NPRL2 were quantitatively greater in A549 and H460 cell lines with WT *p53* genes (Fig. 2, *A* and *C*) than that in H1299 cell line deleted for *p53* gene (Fig. 2*B*). Levels of apoptosis in A549 and H460 cells were comparable with those induced by Ad-p53 in *p53*-deficient H1299 and H358 cells (Fig. 2, *B* and *D*). However, no significant induction of apoptosis was observed in any tumor cell line transduced by Ad-BLU, Ad-RASSF1, Ad-HYAL2, and Ad-HYAL1 (Fig. 2). The levels and time of induction of apoptosis in cells transduced by these Ad-3p vectors correlated with those of reduction of cell numbers in cells treated with the same vectors (Fig. 1), suggesting that suppression of tumor cell growth by these 3p21.3 genes is mediated directly or indirectly through a mechanism of apoptosis.

Suppression of Tumor Growth by Intratumoral Injection of Ad-3p Vectors. To determine whether the observed inhibitory effects of these 3p21.3 genes on tumor cell proliferation *in vitro* could be demonstrated on tumor growth *in vivo,* we evaluated the efficacy of 3p21.3 genes in suppressing tumor growth by direct intratumoral injection of Ad-3p21.3 gene vectors, along with PBS and Ad-EV, Ad-LacZ, and Ad-p53 vectors as controls, into A549 or H1299 tumor xenografts in *nu/nu* mice (Fig. 3). The growth of tumors was recorded from the first injection until 23 days after the last injection. Tumor volumes were normalized by calculating the percentage increase in tumor volume after treatment relative to volume at the beginning of treatment in each group. In both A549 (Fig. 3*A*) and H1299 (Fig. 3*B*) tumor models, all of the tumors treated with Ad-101F6, Ad-FUS1, or Ad-NPRL2 showed significantly suppressed growth ($P < 0.001$), compared with mouse groups treated with Ad-LacZ or Ad-EV controls, whereas no significant effect was observed in Ad-HYAL1-, Ad-BLU (data not shown)-, and Ad-HYAL2 (data not shown)-treated tumors. Moreover, a significantly stronger inhibition of tumor growth was shown in A549 tumors treated with Ad-101F6 and Ad-NPRL2 vectors than in tumors treated with the Ad-p53 vector (Fig. 3*A*).

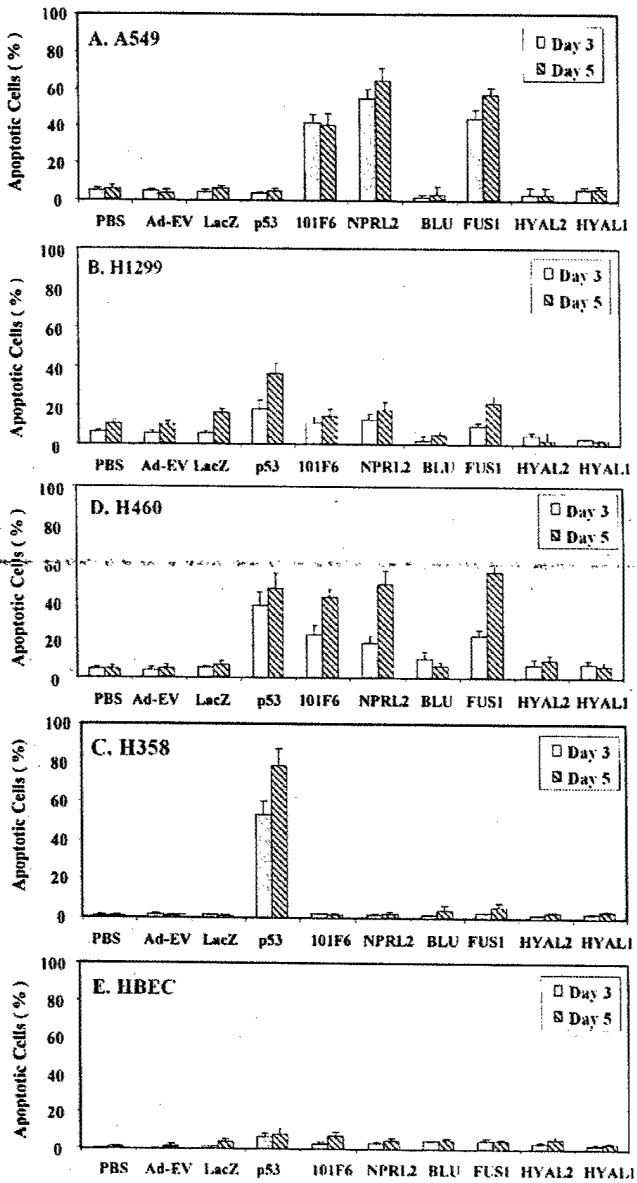

Fig. 2. Induction of apoptosis by exogenous expression of 3p21.3 genes in Ad-3p-transduced human NSCLC cells and normal HBECs. Apoptosis was analyzed by FACS, using TUNEL reaction with FITC-labeled dUTP. Cells were transduced with adenoviral vectors of 3p21.3 genes at an MOI (vp/c) of 5000 for A549 (*A*), 1000 for H1299 (*B*), 5000 for H460 (*C*), 2500 for H358 (*D*), and 1000 for HBEC (*E*), respectively, and PBS, Ad-EV, and p53 were used as controls. Cells were harvested and analyzed for apoptosis at the indicated days post-transduction. The rate of apoptosis is expressed as the percentage of FITC-labeled cells in the total cell population. *Bars,* SDs of the mean in two or three repeated experiments with triplicate treatments and TUNEL reactions for each experiment. The significance of the difference in apoptosis between vector-treated cells and the Ad-EV-, Ad-LacZ-, or PBS-treated controls was analyzed by two-sided Student's *t* test. $P < 0.05$ was considered significant. The differences between the apoptosis induced by the Ad-EV- and Ad-LacZ-transduced cells *versus* PBS-treated controls were not significant ($P = 0.925–0.675$ from different time points and cell lines). The differences between the apoptosis induced in the Ad-101F6-, Ad-FUS1-, and Ad-NPRL2-transduced cells *versus* the Ad-EV-, Ad-LacZ-, or PBS-treated controls were significant in A549 and H460 cells at both 3 and 5 days post-transduction ($P \leq 0.0001–0.005$) and significant *versus* the Ad-EV- and PBS-treated cells in H1299 at 5 days post-transduction ($P \leq 0.02$) but not significant in H358 and HBEC cell lines at both 3 and 5 days post-transduction at all time points ($P \geq 0.85–0.95$), respectively. Induction of apoptosis in Ad-p53-transduced H358 cells was significant at all time points compared with all other treatments ($P < 0.0001$). Induction of apoptosis in cells treated with Ad-BLU, Ad-HYAL2, and Ad-HYAL1 was not significant compared with those treated with PBS, Ad-EV, or Ad-LacZ, in all cell lines at all time points ($P > 0.85$).

Inhibition of Development of Experimental Lung Metastases by Protamine-Adenovirus Complex-mediated 3p21.3 Gene Transfer. A novel formulation using protamine/adenovirus complexes (designated P-Ad) for enhanced systemic delivery of recombinant adenovirus *in vivo* was developed to further explore the potential of 3p21.3 genes in suppressing systemic metastases. An experimental A549 metastatic human lung cancer model (established by i.v. injection of tumor cells) was used to study the effects of 3p21.3 gene transfer on the development of lung metastases in *nu/nu* mice (Fig. 4). The adenoviral 3p21.3 gene vectors were complexed to protamine and delivered via i.v. injection. The development of A549 pulmonary metastases was inhibited significantly, and the numbers of metastatic tumor colonies found on the surfaces of lungs from mice inoculated with A549 cells were reduced by >80% in animals treated with P-Ad-101F6, P-Ad-FUS1, P-Ad-NPRL2, or P-Ad-HYAL2 (70% reduction), compared with those in control treatment groups (Fig. 4). However, no significant reduction of metastatic colony formation was observed in animals treated with P-Ad-HYAL1 and P-Ad-BLU. These data are consistent with results obtained from Ad-3p-treated s.c. tumor xenografts, further supporting the roles of these 3p21.3 genes in suppression of tumor growth and inhibition of tumor progression *in vivo*. Finally, we noted no systemic toxicity to the mice given the systemic injection of PAd-3p complexes.

DISCUSSION

In this study, we used recombinant adenoviral vectors to introduce individual WT 3p21.3 genes into 3p-deficient tumor xenograft or tumor cell lines. The ectopic expression of WT 3p21.3 genes *101F6*, *FUS1*, and *NPRL2* effectively inhibited the growth of 3p-deficient NSCLC A549, H1299, and H460 cells *in vitro* but had no effect on the growth of H358 cells (which remains heterozygous for multiple polymorphic markers in the 3p21.3 650-kb homozygous deletion region) or on the growth of normal HBECs, suggesting the specificity of the exogenous WT 3p21.3 genes in inhibiting tumor cell growth. These findings also indicate the possibility that exogenous expression of 3p21.3 genes will be safe as cancer gene therapy agents because they caused no generalized cytotoxicity to normal cells or in mice treated systemically. The tumor suppressing effects of some TSGs under normal physiological conditions are generally mediated by increased levels of TSG expression in response to the oncogenic and environmental stimuli. These include *p53, WAF1, BAX,* and *BAK* (20), *e.g.,* expression of both endogenous WT *p53* gene and protein increased 6–8-fold after heat treatment of myeloblastic leukemia cells and DNA-binding activity of p53 increased >17-fold after γ-irradiation of human glioblastoma cells (21, 22). The level of 3p21.3 gene expression by the adenoviral vector-mediated 3p21.3 gene transfer in normal HBEC cells was increased ~10–15-fold (data not shown) and is close to the elevated levels of TSG expression induced by environmental stimuli under physiological conditions shown by that of p53.

In most cases, there is loss of heterozygosity at the 3p21.2 locus with no mutations detected in the remaining allele. However, haploinsufficiency can be associated with abrogation of tumor suppressor activity, *e.g.,* the *p27* gene is haploinsufficient for tumor suppression with tumor suppressor activity critically dependent on the absolute level of p27 protein expression (23). Elevated p27 expression inhibits cell cycle progression and promotes apoptosis in human glioma, colon, NSCLC, and mantle cell lymphoma, suggesting that p27 acts as a rheostat rather than as an on/off switch tumor suppressor in suppressing neoplasia (24). Similar to *p27,* some of the 3p21.3 genes are possibly inactivated by haploinsufficincy (10), and the modulation of protein expression may play an important role for their tumor suppressor activities. Furthermore, the overexpression of these 3p21.3

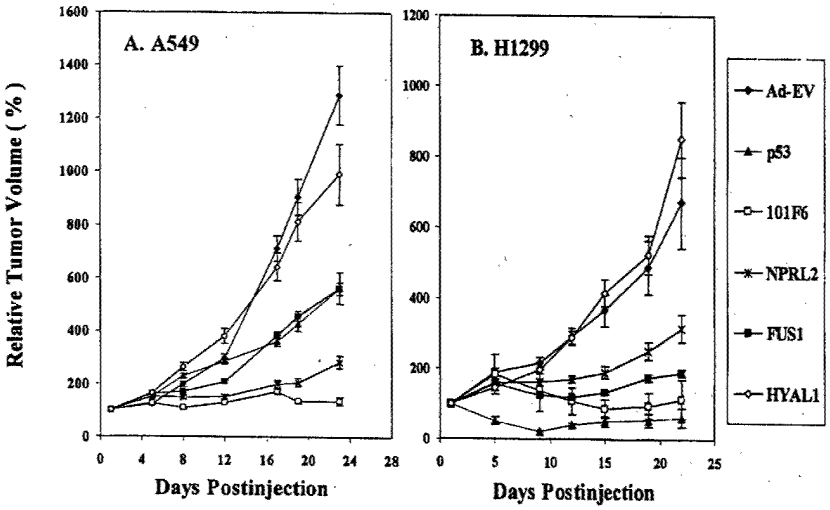

Fig. 3. Effects of intratumoral administration of adenoviral vectors of 3p21.3 genes on growth of human lung cancer A549 (*A*) and H1299 (*B*) s.c. tumors in *nu/nu* mice. When the tumor reached 5–10 mm in diameter at ~2 weeks after tumor inoculation, the tumor was injected with individual adenoviral vectors of 3p21.3 genes *101F6, NPRL2, FUS1,* and *HYAL1* or control vectors Ad-EV and p53, at a dose of 5×10^{10} vp/tumor each in 200 μl of PBS for three times within a week, respectively, and PBS alone was used as a mock control. Results were reported as the mean ± SD in 5–10 mice for each treatment group. Tumor volumes were normalized by the percentage increase of tumor sizes after treatment relative to those at the beginning of the treatment in each group. Mean tumor volumes ±SE from these experiments are shown. ANOVA was performed to determine statistical significance between each treatment group using Statistica software (StatSoft, Inc.), and $P \leq 0.05$ was considered significant. The differences of the tumor volumes in the Ad-101F6-, Ad-FUS1-, and Ad-NPRL2-treated mice *versus* in the Ad-EV-treated mouse controls were statistically significant in both A549 and H1299 tumor models ($P < 0.0001$) after 5 days from the last injection but not significant in Ad-HYAL1 ($P > 0.05$ in both A549 and H1299 tumor models).

genes at higher MOIs may be pharmaceutically appropriate for enhancing their function as cancer therapeutics and may be necessary for proper TSG function to overcome degradation pathways and inactive pathways in the cancer cell. The selectivity of the vectors with respect to growth inhibition and induction of the specific pathway of apoptosis in cancer compared with normal cells further supports their physiological role.

Inhibition of cell proliferation and induction of cell death by activated TSGs, such as *retinoblastoma* (*Rb*) and *p53,* are attributed primarily to these genes' ability to mediate cell cycle arrest and apoptosis (25–27). Because apoptosis is a genetically programmed cellular response to environmental stresses or stimuli, inactivation of TSGs involved in the apoptotic pathways could result in deregulated cell proliferation and tumorigenesis. To elucidate the mechanism governing the inhibition of NSCLC cell growth by 3p21.3 genes, we studied the effects of exogenously expressed 3p21.3 genes on apoptosis mediated by adenoviral vector transduction. Introduction of WT 3p21.3 genes *101F6, FUS1,* and *NPRL2* into the 3p-deficeint A549, H1299, and H460 cells induced apoptosis. However, this was not a generalized feature of 3p21.3 gene overexpression, as the *HYAL2, HYAL1,* and *BLU* genes from this same 120-kb region did not induce a significant increase in apoptosis in the same lung cancer cells. The time and the magnitude of the induction of apoptosis by these 3p21.3 genes were also well correlated with those of the inhibition of growth observed *in vitro*. These observations suggest that the tumor suppressing function mediated by the 3p21.3 genes is through induction of apoptosis.

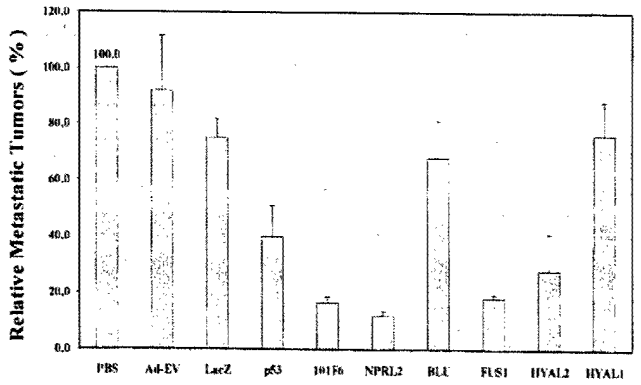

Fig. 4. Effect of systemic administration of protamine-Ad-3p complexes on development of A549 experimental lung metastases in *nu/nu* mice. All animals were i.v. injected with various protamine-adenoviral vector complexes every other 2 days for three times each at a dose of 3×10^{10} vp plus 300 μg of protamine in a total volume of 200 μl/animal, and PBS alone was used as a mock control. Each treatment group consisted of 5–10 animals. Lungs were harvested 2 weeks after the last injection, and metastastic colonies on the surfaces of lung were counted without knowledge of the treatment groups. Development of metastases was represented as the percentages of metastatic colonies formed in protamine-adenovirus complex-treated groups in relation to those in the PBS-treated group (as 100%). *Bars,* SE. Nonparametric *t* test (Wald-Wolfowitz Runs Test) was performed to determine statistical significance between each treatment group using Statistica software (StatSoft, Inc.), and $P \leq 0.05$ was considered significant. A significant inhibition of development of metastases was observed in mice treated with P-Ad-101F6 ($P = 0.002$), P-Ad-NPRL2 ($P = 0.001$), P-Ad-FUS1 ($P = 0.002$), and P-Ad-HYAL2 ($P = 0.014$), respectively, compared with mice treated with PBS, P-Ad-EV, or P-Ad-LacZ but no significant inhibition in mice treated with P-Ad-BLU ($P = 0.818$) or P-Ad-HYAL1 ($P = 0.904$).

To demonstrate whether the observed inhibitory effects of these 3p21.3 genes on tumor cell growth *in vitro* could be reproduced *in vivo,* we evaluated the efficacy of 3p21.3 genes in suppressing tumor growth by directly injecting Ad-3p vectors into A549 or H1299 tumor xenografts in *nu/nu* mice. Growth of both A549 and H1299 tumors was suppressed significantly by treatments with Ad-101F6, Ad-FUS1, and Ad-NPRL2. Furthermore, we explored the tumor suppressing potential of 3p21.3 genes in inhibiting experimental metastases *in vivo* by systemic administration of protamine-Ad-3p complexes. The novel protamine-Ad-3p complexes developed as part of this study allowed us to deliver 3p21.3 genes efficiently to the lung by systemic injection. The development of metastases was inhibited effectively by the protamine-adenovirus complex-mediated transfer of the *101F6, FUS1, HYAL2,* and *NPRL2* genes. These *in vivo* data are consistent with the *in vitro* data, further supporting the roles of 3p21.3 genes as TSGs.

Two of the 3p21.3 genes, *HYAL1* and *RASSF1C,* showed neither tumor suppressor activity *in vitro* nor *in vivo* nor apoptosis-inducing activity *in vitro* in all cell lines tested. Recently, one splicing isoform of one of the genes, *RASSF1A,* has been shown to undergo epigenetic inactivation by promoter region hypermethylation acquired in tumors. This isoform, but not the expressed *RASSF1C* isoform, also exhibits functional tumor suppressing activity. Consistent with these results, we also found no significant effects on growth of NSCLC cells and induction of apoptosis in these NSCLC cells *in vitro* and *in vivo* in our experiments using the Ad-RASSF1C vector (data not shown). The results with *RASSF1A* indicate that it will be important to study all of the genes in the region for loss of expression via tumor-acquired promoter hypermethylation. Alternatively, with 3p allele loss, haploinsufficiency of one or more of these 3p21.3 genes may play a role in tumorigenesis. On the basis of the evidence that multiple contiguous

3p21.3 genes, including *101F6, NPRL2, RASSF1A,* and *FUS1,* exhibited varied degrees of tumor suppressing activity, we propose that genes in this 3p21.3 120-kb region act together as part of a tumor suppressor region to suppress tumor growth through their functional activation of tumor suppressing pathways. Likewise, their inactivation may contribute directly to the development of cancer because of haploinsufficiency, loss of expression, or rarely mutations. In summary, we have demonstrated here for the first time that introduction of several WT 3p21.3 genes (*101F6, NPRL2,* and *FUS1*) contiguously located within a 120-kb region by recombinant adenoviral vector-mediated gene transfer into 3p-deficient tumor xenografts and tumor cell lines efficiently suppressed tumor cell growth and metastases and induced apoptosis *in vitro* and *in vivo*. These results suggest the role of these genes as TSGs. A better understanding of the biological function of genes in this region may result in the development of new strategies for the prevention, early detection, diagnosis, and treatment for lung cancer and other human cancers.

ACKNOWLEDGMENTS

The Minna's Lab thanks Eva Forgacs, Gena Mele, and Adrin Avila for assistance with this work and Dr. Yoshitaka Sekido for his invaluable assistance in identifying and characterizing the genes in this 3p21.3 region.

REFERENCES

1. Zochbauer-Muller, S., Gazdar, A. F., and Minna, J. D. Molecular pathogenesis of lung cancer. Ann. Rev. Physiol., *64:* 681–708, 2002.
2. Fong, K., Sekido, Y., and Minna, J. D. The molecular basis of lung carcinogenesis. *In:* W. B. Coleman and G. Tsongalis (eds.), The Molecular Basis of Human Cancer, pp. 379–405. Totowa, NJ: Humana Press, 2001.
3. Park, I. W., Wistuba, I. I., Maitra, A., Milchgrub, S., Virmani, A. K., Minna, J. D., and Gazdar, A. F. Multiple clonal abnormalities in the bronchial epithelium of patients with lung cancer. J. Natl. Cancer Inst. (Bethesda), *91:* 1863–1868, 1999.
4. Wistuba, I. I., Lam, S., Behrens, C., Virmani, A. K., Fong, K. M., LeRiche, J., Samet, J. M., Srivastava, S., Minna, J. D., and Gazdar, A. F. Molecular damage in the bronchial epithelium of current and former smokers. J. Natl. Cancer Inst. (Bethesda), *89:* 1366–1373, 1997.
5. Wistuba, I. I., Berry, J., Behrens, C., Maitra, A., Shivapurkar, N., Milchgrub, S., Mackay, B., Minna, J. D., and Gazdar, A. F. Molecular changes in the bronchial epithelium of patients with small cell lung cancer. Clin. Cancer Res., *6:* 2604–2610, 2000.
6. Wistuba, I. I., Behrens, C., Virmani, A. K., Mele, G., Milchgrub, S., Girard, L., Fondon, J. W., Garner, H. R., McKay, B., Latif, F., Lerman, M. I., Lam, S., Gazdar, A. F., and Minna, J. D. High resolution chromosome 3p allelotyping of human lung cancer and preneoplastic/preinvasive bronchial epithelium reveals multiple, discontinuous sites of 3p allele loss and three regions of frequent breakpoints. Cancer Res., *60:* 1949–1960, 2000.
7. Girard, L., Zochbauer-Muller, S., Virmani, A. K., Gazdar, A. F., and Minna, J. D. Genome-wide allelotyping of lung cancer identifies new regions of allelic loss, differences between small cell lung cancer and non-small cell lung cancer, and loci clustering. Cancer Res., *60:* 4894–4906, 2000.
8. Maitra, A., Wistuba, I. I., Washington, C., Virmani, A. K., Ashfaq, R., Milchgrub, S., Gazdar, A. F., and Minna, J. D. High-resolution chromosome 3p allelotyping of breast carcinomas and precursor lesions demonstrates frequent loss of heterozygosity and a discontinuous pattern of allele loss. Am. J. Pathol., *159:* 119–130, 2001.
9. Wistuba, I. I., Behrens, C., Milchgrub, S., Bryant, D., Hung, J., Minna, J. D., and Gazdar, A. F. Sequential molecular abnormalities are involved in the multistage development of squamous cell lung carcinoma. Oncogene, *18:* 643–650, 1999.
10. Lerman, M. I., and Minna, J. D. The 630-kb lung cancer homozygous deletion region on human chromosome 3p21.3: identification and evaluation of the resident candidate tumor suppressor genes. Cancer Res., *60:* 6116–6133, 2000.
11. Sekido, Y., Ahmadian, M., Wistuba, I. I., Latif, F., Bader, S., Wei, M. H., Duh, F. M., Gazdar, A. F., Lerman, M. I., and Minna, J. D. Cloning of a breast cancer homozygous deletion junction narrows the region of search for a 3p21.3 tumor suppressor gene. Oncogene, *16:* 3151–3157, 1998.
12. Wu, X., Zhao, Y., Honn, S. E., Tomlinson, G. E., Minna, J. D., Hong, W. K., and Spitz, M. R. Benzo[a]pyrene diol epoxide-induced 3p21.3 aberrations and genetic predisposition to lung cancer. Cancer Res., *58:* 1605–1608, 1998.
13. Burbee, D. G., Forgacs, E., Zochbauer-Muller, S., Shivakumar, L., Fong, K., Gao, B., Randle, D., Kondo, M., Virmani, A., Bader, S., Sekido, Y., Latif, F., Milchgrub, S., Toyooka, S., Gazdar, A. F., Lerman, M. I., Zabarovsky, E., White, M., and Minna, J. D. Epigenetic inactivation of RASSF1A in lung and breast cancers and malignant phenotype suppression. J. Natl. Cancer Inst. (Bethesda), *93:* 691–699, 2001.
14. Dammann, R., Li, C., Yoon, J. H., Chin, P. L., Bates, S., and Pfeifer, G. P. Epigenetic inactivation of a RAS association domain family protein from the lung tumour suppressor locus 3p21.3. Nat. Genet., *25:* 315–319, 2000.
15. Kondo, M., Ji, L., Kamibayashi, C., Tomizawa, Y., Randle, D., Sekido, Y., Yakota, J., Kashuba, V., Zabarovsky, E., Kuzmin, I., Lerman, M., Roth, J. A., and Minna, J. D. Overexpression of candidate tumor suppressor gene FUS1 isolated from the 3p21.3 homozygous deletion region leads to G1 arrest and growth inhibition of lung cancer cells. Oncogene, *20:* 6258–6262, 2001.
16. Fondon, J. W., Mele, G. M., Brezinschek, R. I., Cummings, D., Pande, A., Wren, J., O'Brien, K. M., Kupfer, K. C., Wei, M. H., Lerman, M., Minna, J. D., and Garner, H. R. Computerized polymorphic marker identification, experimental validation and a predicted human polymorphism catalog. Proc. Natl. Acad. Sci. USA, *95:* 7514–7519, 1998.
17. Roehm, N. W., Rodgers, G. H., Hatfield, S. M., and Glasebrook, A. L. An improved colorimetric assay for cell proliferation and viability utilizing the tetrazolium salt XTT. J. Immunol. Methods, *142:* 257–265, 1991.
18. Nishizaki M., Meyn R. E., Atkinson E. N., White R. A., Roth, J. A., and Ji, L. Synergistic inhibition of human lung cancer cell growth by adenovirus-mediated wild-type *p53* gene transfer in combination with docetaxel and radiation therapeutics *in vitro* and *in vivo*. Clin. Cancer Res., *7:* 2683–2689, 2001.
19. Ji, L., Fang, B., Yen, N., Fong, K., Minna, J. D., and Roth, J. A. Induction of apoptosis and inhibition of tumorigenicity and tumor growth by adenovirus vector-mediated fragile histidine triad (FHIT) gene overexpression. Cancer Res., *59:* 3333–3339, 1999.
20. Bishay, K., Ory, K., Lebeau, J., Levalois, C., Olivier, M. F., and Chevillard, S. DNA damage-related gene expression as biomarkers to assess cellular response after γ irradiation of a human lymphoblastoid cell line. Oncogene, *19:* 916–923, 2000.
21. Kastan, M. B., Radin, A. I., Kuerbitz, S. J., Onyekwere, O., Wolkow, C. A., Civin, C. I., Stone, K. D., Woo, T., Ravindranath, Y., and Craig, R. W. Levels of p53 protein increase with maturation in human hematopoietic cells. Cancer Res., *51:* 4279–4286, 1991.
22. Ohnishi, T., Wang, X., Ohnishi, K., Matsumoto, H., and Takahashi, A. p53-dependent induction of WAF1 by heat treatment in human glioblastoma cells. J. Biol. Chem., *271:* 14510–14513, 1996.
23. Fero, M. L., Randel, E., Gurley, K. E., Roberts, J. M., and Kemp, C. J. The murine gene *p27Kip1* is haplo-insufficient for tumour suppression. Nature (Lond.), *396:* 177–180, 1998.
24. Kemp, C. J., Sun, S., and Gurley, K. E. p53 induction and apoptosis in response to radio- and chemotherapy *in vivo* is tumor-type-dependent. Cancer Res., *61:* 327–332, 2001.
25. Evan, G., and Littlewood, T. A matter of life and cell death. Science (Wash. DC), *281:* 1317–1322, 1998.
26. Levine, A. J. p53, the cellular gatekeeper for growth and division. Cell, *88:* 323–331, 1997.
27. Vousden, K. H. p53: death star. Cell, *103:* 691–694, 2000.

Lack of PTEN Expression in Non-Small Cell Lung Cancer Could Be Related to Promoter Methylation[1]

Jean-Charles Soria,[2] Ho-Young Lee,[2] Janet I. Lee,[2] Luo Wang, Jean-Pierre Issa, Bonnie L. Kemp, Diane D. Liu, Jonathan M. Kurie, Li Mao, and Fadlo R. Khuri[3]

Departments of Thoracic/Head and Neck Medical Oncology [J-C. S., H-Y. L., J. I. L., L. W., J. M. K., L. M., F. R. K.], Leukemia [J-P. I.], Pathology [B. L. K.], and Biostatistics [D. D. L.], The University of Texas M. D. Anderson Cancer Center, Houston, Texas 77030

ABSTRACT

Purpose: **The *PTEN* gene at chromosome 10q23.3 is a tumor-suppressor gene that is inactivated in several types of human tumors. Although mutation and homozygous deletion are the most common mechanisms of *PTEN* inactivation, promoter methylation and translational modification can also account for *PTEN* silencing. The aim of this study was to investigate the expression of PTEN protein in primary non-small cell lung cancer (NSCLC) samples and to investigate the promoter methylation status of the gene in a panel of NSCLC cell lines as well as primary tumors.**

Experimental Design: **We analyzed PTEN expression by immunohistochemistry in tissue samples from 125 patients with early-stage NSCLC. We also evaluated *PTEN* promoter methylation status by methylation-specific PCR in 20 microdissected PTEN-negative primary tumors from among the last specimens as well as in a panel of 16 NSCLC cell lines. Western and Northern blotting were performed in the same panel of NSCLC cell lines.**

Results: **Thirty (24%) of the 125 specimens showed a lack of staining for PTEN. *PTEN* methylation was detected in 7 (35%) of the 20 PTEN-negative NSCLC samples and in none of the 10 PTEN-positive NSCLC samples that were microdissected. Furthermore, *PTEN* methylation was observed in 11 (69%) of the 16 NSCLC cell lines tested. *PTEN* mRNA expression was increased in the NCI-H1299 cell line by *in vitro* treatment with the demethylating agent 5-aza-2′-deoxycytidine. *PTEN* methylation was well correlated with PTEN expression in NSCLC cell lines by Western and Northern blot ($P = 0.025$).**

Conclusions: **Although genetic alterations of the *PTEN* gene are rare in NSCLC, loss of PTEN protein is not an uncommon event in early-stage NSCLC. Lack of PTEN expression may be partially explained by promoter methylation.**

INTRODUCTION

Lung cancer is the most common cause of cancer death worldwide, accounting for more deaths than those caused by prostate, breast, and colorectal cancers combined (1). The prognosis for patients with lung cancer is strongly correlated with disease stage at the time of diagnosis: patients with clinical stage I disease have a 5-year survival rate of about 60%, whereas in patients with clinical stage II-IV disease the 5-year survival rate ranges from 40% to less than 5% (2). Improving the survival rate of patients with this disease requires a better understanding of tumor biology and the subsequent development of novel therapeutic strategies.

PTEN/MMAC1/TEP1, located at 10q23.3, is a tumor-suppressor gene that encodes a cytoplasmic protein that has a protein tyrosine phosphatase domain and a domain extensively homologous to the cytoskeletal proteins tensin and auxilin (3). Germ-line mutations of *PTEN* are found in patients with Cowden syndrome, a familial syndrome associated with a predisposition for multiple benign hamartomas and malignant breast, skin, and thyroid neoplasms (3). Somatic mutation or deletion of *PTEN* has been reported in a variety of tumor types, including glioblastoma, melanoma, breast, prostate, renal, and endometrial carcinomas (4–9). Genetic analysis of *PTEN* in NSCLC[4] cancers has demonstrated alterations in *PTEN* in 8–16% of the examined NSCLC cell lines suggesting that *PTEN* is infrequently targeted in NSCLC tumorigenesis (10–13). Because alternative mechanisms such as promoter hypermethylation, alternative splicing of pre-mRNA, and posttranslational modification, may also inactivate gene function, the actual frequency of PTEN abnormalities in NSCLC may be underestimated. To date, few analyses of PTEN protein expression in NSCLC have been performed, and little is known about epigenetic or posttranslational mechanisms that could participate in *PTEN* inactivation.

Received 10/15/01; revised 2/25/02; accepted 2/26/02.

The costs of publication of this article were defrayed in part by the payment of page charges. This article must therefore be hereby marked *advertisement* in accordance with 18 U.S.C. Section 1734 solely to indicate this fact.

[1] Supported in part by Biology, Education, Screening, Chemoprevention, and Treatment (BESCT) Lung Cancer Program, Department of Defense Grant DAMD17-01-1-0689-1 [to F. R. K. (P. I.-Project 3) L. M. (P. I.-Project 1) and W. K. H., P. I.], Cancer Center Grant P30 CA 16620 (to M. D. Anderson Cancer Center), Tobacco Research Fund from State of Texas (to M. D. Anderson Cancer Center), Fondation de France, AP-HP, and Lilly Fondation Grant (to J-C. S).

[2] J-C. S., H-Y. L., and J. I. L. contributed equally to this work.

[3] To whom requests for reprints should be addressed, at Department of Thoracic/Head and Neck Medical Oncology, The University of Texas M. D. Anderson Cancer Center, 1515 Holcombe Boulevard, Houston, TX 77030. Phone: (713) 745-6363; Fax: (713) 796-8655; E-mail: fkhuri@mdanderson.org.

[4] The abbreviations used are: NSCLC, non-small cell lung cancer; PTEN, phosphatase and tensin homologue deleted on chromosome ten; TSA, trichostatin A; MSP, methylation-specific PCR; PIP-3, phosphatidylinositol-3,4,5-triphosphate; HBE, human bronchial epithelial (cells); GAPDH, glyceraldehyde-3-phosphate dehydrogenase; PI3K, phosphoinositol-3-kinase; PKB, protein kinase B.

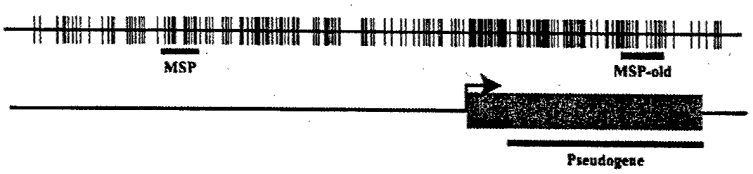

Fig. 1 Map of the PTEN promoter area. *Vertical bars on top*, CpG sites. *Gray box on the bottom*, exon 1; *arrow*, putative transcription start site. *Horizontal lines*, the areas of homology to the *PTEN* pseudogene, the location of the primers used in Salveson *et al.* (*MSP-old*; Ref. 28), and the location of the primers used in the current study (*MSP*). The area shown is 3454 bases long.

To determine PTEN expression in patients with NSCLC and to ascertain whether promoter methylation accounted in part for the loss of PTEN, we examined immunohistochemically the expression pattern of PTEN in 125 patients with early-stage NSCLC and evaluated promoter methylation status in 20 microdissected tumor samples as well as in a panel of 16 NSCLC cell lines.

MATERIALS AND METHODS

Clinical Samples and Immunohistochemical Staining for PTEN Protein. Surgical specimens were obtained from a total of 125 patients with early stages of lung cancer who underwent a surgical resection at the Department of Thoracic and Cardiovascular Surgery at The University of Texas M. D. Anderson Cancer Center. Paraffin-embedded, 4-μm-thick tissue sections from 125 primary tumors were stained for the PTEN protein using a primary rabbit polyclonal anti-PTEN antibody (Zymed Laboratories, San Francisco, CA), as reported previously (14). All of the sections were deparaffinized by using a series of xylene baths and then rehydrated using a graded alcohol series. To retrieve the antigenicity, the tissue sections were microwaved in 10 mM citrate buffer (pH 6.0) once for 2 min. The sections were then immersed in methanol containing 0.3% hydrogen peroxidase for 20 min to block endogenous peroxidase activity and then incubated in 2.5% blocking serum to reduce nonspecific binding. Sections were incubated overnight at 4°C with primary anti-PTEN antiserum (1:50). The sections were then processed using standard avidin-biotin immunohistochemical techniques according to the manufacturer's recommendations (Vector Laboratories, Burlingame, CA). Diaminobenzidine was used as a chromogen, and commercial hematoxylin was used for counterstaining. Adjacent normal-appearing epithelium within the tissue sections served as a positive internal control.

Representative areas of each tissue section were selected, and cells were counted in at least four fields (at ×200). On the basis of the results of the immunohistochemical staining, specimens were classified into three groups, as reported previously (6): increased or equal staining intensity compared with the corresponding normal tissue (++), decreased staining intensity (+), and absence of staining (−). All of the slides were evaluated and scored independently by two investigators (J. I. L. and J-C. S.) who were blinded to the clinical information pertaining to the subjects.

Cell Lines and Culture Conditions. Normal HBE cells were grown from bronchial epithelium that was harvested from fresh surgical specimens obtained from patients undergoing lobectomy procedures. The mucosal layer was sterilely stripped from bronchial specimens, cut into small pieces, and placed on a plastic tissue culture plate containing a thin layer of medium. For each experiment, normal HBE cells from a single patient were used. Normal HBE cells were grown in keratinocyte serum-free medium (Life Technologies, Inc. Grand Island, NY) on standard plastic ware (Falcon; Becton-Dickinson, Bedford, MA) at 37°C in a 5% CO_2 atmosphere. The NSCLC cell lines NCI-H1792, -H1299, -H661, -H596, -H591, -H460, -H441, -H358, -H322, -H292, -H226, and -H157, A549, Calu-6, Calu-1, and SK-MES-1 were routinely maintained in RPMI 1640 supplemented with 10% FCS. The NSCLC cell lines were obtained from the American Type Culture Collection (Manassas, VA). 5-Aza-2′deoxycytidine was added to the RPMI 1640 containing 2% serum.

Tissue Microdissection and Genomic DNA Extraction. Sections (4 μm thick) from formalin-fixed and paraffin-embedded tissue blocks were obtained. Tissue microdissection was performed manually under a stereomicroscope using a 25-gauge needle. Dissected tissues were digested in 200 μl of digestion buffer containing 50 mM Tris–HCl (pH 8.0), 1% SDS, and proteinase K (0.5 mg/ml) at 42°C for 36 h. The digested products were purified by extraction with phenol-chloroform twice. DNA was then precipitated by the ethanol precipitation method in the presence of glycogen (Roche Molecular Biochemicals, Indianapolis, IN) and recovered in distilled water.

MSP. Sample DNA (at least 100 ng) from the microdissected tumor specimens and from NSCLC cell lines, mixed with 1 μg of salmon sperm (Life Technologies, Inc., Gaithersburg, MD), were submitted to chemical modification following the protocol by Herman *et al.* (15). Briefly, DNA was denatured with 2 M NaOH, followed by treatment with 10 mM hydroquinone and 3 M sodium bisulfite (Sigma Chemical Co., St. Louis, MO). After purification in a Wizard SV Plus kit column (Promega, Madison, WI), the DNA was treated with 3 M NaOH and precipitated with three volumes of 100% ethanol, a one-third volume of 10 M NH_4OAc, and 2 μl of glycogen at −20°C. The precipitated DNA was washed with 70% ethanol and dissolved in distilled water. PCR was conducted with primers that were specific for either the methylated or the unmethylated versions of the *PTEN* gene: PTENM forward, 5′-gtttggggatttttttttcgc-3′, and PTENM reverse, 5′-AACCCTTCCTACGCCGCG-3′, for the methylated sequence; PTENU forward, 5′-TATTAGTTTGGGGATTTTTTTTTTGT-3′, and PTENU reverse, 5′-CCCAACCCTTCCTACACCACA-3′, for the unmethylated sequence. Primers location is shown in Fig. 1. The 12.5-μl total reaction volume contained 25 ng of modified DNA, 3% DMSO, all four deoxynucleoside triphosphates (each at 200 μM), 1.5 mM MgCl2, 0.4 μM PCR primers, and 0.625 units of HotStar Taq DNA polymerase (Qiagen, Valencia, CA). Water was substituted for DNA as a negative control, and NCI-H460 cell line

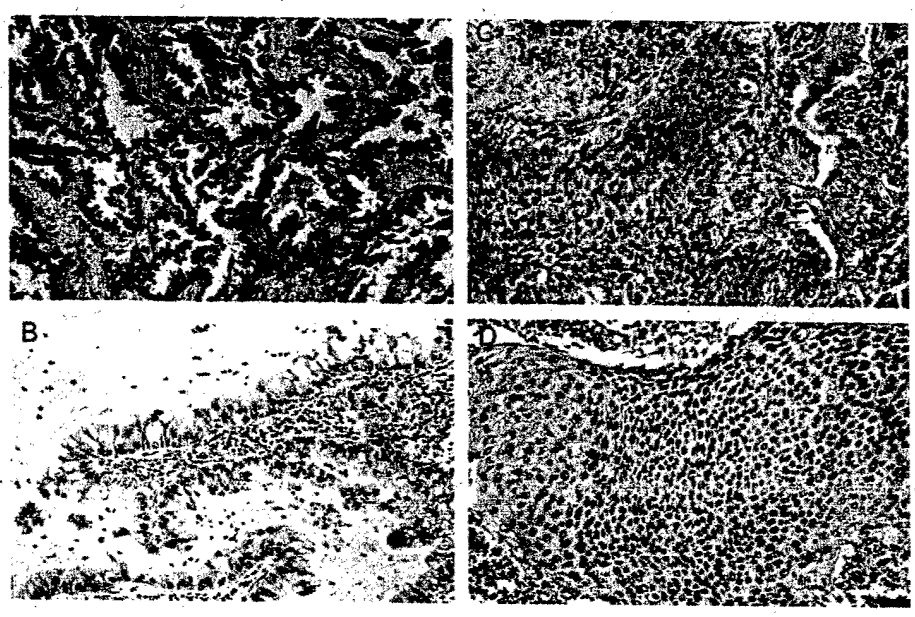

Fig. 2 Immunohistochemical staining patterns of PTEN in early-stage NSCLC. *A*, an adenocarcinoma with most cancer cells expressing PTEN in the cytoplasm. *B*, an adenocarcinoma tumor negative for PTEN expression. *C*, a squamous cell carcinoma tumor with diffuse and strong PTEN expression. *D*, a squamous cell carcinoma tumor with diffusely weak staining. The staining is prominent in the well-differentiated areas. (All panels, ×400).

DNA, treated with SssI Methylase (New England Biolabs, Beverly, MA), was used as a positive control. DNA was amplified by an initial cycle at 95°C for 15 min as required for enzyme activation, followed by 40 cycles of 94°C for 30 s, 60°C for 1 min, and 72°C for 1 min, and ending with a 5-min extension at 72°C in a thermocycler (Applied Biosystems, Foster City, CA). PCR products were separated on 2% agarose gels and visualized after staining with ethidium bromide.

Western Blot Analysis. Whole-cell lysates were prepared in lysis buffer [50 mM HEPES (pH 7.5), 150 mM NaCl, 1.5 mM $MgCl_2$, 1 mM EDTA, 0.2 mM EGTA, 1% NP40, 10% glycerol, 1 mM dithiothreitol, 1 mM phenylmethylsulfonyl fluoride, 20 mM sodium fluoride, 5 mM sodium orthovanadate, 10 mg/ml aprotinin, 10 mg/ml leupeptin, 2 mg/ml pepstatin, and 1 mM benzamidine]. Lysates were incubated for 20 min on ice and centrifugated at 13,000 × *g* for 20 min. The supernatants were collected, and the protein concentration was determined with a protein assay kit (Bio-Rad, Hercules, CA). Cell lysates were electrophoresed using SDS-PAGE and then transferred onto a BA-S-83-reinforced nitrocellulose membrane (Schleicher and Schuell, Inc., Keene, NH). Membranes were immunoblotted overnight at 4°C with a rabbit polyclonal antibody against human PTEN and a goat antibody against β-actin (Santa Cruz Biotechnology, Inc., Santa Cruz, CA) in Tris-buffered saline containing 5% nonfat dry milk. Antibody binding was detected using the ECL kit (Amersham, Inc., Arlington Heights, IL) according to the manufacturer's directions.

5-Aza-2′-deoxycytidine Treatment and Northern Blot Analysis. NCI-H1299 cells were transferred onto a 100-mm^3 dish and, 1 day later, 0.001, 0.01, 0.1, 1, or 5 μM 5-aza-2′-deoxycytidine or 0.001, 0.01, 0.1, 1, or 5 μM TSA were added in RPMI 1640 containing 2% FCS. Cells were changed to a new medium containing 5-aza-2′-deoxycytidine or TSA every day. After 6 days of treatment, the cells were lysed in 4.0 M guanidinium isothiocyanate, and total cellular RNA was extracted. RNA was subjected to electrophoresis (20 μg/lane) on a 1% agarose gel containing 2% formaldehyde, transferred to a Zeta-Probe membrane (Bio-Rad Laboratories), and hybridized to a [γ-^{32}P]dCTP-labeled PTEN or GAPDH probe as a control.

Statistical Analysis. Fisher's exact test or the χ^2 test was used to analyze the association between two categorical variables. All of the tests were two-sided. $P < 0.05$ was considered to be statistically significant.

RESULTS

The usual pattern of positive staining for PTEN in NSCLC was cytoplasmic and not nuclear (Fig. 2). Even when tumor cells were negative for PTEN staining, normal bronchial epithelial cells in the section were positive and were used as an internal positive control of the staining for PTEN. PTEN staining among the tumor specimens was either negative, diffusely weak, strong, or of a heterogeneous pattern of variable intensity. Among the heterogeneously stained specimens, staining was prominent in the well-differentiated areas (Fig. 2*D*). According to our scoring criteria, loss of PTEN expression (−) was noted in 30 (24%) of the 125 NSCLC specimens. Weak expression (+) was seen in 57 (46%) of the tumors, and strongly positive expression (++) was seen in 38 (30%) of the tumors. The frequency of PTEN expression did not differ significantly by tumor-node-metastasis stage, sex, smoking status, age, race, and histological subtype between the group with PTEN positive staining (+ or ++) and the group with PTEN negative staining (−; Table 1). Survival times were similar for patients with PTEN-negative tumors and with PTEN-positive tumors (P = 0.88, log rank test; data not shown).

To understand the mechanism explaining loss of PTEN expression in 24% of 125 NSCLC patients, we manually microdissected 20 randomly selected PTEN-negative slides along with 10 PTEN-positive slides. MSP was performed on genomic

Table 1 PTEN status in early-stage NSCLC tumor specimens from 125 patients according to clinicopathological features

Variable	No. of patients (n = 125)	PTEN expression		P
		Positive (n = 95)	Negative (n = 30)	
Age (yr) median (range)	63 (39–83)	64.5 (41–82)	64 (39–83)	0.73
Sex				
Male	93	70	23	0.81
Female	32	25	7	
Race				
White	110	84	26	0.75
Other	15	11	4	
Smoker				
Yes	107	87	20	0.5[a]
No	8	6	2	
Unknown	10	2	8	
Histology of tumors				
Squamous cell carcinoma	50	38	12	1
Adenocarcinoma and others	75	57	18	
TNM stage				
$T_1N_0M_0$	64	45	19	0.14
$T_2N_0M_0$	61	50	11	
5-yr overall survival rate (95% CI)	52.3% (44.2–61.9%)	53% (43.8–64.2%)	50% (35–71.5%)	

[a] P was calculated comparing smoking *versus* nonsmoking patients.

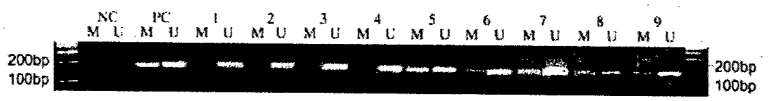

Fig. 3 PTEN promoter methylation status in PTEN-positive (*Lanes 1-4*) and PTEN-negative primary lung cancers (*Lanes 5–9*). *NC*, negative control; *PC*, positive control; *M*, amplified product with primers recognizing methylated sequence; *U*, amplified product with primers recognizing unmethylated sequence.

DNA extracted from those samples (Fig. 3). No methylation was found in the 10 PTEN-positive samples, whereas a methylated band was observed in 7 (35%) of the PTEN-negative samples. To further explore *PTEN* promoter methylation status, we evaluated a panel of 16 NSCLC cell lines. Overall, 11 (69%) of the 16 NSCLC cell lines displayed a methylated band (NCI-H1792, -H1299, -H661, -H441, -H358, -H322, -H292, -H157, Calu-6, Calu-1, and SK-MES-1). The following cell lines only displayed an unmethylated band: NCI-H226, -H460, -H591, -H596, and A549. The NSCLC cell line NCI-H1299 displayed a clear methylated band and had very low levels of *PTEN* mRNA, making it a suitable candidate for treatment with the demethylating agent 5-aza-2′-deoxycytidine. A net increase of *PTEN* mRNA was seen after treatment of NCI-H1299 cells with 5-aza-2′-deoxycytidine (Fig. 4) but not with TSA (data not shown), confirming the role of the 5′ region CpG methylation in regulating *PTEN* expression.

We further evaluated the correlation between *PTEN* promoter methylation status and PTEN expression by Western blot analysis in the same panel of 16 NSCLC cell lines. PTEN expression by Western blot in the NSCLC cell lines was either absent, weak, or strong (Fig. 5). Eleven cell lines displayed a methylated band: of these 11, 5 had a weak PTEN band, and 5 had no PTEN band detectable by Western blotting. Among the five cell lines without a methylated band by MSP, four had a strong PTEN band by Western blotting. The presence of a methylated band by MSP was statistically correlated with weak

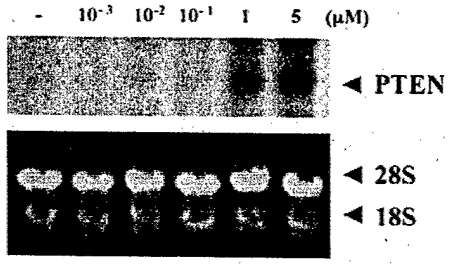

Fig. 4 Effect of 5-aza-2′deoxycytidine on PTEN expression. NCI-H1299 cells cultured *in vitro* were treated with 5-aza-2′deoxycytidine at concentrations of 0.001, 0.01, 0.1, 1, and 5 μM. Expression of PTEN was detected by Northern blot. A GAPDH probe was used as control for the integrity of RNA in all samples.

or absent PTEN expression by Western blotting (P = 0.025, Fisher's exact test; Fig. 6). Northern blotting further confirmed a low mRNA message in the NSCLC cell lines that had a methylated band and a weak or absent PTEN band by Western blot (Fig. 6).

DISCUSSION

The *PTEN* gene product dephosphorylates tyrosine and serine/threonine residues and exhibits phosphatase activities with both protein and lipid substrates (16, 17). The major

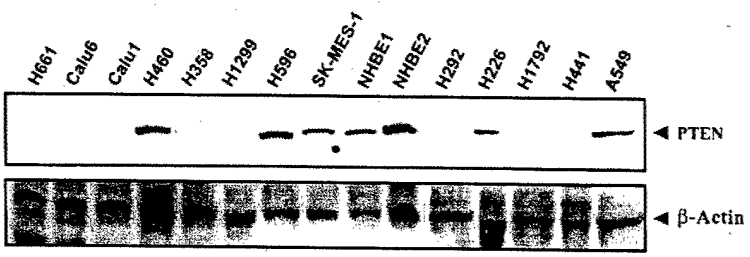

Fig. 5 PTEN expression evaluated by Western blot in a panel of NSCLC cell lines and in two normal HBE cells. A rabbit polyclonal antibody against human PTEN and a goat antibody against β-actin were used to probe the whole-cell extracts.

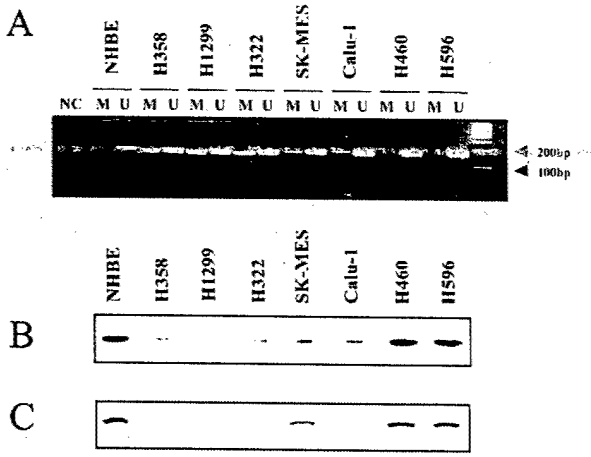

Fig. 6 PTEN promoter methylation was evaluated by MSP (*A*). NSCLC cell lines with a methylated band usually had a weak or absent PTEN band as shown by Western blot analysis (*B*). These same cell lines also displayed low levels of mRNA in Northern blots (*C*).

substrate of PTEN is PIP-3, a product of PI3K (18). The loss of PTEN function increases the concentration of PIP-3, which in turn leads to Akt hyperactivation, which suggests that the tumor-suppressor function of PTEN is exerted through the negative regulation of the PI3K/Akt cell survival pathway (3, 19, 20). The loss of PTEN expression results in increased Akt activity and continued cell survival and cell proliferation. In studied glioma, breast, and prostate cancer cell lines, *PTEN* has been shown to mediate G_1 cell cycle arrest and/or apoptosis through the suppression of the PI3K/Akt pathway (21). PTEN, therefore, seems to play an important role in modulating cell cycle progression and/or apoptosis. Although the protein phosphatase activity of PTEN is not considered to be as important as its lipid phosphatase activity for tumor suppression, the PTEN function as protein phosphatase has been implicated in the inhibition of cell migration and invasion via dephosphorylation of focal adhesion kinase (FAK), a molecule critical in the regulation of integrin signaling (22–24) and also in the inhibition of cell cycle progression (24).

Recently, frequent genetic alterations and loss of expression of the *PTEN* gene have been found in several malignant neoplasms (4–9). The studies of *PTEN* in NSCLC have focused exclusively on searching for mutations or deletions of the gene, with little emphasis on abnormalities at the protein level (10–13). In one study of NSCLC cell lines, homozygous deletions of *PTEN* were reported in 2 (8%) of 25 cell lines tested (10). Two subsequent studies, however, failed to demonstrate mutation of *PTEN* in the NSCLC samples studied, neither in cell lines nor in primary tumors (11, 13). Nevertheless, Forgacs *et al.* (12) described point mutations in 3 (16.7%) of 18 NSCLC cell lines analyzed (12). Using immunohistochemical analysis of 125 NSCLC patients, we showed that the rate of PTEN inactivation at the protein level is more frequent (24%) than that identified at the genetic level (0–16.7%). Interestingly, one previous study (25) that screened a wide variety of human neoplastic tissues, also reported PTEN protein loss in 25% of the NSCLC samples tested. We did not find any significant correlation between the loss of PTEN and clinicopathological characteristics in our NSCLC patients. Furthermore, no association was found between PTEN expression and survival. This is in contrast to the results of a recent report in which patients with breast cancer who lacked PTEN expression in their tumor had a shorter survival time (26). Tissue specificity or technical differences (*e.g.*, different antibody used for immunohistochemical evaluation) may account for these different results.

The loss of PTEN expression in 24% of 125 patients with early-stage NSCLC suggests that abrogation of PTEN function may occur through multiple mechanisms. Loss of PTEN expression may be explained by decreased protein synthesis, elevated protein degradation or turnover, or other posttranslational modifications. Another possible mechanism is the epigenetic inactivation of the gene through hypermethylation of the promoter region (27, 28). Indeed, inactivation of other tumor-suppressor genes by methylation has been previously reported in patients with NSCLC (29, 30). We found promoter methylation in 7 (35%) of 20 PTEN-negative microdissected tumors, whereas none of the 10 PTEN-positive microdissected tumors displayed a methylated band. In the 16 NSCLC cell lines, we found methylation in 69% of the cell lines tested. The higher percentage of methylation found in the lung cancer cell lines compared with primary tumors might be explained by additional changes acquired in culture or by the fact that the tumor cell lines were derived from more aggressive and more advanced tumors (stage III and IV). Furthermore DNA, quality and preservation in the sections from formalin-fixed and paraffin-embedded tissue blocks might not always be optimal. This could partially explain why only 35% of the PTEN-negative sections displayed a methylated band. Additional mechanisms (*e.g.*, posttranslational modifications) could also account for the lack of PTEN expression in some of the primary tumor samples

tested. It is noteworthy that our primer design for *PTEN* MSP differed from the one previously reported by Salvesen *et al.* (28). Indeed, through BLAST search, we have found extensive homology between the *PTEN* DNA region explored by Salvesen *et al.* (28) and the chromosome 9 duplication of the T-cell receptor β gene (AF029308), as well as with the highly conserved processed *PTEN* pseudogene (31). Therefore, we have designed primers to explore a CpG island, with no homology, located ~1.9 kb upstream from the region evaluated by Salvesen *et al.* (28). Fig. 1 represents the PTEN promoter area with the different CpG islands. It is not clear to date, which CpG island in the very large *PTEN* upstream regulatory region is best related to the gene expression. An additional fact that supports the importance of *PTEN* methylation in inactivating this gene is the efficacy of the demethylating agent 5-aza-2′-deoxycytidine in increasing *PTEN* mRNA in NCI-H1299 cell line. It is noteworthy that TSA treatment had no effect on *PTEN* expression, thus highlighting the specificity of the demethylating effect of 5-aza-2′-deoxycytidine. Taken together, these findings suggest that the methylation of *PTEN* may be an important mechanism for silencing this gene in NSCLC.

Our findings are in line with similar findings reported in endometrial cancer (28) and suspected in ovarian carcinomas and melanoma (16, 32). In fact, the loss of *PTEN* function in endometrial, breast, prostate, ovarian, and melanocytic tumors is more frequent than can be adequately explained by structural genomic changes alone (33). We believe that reports on *PTEN* methylation are few because proving an epigenetic mechanism of *PTEN* silencing is technically challenging. Indeed, one has to take into account the large size (>250 kb) of the *PTEN* upstream regulatory region, the existence of a highly conserved processed pseudogene with homology maintained up to 1 kb upstream from the translational start site, and technical challenges in linking epigenetic events with expression level (31, 33).

The elucidation of the mechanism that mediates the loss of PTEN expression has important clinical implications. The role of PI3K/Akt/PKB in apoptosis and survival, as well as the effects of dysregulation of the PI3K/Akt/PKB pathway in the pathogenesis of a large fraction of human cancer, has been identified (34–37). Because demethylating agents are under clinical evaluation, our finding may provide an advantage in therapeutic strategies, especially in the treatment of NSCLC, in which constitutive activation of Akt/PKB occurs at a high frequency (34).

In summary, we have demonstrated that the loss of PTEN is not a rare event in NSCLC, although genetic alterations of the *PTEN* gene are rare in this setting. The lack of PTEN expression may be partially explained by promoter methylation. We found methylation of *PTEN* in 35% of the primary tumors and in 69% of the NSCLC cell lines tested. Moreover, we were able to show that methylation of this gene is reversible with 5-aza-2′-deoxycytidine. Our findings of a frequent acquired tumor-related epigenetic alteration favor the candidacy of *PTEN* as a tumor suppressor gene also subject to methylation in addition to point mutations and homozygous deletions.

REFERENCES

1. Greenlee, R. T., Hill-Harmon, B. B., Murray, T., and Thun, M. Cancer statistics, 2001. CA Cancer J. Clin., *51:* 16–36, 2001.

2. Mountain, C. T. Revision in the international system for staging of lung cancer. Chest, *111:* 1710–1717, 1997.

3. Di Cristofano, A. D., and Pandolfi, P. P. The multiple roles of PTEN in tumor suppression. Cell, *100:* 387–390, 2000.

4. Duerr, E. M., Rollbrocker, B., Hayashi, Y., Peters, N., Meyer-Puttlitz, B., Louis, D. N., Schramm, J., Wiestler, O. D., Parsons, R., Eng, C., and von Deimling, A. PTEN mutations in gliomas and glioneuronal tumors. Oncogene, *16:* 2259–2264, 1998.

5. Tsao, H. S., Zhang, X., Benoit, E., and Haluska, F. G. Identification of PTEN/MMAC 1 alterations in uncultured melanomas and melanoma cell lines. Oncogene, *16:* 3397–3402, 1998.

6. Perren, A., Weng, L-P., Boag, A. H., Ziebold, U., Thakore, K., Dahia, P. L., Komminoth, P., Lees, J. A., Mulligan, L. M., Mutter, G. L., and Eng, C. Immunohistochemical evidence of loss of PTEN expression in primary ductal adenocarcinomas of the breast. Am. J. Pathol., *155:* 1254–1260, 1999.

7. Cairns, P., Okami, K., Halachmi, S., Halachmi, N., Esteller, M., Herman, J. G., Jen, J., Isaacs, W. B., Bova, G. S., and Sidransky, D. Frequent inactivation of PTEN/MMAC1 in primary prostate cancer. Cancer Res., *57:* 4997–5000, 1997.

8. Mutter, G. L., Lin, M-C., Fitzgerald, J. T., Kum, J. B., Baak, J. P., Lees, J. A., Weng, L. P., and Eng, C. Altered PTEN expression as a diagnostic marker for the earliest endometrial precancers. J. Natl. Cancer Inst. (Bethesda), *92:* 924–930, 2000.

9. Kondo, K., Yao, M., Kobayashi, K., Ota, S., Yoshida, M., Kaneko, S., Baba, M., Sakai, N., Kishida, T., Kawakami, S., Uemura, H., Nagashima, Y., Nakatani, Y., and Hosaka, M. PTEN/MMAC1/TEP1 mutations in human primary renal-cell carcinomas and renal carcinoma cell lines. Int. J. Cancer, *91:* 219–224, 2001.

10. Kohno, T., Takahashi, M., Manda, R., and Yokota, J. Inactivation of the *PTEN/MMAC1/TEP1* gene in human lung cancers. Genes Chromosomes Cancer, *22:* 152–156, 1998.

11. Yokomizo, A., Tindall, D. J., Drabkin, H., Gemmill, R., Franklin, W., Yang, P., Sugio, K., Smith, D. I., and Liu, W. PTEN/MMAC1 mutations identified in small cell, but not in non-small cell lung cancers. Oncogene, *17:* 475–479, 1998.

12. Forgacs, E., Biesterveld, E. J., Sekido, Y., Fong, K., Muneer, S., Wistuba, I. I., Milchgrub, S., Brezinschek, R., Virmani, A., Gazdar, A. F., and Minna, J. D. Mutation analysis of the *PTEN/MMAC1* gene in lung cancer. Oncogene, *17:* 1557–1565, 1998.

13. Hosoya, Y., Gemma, A., Seike, M., Kurimoto, F., Uematsu, K., Hibino, S., Yoshimura, A., Shibuya, M., and Kudoh S. Alteration of the *PTEN/MMAC1* gene locus in primary lung cancer with distant metastasis. Lung Cancer, *25:* 87–93, 1999.

14. Lee, J. I., Soria, J. C., Hassan, K. A., El-Naggar, A. K., Tang, X., Liu, D. D., Hong, W. K., and Mao, L. Loss of PTEN expression as a prognostic marker for tongue cancer. Arch. Otolaryngol. Head Neck Surg., *127:* 144–145, 2001.

15. Herman, J. G., Graff, J. R., Myohanen, S., Hamilton, S. R., Nelkin, B. D., and Baylin, S. B. Methylation-specific PCR. A novel PCR assay for methylation status of CpG islands. Proc. Natl. Acad. Sci. USA, *93:* 9821–9826, 1996.

16. Ali, I. U., Schriml, L. M., and Dean, M. Mutational spectra of PTEN/MMAC1: a tumor suppressor with lipid phosphatase activity. J. Natl. Cancer Inst. (Bethesda), *91:* 1922–1932, 1999.

17. Li, D. M., and Sun, H. TEP1, encoded by a candidate tumor suppressor locus, is a novel protein tyrosine phosphatase regulated by transforming growth factor β. Cancer Res., *57:* 2124–2129, 1997.

18. Myers, M. P., Pass, I., Batty, I. H., Van der Kaay, J., Stolarov, J. P., Hemmings, B. A., Wigler, M. H., Downes, C. P., and Tonks, N. K. The lipid phosphatase activity of PTEN is critical for its tumor suppressor function. Proc. Natl. Acad. Sci. USA, *95:* 13513–13518, 1998.

19. Furnari, F. B., Huang, H. J., and Cavenee, W. K. The phosphoinositol phosphatase activity of PTEN mediates a serum-sensitive G_1 growth arrest in glioma cells. Cancer Res., *58:* 5002–5008, 1998.

20. Stambolic, V., Suzuki, A., de la Pompa, J. L., Brothers, G. M., Mirtsos, C., Sasaki, T., Ruland, J., Penninger, J. M., Siderovski, D. P., and Mak, T. W. Negative regulation of PKB/Akt-dependent cell survival by the tumor suppressor PTEN. Cell, *95:* 29–39, 1998.

21. Lu, Y., Lin, Y. Z., LaPushin, R., Cuevas, B., Fang, X., Yu, S. X., Davies, M. A., Khan, H., Furui, T., Mao, M., Zinner, R., Hung, M. C., Steck, P., Siminovitch, K., and Mills, G. B. The *PTEN/MMAC1/TEP* tumor suppressor gene decreases cell growth and induces apoptosis and anoikis in breast cancer cells. Oncogene, *18:* 7034–7035, 1999.

22. Tamura, M., Gu, J., Matsumoto, K., Aota, S., Parsons, R., and Yamada, K. M. Inhibition of cell migration, spreading, and focal adhesions by tumor suppressor PTEN. Science (Wash. DC), *280:* 1614–1617, 1998.

23. Tamura, M., Gu, J., Takino, T., and Yamada, K. M. Tumor suppressor PTEN inhibition of cell invasion, migration, and growth: differential involvement of focal adhesion kinase and p130Cas. Cancer Res., *59:* 442–449, 1999.

24. Tamura, M., Gu, J., Danen, E. H., Takino, T., Miyamoto, S., and Yamada, K. M. PTEN interactions with focal adhesion kinase and suppression of the extracellular matrix-dependent phosphatidylinositol 3-kinase/Akt cell survival pathway. J. Biol. Chem., *274:* 20693–20703, 1999.

25. Torres, J., Navarro, S., Rogla, I., Ripoll, F., Lluch, A., Garcia-Conde, J., Llombart-Bosch, A., Cervera, J., and Pulido, R. Heterogeneous lack of expression of the tumour suppressor PTEN protein in human neoplastic tissues. Eur. J. Cancer, *37:* 114–121, 2001.

26. Depowski, P. L., Rosenthal, S. I., and Ross, J. S. Loss of expression of the *pten* gene protein product is associated with poor outcome in breast cancer. Mod. Pathol., *14:* 672–676, 2001.

27. Whang, Y. E., Wu, X., Suzuki, H., Reiter, R. E., Tran, C., Vessella, R. L., Said, J. W., Isaacs, W. B., and Sawyers, C. L. Inactivation of the tumor suppressor PTEN/MMAC1 in advanced human prostate cancer through loss of expression. Proc. Natl. Acad. Sci. USA, *95:* 5246–5250, 1998.

28. Salvesen, H. B., MacDonald, N., Ryan, A., Jacobs, I. J., Lynch, E. D., Akslen, L. A., and Das, S. PTEN methylation is associated with advanced stage and microsatellite instability in endometrial carcinoma. Int. J. Cancer, *91:* 22–26, 2001.

29. Belinsky, S. A., Nikula, K. J., Palmisano, W. A., Michels, R., Saccomano, G., Gabrielson, E., Baylin, S. B., and Herman, J. G. Aberrant methylation of $p16^{ink4a}$ is an early event in lung cancer and a potential biomarker for early diagnosis. Proc. Natl. Acad. Sci. USA, *95:* 11891–11896, 1998.

30. Zochbauer-Muller, S., Fong, K. M., Virmani, A. K., Geradts, J., Gazdar, A. F., and Minna, J. D. Aberrant promoter methylation of multiple genes in non-small cell lung cancers. Cancer Res., *61:* 249–255, 2001.

31. Dahia, P. L., FitzGerald, M. G., Zhang, X., Marsh, D. J., Zheng, Z., Pietsch, T., von Deimling, A., Haluska, F. G., Haber, D. A., and Eng, C. A highly conserved processed *PTEN* pseudogene is located on chromosome band 9p21. Oncogene, *16:* 2403–2406, 1998.

32. Kurose, K., Zhou, X. P., Araki, T., Cannistra, S. A., Maher, E. R., and Eng, C. Frequent loss of PTEN expression is linked to elevated phosphorylated Akt levels, but not associated with p27 and cyclin D1 expression, in primary epithelial ovarian carcinomas. Am. J. Pathol., *158:* 2097–2106, 2001.

33. Mutter, G. L. PTEN, a protean tumor suppressor. Am. J. Pathol., *158:* 1895–1898, 2001.

34. Brognard, J., Clark, A. S., Ni, Y., and Dennis P. A. Akt/protein kinase B is constitutively active in non-small cell lung cancer cells and promotes cellular survival and resistance to chemotherapy and radiation. Cancer Res., *61:* 3986–3997, 2001.

35. Kauffmann-Zeh, A., Rodriguez-Viciana, P., Ulrich, E., Gilbert, C., Coffer, P., Downward, J., and Evan, G. Suppression of c-Myc-induced apoptosis by Ras signaling through PI(3)K and PKB. Nature (Lond.), *385:* 544–548, 1997.

36. Khwaja, A., Rodriguez-Viciana, P., Wennstrom, S., Warne, P., and Downward, J. Matrix adhesion and ras transformation both activate a phosphoinositide 3-OH kinase and protein kinase B/Akt cellular survival pathway. EMBO J., *16:* 2783–2793, 1997.

37. Chen, R. H., Su, Y. H., Chuang, R. L., and Chang. T. Y. Suppression of transforming growth factor-β-induced apoptosis through a phosphatidylinositol 3-kinase/Akt-dependent pathway. Oncogene, *17:* 1959–1968, 1998.

hTERT Expression Is a Prognostic Factor of Survival in Patients with Stage I Non-Small Cell Lung Cancer[1]

Luo Wang, Jean-Charles Soria, Bonnie L. Kemp, Diane D. Liu, Li Mao, and Fadlo R. Khuri[2]

Departments of Thoracic/Head and Neck Medical Oncology [L. W., J-C. S., L. M., F. R. K.], Pathology [B. L. K.], and Biostatistics [D. D. L.], The University of Texas M. D. Anderson Cancer Center, Houston, TX 77030

ABSTRACT

Activation of telomerase plays a critical role in unlimited proliferation and immortalization of cells. The purpose of this study was to evaluate the significance of human telomerase reverse transcriptase catalytic subunit (hTERT) as a prognostic marker.

The expression of hTERT in a large population of 153 patients with stage I non-small cell lung cancer was analyzed using the *in situ* hybridization technique.

We found that diffuse and clear hTERT expression was present in 51 (33%) of 153 patients. Kaplan-Meier analysis showed that hTERT expression was associated with shorter overall survival ($P = 0.04$), shorter disease-specific survival ($P = 0.03$), and shorter disease-free survival ($P = 0.02$). Multivariate analysis confirmed this independent prognostic value of hTERT expression.

Our results indicated that hTERT mRNA expression is associated with malignant tumor progression and poor outcome. hTERT may serve as a useful marker to identify patients with poor prognosis and to select patients with early-stage non-small cell lung cancer who might benefit from adjuvant treatment.

INTRODUCTION

Lung cancer retains the leading position in cancer-related deaths in the United States. In 2002, it is estimated that there will be 154,900 deaths and 169,400 new cases from lung and bronchial cancer in the United States, compared with 156,900 deaths and 164,100 new cases in 2000 (1). NSCLC[3] comprises more than 80% of lung cancers, and complete surgical resection of primary tumors in early-stage disease is the only potentially curative treatment. For patients with stage I NSCLC (about 17% of all patients with NSCLC), the average 5-year survival rate is about 60%. Adjuvant cytotoxic chemotherapy has been proposed and evaluated in the setting of NSCLC, and it offers limited hope of improving prognosis (2). One area of intense research on early-stage NSCLC is the identification of molecular markers to complement TNM staging to fully assess the prognosis of patients and to evaluate the effects of novel chemotherapy agents and regimens (3). Such prognostic markers include a wide variety of protein molecular markers that can be classified by different antibodies as molecular genetic markers, metastatic propensity markers, differentiation markers, and proliferation markers (3). Other markers have been evaluated at the mRNA level including retinoic acid receptor-β, cyclooxygenase-2, vascular endothelial growth factor, MMP-2 and -9, E-cadherin, angiopoietin-2, and CD44. These markers have been associated with clinicopathological variables and survival time in patients with NSCLC (4–8).

Telomerase is a ribonucleoprotein enzyme that lengthens chromosome ends that have been shortened during successive cycles of cell division (9). Telomerase is expressed in up to 85% of NSCLCs (10, 11), and its activation plays a critical role in tumorigenesis by sustaining cellular immortality (12, 13). Hahn *et al.* (14) proved that disruption of the intracellular pathways regulated by large T antigen, oncogenic *ras*, and telomerase suffices to create a human tumor cell. The components of human telomerase include an RNA subunit (hTERC), a catalytic protein subunit (hTERT), and other telomerase-associated proteins (15). It has been shown that the expression pattern of hTERT is closely associated with telomerase activity (16–18). The recent development of ISH techniques that can reliably detect hTERT mRNA has made it possible to examine the expression of this critical telomerase component at the single-cell level (18–21). In our previous study (22), we evaluated hTERT expression in bronchial biopsy samples and found that it was a frequent event and appeared at a very early stage in cigarette smoking-induced lung carcinogenesis, making it clearer that telomerase plays a critical role in tumorigenesis. Because we have established a reliable ISH technique for detecting hTERT mRNA expression in paraffin-embedded tissue, we decided to evaluate the prognostic value of hTERT in a relatively homogeneous tumor, in a population of 153 patients with stage I NSCLC.

Received 2/26/02; revised 6/3/02; accepted 6/3/02.

The costs of publication of this article were defrayed in part by the payment of page charges. This article must therefore be hereby marked *advertisement* in accordance with 18 U.S.C. Section 1734 solely to indicate this fact.

[1] Funded by BESCT (Biology, Education, Screening, Chemoprevention, and Treatment) Lung Cancer Program, Department of Defense Grant DAMD17-01-1-0689-1 projects 1 and 3 (to L. M. and F. R. K.), Cancer Center Grant P30 CA-16620 (to M. D. Anderson Cancer Center), Tobacco Research Fund from the State of Texas (to M. D. Anderson Cancer Center), and Fondation de France, AP-HP, and a Lilly Foundation grant (to J-C. S.).

[2] To whom requests for reprints should be addressed, at Department of Thoracic/Head and Neck Medical Oncology, The University of Texas M. D. Anderson Cancer Center, Box 432, 1515 Holcombe Boulevard, Houston, TX 77030. Phone: (713) 792-6363; Fax: (713) 796-8655; E-mail: fkhuri@mdanderson.org.

[3] The abbreviations used are: NSCLC, non-small cell lung cancer; hTERT, human telomerase reverse transcriptase subunit; ISH, *in situ* hybridization; MMP, matrix metalloprotease; hnRNP A1, heterogeneous nuclear ribonucleoprotein A1; TRAP, telomeric repeat amplification protocol; TNM, tumor node metastasis; CI, confidence interval; SCC, squamous cell carcinoma.

MATERIALS AND METHODS

Clinical Samples and Preparation of Slides. Five hundred ninety-five consecutive patients with stage I NSCLC underwent definitive surgical resection, defined as a lobectomy or a pneumonectomy, from 1975 to 1993 at The University of Texas M. D. Anderson Cancer Center. We retrospectively examined 153 cases for which both tissue samples as well as data from a median follow-up period of more than 5 years were available. All available tissue blocks for each patient were reviewed for the presence of tumor by a thoracic pathologist (B. L. K.). To prevent RNA degradation in the tissue blocks during sectioning, we used glass slides that were pretreated with diethylpyrocarbonate-treated water (Sigma Chemical Co., St. Louis, MO) and coated with poly-lysine (Sigma Chemical Co.). The patient population was identified through a search of the Tumor Registry Database maintained by the Department of Medical Informatics at M. D. Anderson Cancer Center. The study was reviewed and approved by the institution's Surveillance Committee to allow us to obtain the tissue blocks and all pertinent follow-up information.

Generation of Single-Strand-specific Riboprobes. The riboprobe used in the present study, a 430-bp EcoRV-BamHI fragment of the full-length hTERT cDNA, is identical to the one initially reported by Kolquist *et al.* in 1998 (18). We have successfully tested this probe in 532 paraffin-embedded sections of bronchial origin, in a previous study (22). Although larger than the classical 50–300-bp probes usually developed for ISH, this probe remains well in the range of previous probes used to evaluate hTERT by ISH (18–22). Part of exon 1 from hnRNP A1 was used as a control to verify sample quality.

Both cDNA fragments were cloned into the pCRII-TOPO vector (Invitrogen, Carlsbad, CA). The single-strand-specific riboprobes were generated by using *in vitro* transcription. In brief, the plasmid was linearized with EcoRV and then transcribed *in vitro* with SP6 RNA polymerase (Promega, Madison, WI) using a DIG RNA labeling kit (Roche Diagnostics, Inc., Indianapolis, IN). The resulting digoxigenin-labeled RNA probe was mixed with RNase inhibitor (Roche Diagnostics, Inc.) and stored in aliquots at −80°C.

RNA ISH. ISH was performed as described previously (22). Briefly, the sections were deparaffinized in xylene and then gradually rehydrated in decreasing concentrations of ethanol. They were then treated with 2.5 μg/ml proteinase K (Roche Diagnostics, Inc.), post-fixed in 4% paraformaldehyde, and acetylated in 0.25% acetic anhydride/0.1 M triethanolamine (Sigma Chemical Co.). After dehydrating in increasing concentrations of ethanol and air-drying, the sections were hybridized with the probe at 42°C for 4 h by incubating in hybridization buffer [400–800 ng/ml of either hTERT or hnRNP A1 riboprobe, 10% 20× SSC, 50% deionized formamide, 5% dextran sulfate, 2% 100× Denhardt's solution (2% Ficoll 400, 2% povidone, and 2% BSA), 10 mM DTT, 250 μg/ml predenatured salmon sperm DNA, and 200 μg/ml yeast tRNA]. The sections were then washed two times for 5 min in 2× SSC and then for 2 h in 2× SSC containing 0.05% Triton X-100 and 2% normal sheep serum (Sigma Chemical Co.) with agitation at room temperature. After being briefly rinsed in buffer 1 [0.1 M maleic acid and 0.15 M NaCl (pH 7.5)], the sections were washed in buffer 1 containing 0.3% Triton X-100 and 2% normal sheep serum for another 30 min at room temperature.

Detection was performed using the DIG Nucleic Acid Detection Kit (Roche Diagnostics, Inc.) according to the manufacturer's directions. Anti-DIG alkaline phosphotase-conjugated antibody was diluted 1:500. Nitro-blue tetrazolium and 5-bromo-4-chloro-3-indolyl phosphate were used as chromogens. Slides were then rinsed in TE buffer [10 mM Tris-HCl/1 mM EDTA (pH 8)] and mounted with Aqua-Mount medium (Fisher, Houston, TX).

Determination of Positive hTERT Expression. As reported by Falchetti *et al.* (21), only slides displaying a clear cytoplasmic signal could be considered as positive. More specifically, our slides were rated as positive if such a definite and clear signal was present in at least two large areas (×200 magnification) on the slide. Slides with faint signal, the absence of signal, or only focal positivity were considered to be negative. We did not grade the intensity of the hybridization signals.

To confirm RNA preservation in hTERT-negative slides, we randomly selected 33 such negative slides and detected the expression of the major splicing factor hnRNP A1. Because hnRNP A1 is one of the most abundant splicing factors in human cells, this probe was a good control to check mRNA quality.

Statistical Analysis. All statistical analyses were performed using SAS software (version 6.12; SAS Institute, Inc., Cary, NC). Overall, disease-specific and disease-free survival rates were calculated using the Kaplan-Meier method. All survival times were calculated from the date of surgery. The overall survival statistic accounted for all deaths (cancer related or not). Disease-specific survival time was calculated from the date of surgery to death from cancer-related causes. Disease-free survival time was calculated from the date of surgery to relapse or death from cancer-related causes. The χ^2 test was used to test the association between two categorical variables. The Wilcoxon rank-sum test was used for differences in median of age. We used the Cox proportional hazards model for univariate analysis to evaluate the association between survival time and risk factors and for multivariate analysis to model the risks of hTERT expression on survival time, with adjustment for clinical and histopathological parameters (age, sex, race, tumor histology, tumor size). All *P*s were determined by two-sided tests. *P*s less than 0.05 were considered statistically significant.

RESULTS

A total of 153 cases that had adequate tumor specimen and ≥5-year follow-up information were analyzed for hTERT mRNA expression in this study. The study population consisted of 115 men and 38 women; 136 patients were white, and 17 patients were of other ethnicities (Table 1). Patient ages ranged from 37–85 years old, with a median age of 63.4 ± 9.2 years old. Histological subtypes included 66 cases of SCC, 59 cases of adenocarcinoma, 12 cases of bronchioalveolar carcinoma, 5 cases of large cell carcinoma, 5 cases of adenosquamous carcinoma, and 6 unclassified cases. Thirty-nine patients died of lung cancer. The other patients died of heart disease (21 cases), respiratory diseases (15 cases), other organ failures (6 cases), and unknown causes (24 cases). The probability of 5-year over-

Table 1 hTERT expression status in stage I NSCLC tumors according to clinicopathological features of patients

Variable	Total no. of patients (n = 153)	hTERT expression		P
		Positive (n = 51)	Negative (n = 102)[a]	
Age (mean ± SD)	63.4 ± 9.2	64.3 ± 9.5	62.9 ± 9.1	0.38
Sex				
Male	115	40	75	0.51
Female	38	11	27	
Race				
White	136	42	94	0.09
Other	17	9	8	
Smoker				
Yes	137	47	90	1[b]
No	7	2	5	
Unknown	9	2	7	
Tumor histology				
SCC	66	27	39	0.08
Adenocarcinoma and others	87	24	63	
TNM stage				
T1N0M0	75	27	48	0.49
T2N0M0	78	24	54	
5-year overall survival rate (95% CI)	56.1% (48.7%, 64.6%)	42.7% (30.9%, 58.8%)	62.9% (54.1%, 73.1%)	

[a] This number included 36 cases in which the signal was faint or focal.
[b] The P was calculated to compare smoking and nonsmoking patients.

all survival for the whole population was 56.1% (95% CI, 48.7–64.6%).

By using the hTERT riboprobe, we detected diffuse and clear hTERT mRNA expression in tumor cell nests as well as in some infiltrating tumor lymphocytes (Fig. 1). In pilot experiments, the positive hybridization signal was always cytoplasmic and was abrogated by RNase treatment of the sections before hybridization with the riboprobe, suggesting that the signal was related to the presence of hTERT mRNA. The hybridization signal for hTERT mRNA in the tumorous area of positive samples ranged in intensity from low or moderate to strongly positive and was detectable in the vast majority of cells examined (Fig. 1). Interestingly, we found hTERT-positive cases in all of the histological subtypes we tested (Fig. 1). Slides that were negative for hTERT mRNA (*i.e.*, that had no hybridization signal or only focal positivity) also contained different histological subtypes (Fig. 2). We clearly detected hnRNP A1 mRNA, used as a positive control, in all 33 of the randomly selected hTERT-negative slides, therefore ruling out false-negativity related to RNA degradation (Fig. 2).

Among these 153 cases screened for hTERT expression by ISH, the percentage of tumors that were hTERT positive was 33.3% (51 cases). The positive slides were randomly distributed in the different years of surgery, and statistical analysis did not show any difference between the positive rates of slides by year (data not shown). The association between hTERT expression and the general clinicopathological characteristics of the patients is shown in Table 1. There was no statistical significance between age, sex, tumor size (T1N0M0 *versus* T2N0M0), and smoking status between the hTERT-positive cases and the hTERT-negative cases. Only seven patients were nonsmokers, thereby preventing any definitive conclusion regarding the association between hTERT expression and smoking. There was a trend, but no statistical significance, toward more cases with positive expression of hTERT in Caucasians (P = 0.09).

We subsequently analyzed the relationship between hTERT expression and length of survival. The median follow-up time for the patient population was 10.5 years. Fig. 3*A* shows the overall survival curves analyzed using the Kaplan-Meier method. Patients with tumors that were hTERT positive had a shorter survival time than did patients with tumors that were hTERT negative (P = 0.04; log-rank test). The 5-year overall survival rate for patients whose tumors were hTERT positive was 42.7% (95% CI, 30.9–58.8%) and 62.9% (95% CI, 54.1–73.1%) for patients whose tumors were hTERT negative (Table 1). Fig. 3*B* shows that patients with positive hTERT expression had significantly shorter disease-specific survival times than did patients with negative hTERT expression (P = 0.03; log-rank test). A comparison of disease-free survival curves in hTERT-negative and hTERT-positive patients yielded similar results (P = 0.02; log-rank test; Fig. 3*C*).

The univariate Cox proportional hazards model was used to evaluate the association between hTERT expression, clinicopathological variables (age, sex, race, histological subtype, TNM stage), and survival time. Table 2 shows the results on disease-specific survival time. In a multivariate Cox proportional hazards model, among all clinicopathological variables, hTERT expression was the only significant independent prognostic indicator for disease-specific survival.

DISCUSSION

Numerous prognostic factors have been identified in patients with early-stage NSCLC that might enable classification of such patients into different subsets corresponding to different risks of recurrence following complete resection. Most of the markers are proteins that can be detected by immunohistochemistry assays based on the antigen-antibody reaction. These markers, in general, can be classified into four groups: molecular genetic markers such as K-*ras*/p21 protein, p53 protein, C-erbB-

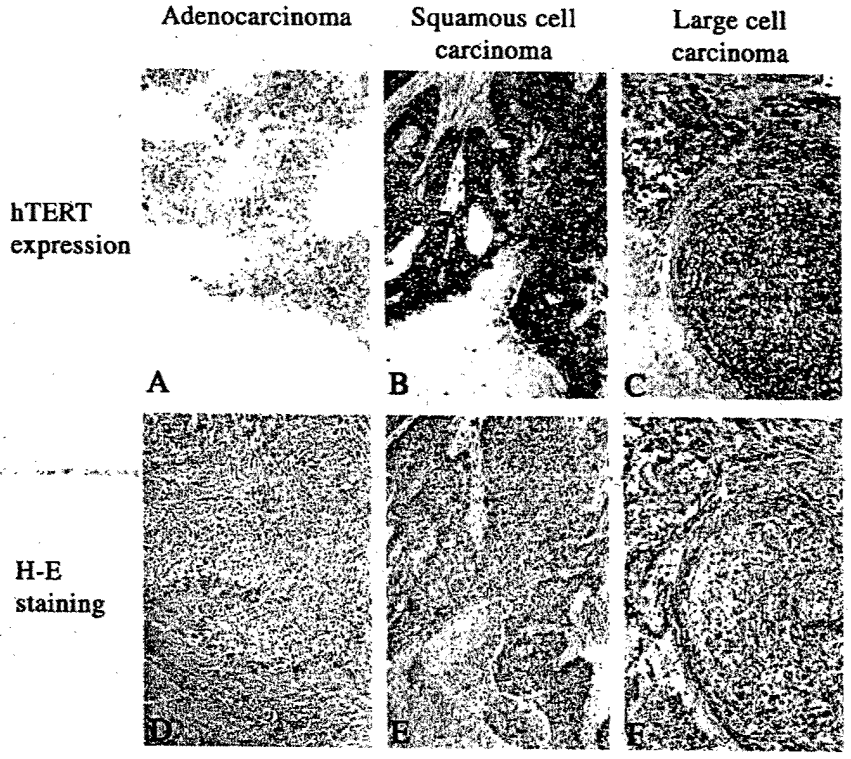

Fig. 1 hTERT expression detected by ISH in an adenocarcinoma (*A*), a SCC (*B*), and a large cell carcinoma (*C*). Magnification, ×100. Panels *D*, *E*, and *F* represent Hematoxylin and Eosin stained samples from the same tumors and adjacent slices to panels *A*, *B*, and *C*.

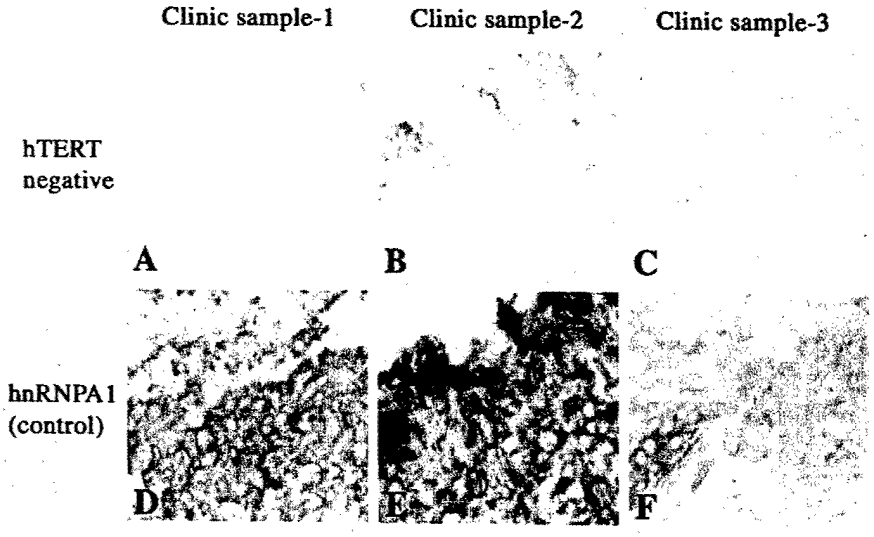

Fig. 2 Sample quality detected by ISH with hnRNP A1 as the control in hTERT-negative cases. Magnification, ×200.

2/p185, bcl-2 protein, and Rb protein; metastatic propensity markers such as CK18 protein, cathepsin B protein, factor VIII and type IV collagen; differentiation markers such as the ABH blood group antigen and the Lewis-related antigen; and proliferation markers such as Ki-67 nuclear antigen and proliferating cell nuclear antigen (3).

Because the major value of prognostic markers is to guide postresection treatment in early-stage NSCLC, the ability to identify patients with a high risk of cancer-related events such as recurrence or metastasis will help to determine whether adjuvant therapy is needed and to evaluate its effect. However, no conclusions have been reached about which marker or markers are better for forecasting patients' outcomes. Therefore, one of the major current interests in this field is to evaluate other novel

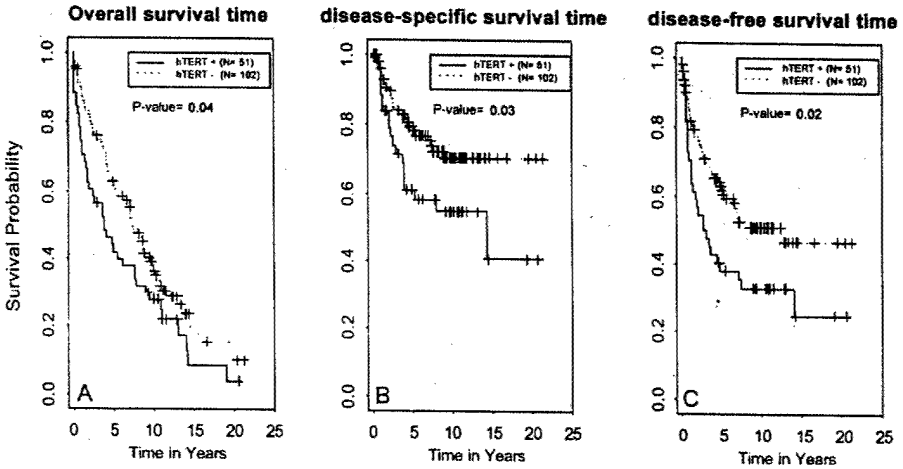

Fig. 3 Survival analysis of 153 patients with stage I NSCLC based on the classification of hTERT-positive and -negative mRNA expression. *A*, overall length of survival; *B*, disease-specific survival time; *C*, length of disease-free survival.

Table 2 A univariate Cox proportional hazards model applied to disease-specific survival time

Variable	Hazard ratio	95% CI	*P*
Age	1.0	0.98–1.05	0.51
Sex (male or female)	1.1	0.57–2.14	0.77
Race (white or other)	0.56	0.25–1.25	0.15
Histological subtype (SCC or other)	0.76	0.41–1.42	0.39
Tumor size (T1 or T2)	1.03	0.57–1.86	0.92
hTERT (+ or −)	1.90	1.04–3.45	0.036

markers. Some effort has been put forth to test mRNA markers such as retinoic acid receptor-β, cyclooxygenase-2, vascular endothelial growth factor, MMP-2, MMP-9, E-cadherin, angiopoietin-2, and CD44 (4–8).

Telomerase activity has been described as an independent marker of poor prognostic in different human tumors such as neuroblastoma, gastric cancer, breast cancer, colon cancer, cervical cancer, and meningioma (23–28). In patients with NSCLC, a conclusion regarding the prognostic value of telomerase activity remains unclear. Hiyama *et al.* (29) first observed a high level of telomerase activity in primary tumors and corresponding metastatic lesions. However, Albanell *et al.* (30) found only a weak association between telomerase activity and unfavorable prognosis in a mixed population of 99 patients with stages I–IV NSCLC. Komiya *et al.* (31) examined the expression of hTERT mRNA in tumor specimens from 68 patients by using RT-PCR and did not find a correlation between hTERT status and any common clinical features, except age. However, Marchetti *et al.* (32) evaluated the activity of the telomerase enzyme detected by the TRAP assay in tumors and adjacent noncancerous lung tissue samples obtained from 107 consecutive patients with pathological stage I operable NSCLC. They found telomerase activity in 66 of 107 tumors but in none of the corresponding adjacent noncancerous lung tissue samples. They also found a statistically significant association between telomerase activity and both disease-free and overall survival times. Kumaki *et al.* (33), Arinaga *et al.* (34), and Satoshi *et al.* (35) reported different conclusions.

We considered that such contradictions in the literature could be attributed to analysis of heterogeneous populations with few patients with stage I NSCLC, and to the different techniques used to detect telomerase activity or expression. To address these issues, we decided to use ISH to measure the mRNA expression level of hTERT in a large population of 153 patients with stage I NSCLC for which complete follow-up information was available. Because the tumor samples had been stored for a long time (8–26 years), we anticipated that sample quality would be the first major problem in getting a correct signal. The second major issue for successful ISH is the probe. A single-strand riboprobe can yield a more specific signal than that of a standard double-strand cDNA probe labeled mostly by the random-primer method. The size and sequence of the riboprobe are also very important for successful ISH. The major component of human telomerase is hTERT, and it has been proven that the expression pattern of hTERT is closely associated with actual telomerase activity (16–18). On the basis of the analysis of the hTERT genomic sequence, we selected the most conserved region, from exon 7 to exon 12, as the probe, which also corresponded to the catalytic domain of this enzyme. The result is shown in Fig. 1. We are convinced that the hTERT ISH is a reliable technique. It can possibly be developed as a clinical assay, and, in fact, in a clinical trial of n-(4-hydroxyphenyl) retinamide, a compound derived from 13-*cis*-retinoic acid, we successfully used ISH to evaluate its effect on hTERT expression in the bronchial epithelium of smokers (22).

One major concern generated by our results is the low percentage (33%) of hTERT-positive cases reported in contrast to previous studies reporting telomerase activity in up to 85% of NSCLCs. We believe that this apparent discrepancy can be explained by the specific technique (ISH) and the strict criteria used in our study in comparison to the very sensitive TRAP assay. It is very important to point out that the TRAP assay does not account for tumor heterogeneity, and, therefore, tumors with few telomerase-positive cells appear telomerase positive in the same way as tumors in which most cells are telomerase positive. Furthermore, most previous studies on telomerase have been carried out in heterogeneous populations including patients with

stages I–IV disease (29–31). Marchetti *et al.* (32) reported a hTERT positivity rate of 66% by RT-PCR in stage I NSCLC. Falchetti *et al.* (21) investigated the expression of hTERT in 34 samples from patients with primary *de novo* glioblastoma multiforme by ISH, RT-PCR, TRAP activity assay, and telomere restriction fragment Southern blotting. They found that 60% of the cases were hTERT positive by ISH and could be classified into two groups: those with diffuse and those with focal hTERT expression. However, some studies have shown that telomerase activity can be detected at high, moderate, and low levels (26, 28). In cell lines, we found that the ISH signal generally corresponded to the level of telomerase activity detected by TRAP assay (data not shown). We considered that the focal hTERT expression does not seem to represent strong telomerase activity and decided to classify the cases with hTERT focal expression as negative.

In this study, even with our criteria, which are stricter than those used in other studies, a definite association exists between hTERT expression and all of the clinically relevant outcomes. This strongly supports our notion that substantial hTERT mRNA expression could be an ideal marker for assessing prognosis of patients with early-stage NSCLC and evaluating the effect of new chemotherapeutic agents.

In conclusion, based on a large population of patients with stage I NSCLC, our results indicate that hTERT mRNA expression is associated with malignant tumor progression, thereby making it a potentially suitable prognostic marker. ISH of hTERT expression may be used to distinguish patients with poor prognosis and to potentially guide the regimen of adjuvant chemotherapy for patients with early-stage NSCLCs. Nevertheless, confirmatory studies by independent groups, using ISH or alternative techniques (RT-PCR, TRAP), are necessary.

ACKNOWLEDGMENTS

We thank Julia M. Starr for editing the manuscript and Lakshmi Kakarala for histological assistance.

REFERENCES

1. Jamal, A., Thomas, A., Murray, T., and Thun, M. Cancer Statistics, 2002. Ca. Cancer J. Clin., *52:* 23–47, 2002.

2. Non-small Cell Lung Cancer Collaborative Group. Chemotherapy in non-small cell lung cancer: a meta-analysis using updated data on individual patients from 52 randomised clinical trials. Br. Med. J., *311:* 899–909, 1995.

3. Strauss, G. M. Prognostic markers in resectable non-small cell lung cancer. Hematol. Oncol. Clin. North Am., *11:* 409–434, 1997.

4. Khuri, F. R., Wu, H., Lee, J. J., Kemp, B. L., Lotan, R., Lippman, S. M., Feng, L., Hong, W. K., and Xu, X. C. Cyclooxygenase-2 overexpression is a marker of poor prognosis in stage I non-small cell lung cancer. Clin. Cancer Res., *7:* 861–867, 2001.

5. Khuri, F. R., Lotan, R., Kemp, B. L., Lippman, S. M., Wu, H., Feng, L., Lee, J. J., Cooksley, C. S., Parr, B., Chang, E., Walsh, G. L., Lee, J. S., Hong, W. K., and Xu, X. C. Retinoic acid receptor-β as a prognostic indicator in stage I non-small-cell lung cancer. J. Clin. Oncol., *18:* 2798–2804, 2000.

6. Wong, M. P., Chan, S. Y., Fu, K. H., Leung, S. Y., Cheung, N., Yuen, S. T., and Chung, L. P. The angiopoietins, tie2 and vascular endothelial growth factor are differentially expressed in the transformation of normal lung to non-small cell lung carcinomas. Lung Cancer, *29:* 11–22, 2000.

7. Pirinen, R., Hirvikoski, P., Bohm, J., Kellokoski, J., Moisio, K., Viren, M., Johansson, R., Hollmen, S., and Kosma, V. M. Reduced expression of CD44v3 variant isoform is associated with unfavorable outcome in non-small cell lung carcinoma. Hum. Pathol., *31:* 1088–1095, 2000.

8. Herbst, R. S., Yano, S., Kuniyasu, H., Khuri, F. R., Bucana, C. D., Guo, F., Liu, D., Kemp, B. L., Lee, J. J., Hong, W. K., and Fidler, I. J. Differential expression of E-cadherin and type IV collagenase genes predicts outcome in patients with stage I non-small cell lung carcinoma. Clin. Cancer Res., *6:* 790–797, 2000.

9. Greider, C. W., and Blackburn, E. H. Identification of a specific telomere terminal transferase activity in Tetrahymena extracts. Cell, *43:* 405–413, 1985.

10. Hiyama, K., Hiyama, E., Ishioka, S., Yamakido, M., Inai, K., Gazdar, A. F., Piatyszek, M. A., and Shay, J. W. Telomerase activity in small-cell and non-small-cell lung cancers. J. Natl. Cancer Inst., *87:* 895–902, 1995.

11. Albanell, J., Lonardo, F., Rusch, V., Engelhardt, M., Langenfeld, J., Han, W., Klimstra, D., Venkatraman, E., Moore, M. A., and Dmitrovsky, E. High telomerase activity in primary lung cancers: association with increased cell proliferation rates and advanced pathologic stage. J. Natl. Cancer Inst., *89:* 1609–1615, 1997.

12. Dhaene, K., Van Marck, E., and Parwaresch, R. Telomeres, telomerase and cancer: an up-date. Virchows Arch., *437:* 1–16, 2000.

13. Kim, N. W., Piatyszek, M. A., Prowse, K. R., Harley, C. B., West, M. D., Ho, P. L., Coviello, G. M., Wright, W. E., Weinrich, S. L., and Shay, J. W. Specific association of human telomerase activity with immortal cells and cancer. Science (Wash DC), *266:* 2011–2015, 1994.

14. Hahn, W. C., Counter, C. M., Lundberg, A. S., Beijersbergen, R. L., Brooks, M. W., and Weinberg, R. A. Creation of human tumour cells with defined genetic elements. Nature (Lond.), *400:* 464–468, 1999.

15. Feng, J., Funk, W. D., Wang, S. S., Weinrich, S. L., Avilion, A. A., Chiu, C. P., Adams, R. R., Chang, E., Allsopp, R. C., Yu, J., Le, S., West, M. D., Harley, C. B., Andrews, W. H., Greider, C. W., and Villeponteau, B. The RNA component of human telomerase. Science (Wash DC), *269:* 1236–1241, 1995.

16. Meyerson, M., Counter, C. M., Eaton, E. N., Ellisen, L. W., Steiner, P., Caddle, S. D., Ziaugra, L., Beijersbergen, R. L., Davidoff, M. J., Liu, Q., Bacchetti, S., Haber, D. A., and Weinberg, R. A. hEST2, the putative human telomerase catalytic subunit gene, is up-regulated in tumor cells and during immortalization. Cell, *90:* 785–795, 1997.

17. Nakamura, T. M., Morin, G. B., Chapman, K. B., Weinrich, S. L., Andrews, W. H., Lingner, J., Harley, C. B., and Cech, T. R. Telomerase catalytic subunit homologs from fission yeast and human. Science (Wash DC), *277:* 955–959, 1997.

18. Kolquist, K. A., Ellisen, L. W., Counter, C. M., Meyerson, M., Tan, L. K., Weinberg, R. A., Haber, D. A., and Gerald, W. L. Expression of TERT in early premalignant lesions and a subset of cells in normal tissues. Nat. Genet., *19:* 182–186, 1998.

19. Nakano, K., Watney, E., and McDougall, J. K. Telomerase activity and expression of telomerase RNA component and telomerase catalytic subunit gene in cervical cancer. Am. J. Pathol., *153:* 857–864, 1998.

20. Liu, K., Schoonmaker, M. M., Levine, B. L., June, C. H., Hodes, R. J., and Weng, N. P. Constitutive and regulated expression of telomerase reverse transcriptase (hTERT) in human lymphocytes. Proc. Natl. Acad. Sci. USA, *96:* 5147–5152, 1999.

21. Falchetti, M. L., Pallini, R., D'Ambrosio, E., Pierconti, F., Martini, M., Cimino-Reale, G., Verna, R., Maira, G., and Larocca, L. M. In situ detection of telomerase catalytic subunit mRNA in glioblastoma multiforme. Int. J. Cancer, *88:* 895–901, 2000.

22. Soria, J. C., Moon, C., Wang, L., Hittelman, W. N., Jang, S. J., Sun, S. Y., Lee, J. J., Liu, D., Kurie, J. M., Morice, R. C., Lee, J. S., Hong, W. K., and Mao, L. Effects of *N*-(4-hydroxyphenyl) retinamide on hTERT expression in the bronchial epithelium of smokers. J. Natl. Cancer Inst., *93:* 1257–1263, 2001.

23. Hiyama, E., Hiyama, K., Yokoyama, T., Matsuura, Y., Piatyszek, M. A., and Shay, J. W. Correlating telomerase activity levels with human neuroblastoma outcomes. Nat. Med., *1:* 249–255, 1995.

24. Hiyama, E., Yokoyama, T., Tatsumoto, N., Hiyama, K., Imamura, Y., and Murakami, Y. Telomerase activity in gastric cancer. Cancer Res., *55:* 3258–3262, 1995.

25. Kim, N. W., Levitt, D., Huang, G., Wu, F., Osborne, K., and Clark, G. Correlation of telomerase with prognostic indicators of breast cancer. Proc. Am. Assoc. Cancer Res., *37:* 561–562, 1996.

26. Clark, G. M., Osborne, C. K., Levitt, D., Wu, F., and Kim, N. W. Telomerase activity and survival of patients with node-positive breast cancer. J. Natl. Cancer Inst., *89:* 1874–1881, 1997.

27. Wisman, G. B. A., De Jong, S., Meersma, G. J., Helder, M. N., Hollema, H., de Vries, E. G. E., Keith, W. N., and van der Zee, A. G. J. Telomerase in (pre)neoplastic cervical disease. Hum. Pathol., *31:* 1304–1312, 2000.

28. Tatsumoto, N., Hiyama, E., Murakami, Y., Imamura, Y., Shay, J. W., Matsuura, Y., and Yokoyama, T. High telomerase activity is an independent prognostic indicator of poor outcome in colorectal cancer. Clin. Cancer Res., *6:* 2696–2701, 2000.

29. Hiyama, K., Hiyama, E., Ishioka, S., Yamakido, M., Inai, K., Gazdar, A. F., Piatyszek, M. A., and Shay, J. W. Telomerase activity in small-cell and non-small-cell lung cancer. J. Natl. Cancer Inst., *87:* 895–902, 1995.

30. Albanell, J., Leonardo, F., Rusch, V., Engelhardt, M., Langenfeld, J., Han, W., Klimstra, D., Venkatraman, E., Moore, M. A. S., and Dmitrovsky, E. High telomerase activity in primary lung cancer: association with increased cell proliferation rates and advanced pathologic stage. J. Natl. Cancer Inst., *89:* 1609–1615, 1997.

31. Komiya, T., Kawase, I., Nitta, T., Yasumitsu, T., Kikui, M., Fukuoka, M., Nakagawa, K., and Hirashima, T. Prognostic significance of hTERT expression in non-small cell lung cancer. Int. J. Oncol., *16:* 1173–1177, 2000.

32. Marchetti, A., Bertacca, G., Buttitta, F., Chella, A., Quattrocolo, G., Angeletti, C. A., and Bevilacqua, G. Telomerase activity as a prognostic indicator in stage I non-small cell lung cancer. Clin. Cancer Res., *5:* 2077–2081, 1999.

33. Kumaki, F., Kawai, T., Hiroi, S., Shinomiya, N., Ozeki, Y., Ferrans, V. J., and Torikata, C. Telomerase activity and expression of human telomerase RNA component and human telomerase reverse transcriptase in lung carcinomas. Hum. Pathol., *32:* 188–195, 2001.

34. Arinaga, M., Shimizu, S., Gotoh, K., Haruki, N., Takahashi, T., Takahashi, T., and Mitsudomi, T. Expression of human telomerase subunit genes in primary lung cancer and its clinical significance. Ann. Thorac. Surg., *70:* 401–405, 2000.

35. Satoshi, T., Toshihiro, O., Akira, O., Hideyuki, I., and Kosei, Y. Prognostic impact of telomerase activity in non-small cell lung cancers. Ann. Surg., *230:* 715–720, 1999.

Oncogene (2003) 22, 615–626

www.nature.com/onc

CACNA2D2-mediated apoptosis in NSCLC cells is associated with alterations of the intracellular calcium signaling and disruption of mitochondria membrane integrity

Giovanni L Carboni[1,3], Boning Gao[2], Masahiko Nishizaki[1], Kai Xu[1], John D Minna[2], Jack A Roth[1] and Lin Ji[1]

[1]*Section of Thoracic Molecular Oncology, Department of Thoracic and Cardiovascular Surgery, The University of Texas MD Anderson Cancer Center, Houston, TX 77030, USA;* [2]*Department of Internal Medicine and Pharmacology, Hamon Center for Therapeutic Oncology Research, University of Texas Southwestern Medical Center, Dallas, TX 75390, USA;* [3]*Division of General Thoracic Surgery, University Hospital Bern, Switzerland*

The CACNA2D2 gene, a new subunit of the Ca^{2+}-channel complex, was identified in the homozygous deletion region of chromosome 3p21.3 in human lung and breast cancers. Expression deficiency of the CACNA2D2 in cancer cells suggests a possible link of it to Ca^{2+} signaling in the pathogenesis of lung cancer and other cancers. We investigated the effects of overexpression of CACNA2D2 on intracellular Ca^{2+} contents, mitochondria homeostasis, cell proliferation, and apoptosis by adenoviral vector-mediated wild-type CACNA2D2 gene transfer in 3p21.3-deficient nonsmall cell lung cancer cell lines. Exogenous expression of CACNA2D2 significantly inhibited tumor cell growth compared with the controls. Overexpression of CACNA2D2 induced apoptosis in H1299 (12.5%), H358 (13.7%), H460 (22.3%), and A549 (50.1%) cell lines. Levels of intracellular free Ca^{2+} were elevated in AdCACNA2D2-transduced cells compared with the controls. Mitochondria membrane depolarization was observed prior to apoptosis in Ad-CACNA2D2 and Adp53-transduced H460 and A549 cells. Release of cyt *c* into the cytosol, caspase 3 activation, and PARP cleavage were also detected in these cells. Together, these results suggest that one of the pathways in CACNA2D2-induced apoptosis is mediated through disruption of mitochondria membrane integrity, the release of cyt *c*, and the activation of caspases, a process that is associated with regulation of cytosolic free Ca^{2+} contents.
Oncogene (2003) **22,** 615–626. doi:10.1038/sj.onc.1206134

Keywords: tumor suppressor genes; apoptosis; calcium channel proteins; human chromosome 3p21.3; lung cancer

Introduction

The novel gene CACNA2D2 has recently been identified in the homozygous deletion region of chromosome 3p21.3 in human lung and breast cancers (Gao *et al.*, 2000, Lerman and Minna, 2000). It is characterized structurally as a new $\alpha 2\delta 2$ auxiliary subunit of the voltage-activated calcium channel (VACC) protein complex. The CACNA2D2 gene spans an ~140 kb genomic locus in the 3p21.3 region, consists of at least 40 exons, and is expressed as a 5.5–5.7 kb mRNA. The CACNA2D2 protein consists of 1146 amino acids with a predicted molecular mass of 130 kDa (Gao *et al.*, 2000). Three splicing variants of CACNA2D2 mRNA have been detected, which result in two protein isoforms with different N-terminals (Angeloni *et al.*, 2000). The CACNA2D2 protein shows a 56% amino-acid sequence homology to that of the $\alpha 2\delta 1$ subunit of the VACC complexes and shares a similar secondary and tertiary structure with the CACNA2D1, as suggested by the analysis of hydrophobicity, potential glycosylation sites, and bridge-forming cysteines of the primary sequence (Angeloni *et al.*, 2000). The CACNA2D2 protein is highly expressed in normal lung tissue, but either absent or underexpressed in more than 50% of lung cancers (Gao *et al.*, 2000). Since cancer cells are deficient in CACNA2D2, it has been suggested that CACNA2D2 could be a tumor suppressor gene linking Ca^{2+} signaling with the pathogenesis of lung cancer and other cancers (Gao *et al.*, 2000).

Growing evidence has demonstrated that Ca^{2+} signaling regulates and controls diverse cellular processes such as cell fertilization, development, proliferation, learning and memory, contraction and secretion, and cell death (Berridge *et al.*, 1998, 2000). The universality of calcium as an intracellular messenger depends on the enormous range of timing, spatial, and temporal signals it can create in the complicated cellular processes (Berridge *et al.*, 1998, 2000). Alteration of the spatial and temporal balances of intracellular calcium by either environmental stimuli or calcium effectors can result in cell death by both necrosis and apoptosis (Lemasters *et al.*, 1998; Berridge *et al.*, 2000; Zhu *et al.*, 2000).

Early loss of CACNA2D2 expression in the pathogenesis of lung cancer (Angeloni *et al.*, 2000), inactivation of expression of other calcium channel-related

*Correspondence: L Ji, Department of Thoracic and Cardiovascular Surgery, Box 445, The University of Texas MD Anderson Cancer Center, 1515 Holcombe Blvd, Houston, TX 77030, USA;
E-mail: lji@mail.mdanderson.org
Received 7 July 2002; revised 4 October 2002; accepted 8 October 2002

proteins such as calcium/calmodulin-dependent death-associated protein kinase (DAPK) (Raveh and Kimchi, 2001) and CACNA1G by promoter hypermethylation in various human cancers (Toyota *et al*., 1999; Ueki *et al*., 2000; Zochbauer-Muller *et al*., 2001), and the growing role of Ca^{2+} signaling in cell regulation (Berridge *et al*., 2000), and especially its involvement in the mitochondria-mediated apoptotic pathway (Rutter and Rizzuto, 2000; Zhu *et al*., 2000), motivated us to further investigate the function of the calcium channel protein CACNA2D2 in the regulation of cell proliferation and cell death and in the pathogenesis of human cancers. This study encompasses the effect of the ectopic expression of CACNA2D2 on mitochondria homeostasis, cell proliferation, apoptosis, and intracellular Ca^{2+} contents by adenoviral vector-mediated wild-type (wt)-CACNA2D2 gene transfer in various 3p21.3-deficient NSCLC cell lines. We demonstrated that CACNA2D2-induced apoptosis was mediated through a cellular process involved in the regulation of the intracellular Ca^{2+} contents, the disruption of mitochondria membrane integrity, the release of cyt *c*, and the activation of downstream caspases.

Results

Exogenous expression of CACNA2D2 inhibits tumor cell growth

To evaluate whether the CACNA2D2 could function as a tumor suppressor or a cell death mediator by inhibition of tumor cell growth in lung cancer, we performed a series of experiments to study the effect of ectopic expression of the CACNA2D2 gene on cell proliferation in various Ad-CACNA2D2-transduced human NSCLC cell lines NCI-H1299, NCI-H460, NCI-H358, and A549, with varying status of 3p21.3 markers (Figure 1). Cells from each line were transduced *in vitro* by the Ad-CACNA2D2 vector administered at various MOIs, and cells treated with PBS, the empty vector Ad-EV, Ad-LacZ, or Ad-GFP were used as controls. The transduction efficiency was determined by examining the GFP-expressing cells in the Ad-GFP transduced cell population under a fluorescence microscope. The transduction efficiency of the adenoviral vectors was greater than 80% at the highest MOI applied for each cell line. Expression of CACNA2D2 was verified by RT-PCR analysis (Figure 1a) and Western blot analysis (Figure 1b), respectively, in Ad-CACNA2D2-transduced NSCLC cells. The transfection by plasmid DNA and the transduction by adenoviral vector are less efficient in A549, H460, and H358 cells than those in H1299 cells. Although the transcription of CACNA2D2 could be detected by RT-PCR (Figure 1a), the protein expression could only be detected at a trace amount by Western blot analysis (Figure 1b) in the CACNA2D2-containing plasmid DNA-transfected A459, H460, and H358 cells. A significantly elevated expression of CACNA2D2 proteins could be detected in all cell lines transduced by the Ad-CACN vector (Figure 1b).

We analysed cell proliferation by determining the viability of cells at 2 and 5 days post-transduction, respectively. Tumor cell growth was significantly inhibited in all the cell lines transduced by the Ad-CACNA2D2 vector 5 days after transduction, compared with what we observed with untreated cells (PBS) or those treated with Ad-EV and Ad-LacZ controls (Figure 1c). The A549 cell line appeared to be the most sensitive to the ectopic expression of CACNA2D2 and showed a more than 60% reduction in cell viability at day 5 (Figure 1c, A549), while moderate reduction of cell viability was observed in Ad-CACNA2D2-transduced H358 (44%), H460 (42%), and H1299 (28%) cells (Figure 1c). Adp53 was used as a positive control and was less effective than Ad-CACNA2D2 in A549 and H460, which contain wt-p53. No significant effect on cell viability was observed in controls treated with PBS, AdEV, and Ad-LacZ.

The effect of enforced expression of the wt-CACNA2D2 gene on tumor growth was further evaluated *in vivo* by direct intratumoral injection of Ad-CACNA2D2 vector, along with PBS and Ad-LacZ vector as controls, into human NSCLC H460 tumor xenografts in *nu/nu* mice (Figure 1d). The growth of tumors was recorded from the first injection until about 20 days after the last injection. Tumor volumes were normalized by calculat-

Figure 1 Adenoviral vector-mediated ectopic expression of CACNA2D2 gene inhibited NSCLC cell growth *in vitro*. (**a**) Expression of the CACNA2D2 gene in Ad-CACNA2D2 (CACN)-transduced NSCLC cells by RT–PCR analysis. Total RNAs were prepared from H1299, A549, H460, and H358 cells transduced by the Ad-CACNA2D2 vector for 48 h at MOIs of 1000 and 2500 vp/c, respectively, and the RNA prepared from cells transfected with a CACNA2D2-expressing plasmid DNA (pLJ58) was used as a positive control. The RNA samples were treated with DNAse prior to the RT reaction. (**b**) Western blot analysis of expression of CACNA2D2 protein. The crude protein lysates were prepared from NSCLC cells treated in the same way as described for RNA sample preparation in **a**. The rabbit anti-CACNA2D2 polyclonal antibodies were used for blotting. (**c**) XTT assay shows the effect of ectopic expression of CACNA2D2 on tumor cell viability. Cells from NSCLC cell lines A549, H460, H1299, and H358 were tranduced with Ad-CACNA2D2 vectors (CACN) at varied MOIs: 2500 for A549, 4000 for H460, 1000 for H1299, and 2000 vp/c for H358 cells. Untreated (PBS), Ad-EV (EV) treated, and Ad-LacZ(LacZ)-treated cells were used as negative controls and Adp53(p53)-treated cells as a positive control, at the same MOIs as CACN-treated cells for each cell line. Cell viability was calculated relative to that of untreated (PBS) controls. Differences were significant in the CACN-transduced cells compared to the untreated (PBS) control cells ($P=0.021$ in H1299, $P<0.0001$ in H358, H460, and A549 cells) and to the Ad-LacZ-transduced cells ($P<0.0001$ in H358, H460, and A549 cells) after 5 days of transduction. Differences between CACN-treated cells and controls were not significant in the H1299 cell line. (**d**) Effects of intratumoral administration of CACN on growth of human lung cancer H460 subcutaneous tumors in *nu/nu* mice. Results were reported as the mean ± s.d. in five to 10 mice for each treatment group. Tumor volumes were normalized by the percentage increase of tumor sizes after treatment relative to those at the beginning of the treatment in each group. Mean tumor volumes ± s.e. from these experiments are shown. The differences of the tumor volumes in the CACN-treated mice versus the PBS- and Ad-LacZ-treated controls were significant ($P<0.0001$ and 0.015, respectively)

ing the percentage increase in tumor volume after treatment relative to volume at the beginning of treatment in each group. A significant suppression of tumor growth was observed in H460 tumors treated with Ad-CACNA2D2 vector compared with those control groups treated with PBS ($P<0.0001$) and with Ad-LacZ ($P=0.015$) (Figure 1d). These results obtained *in vivo* are consistent with those observed *in vitro* for effects on inhibition of tumor cell growth and induction of apoptosis in the same cell line.

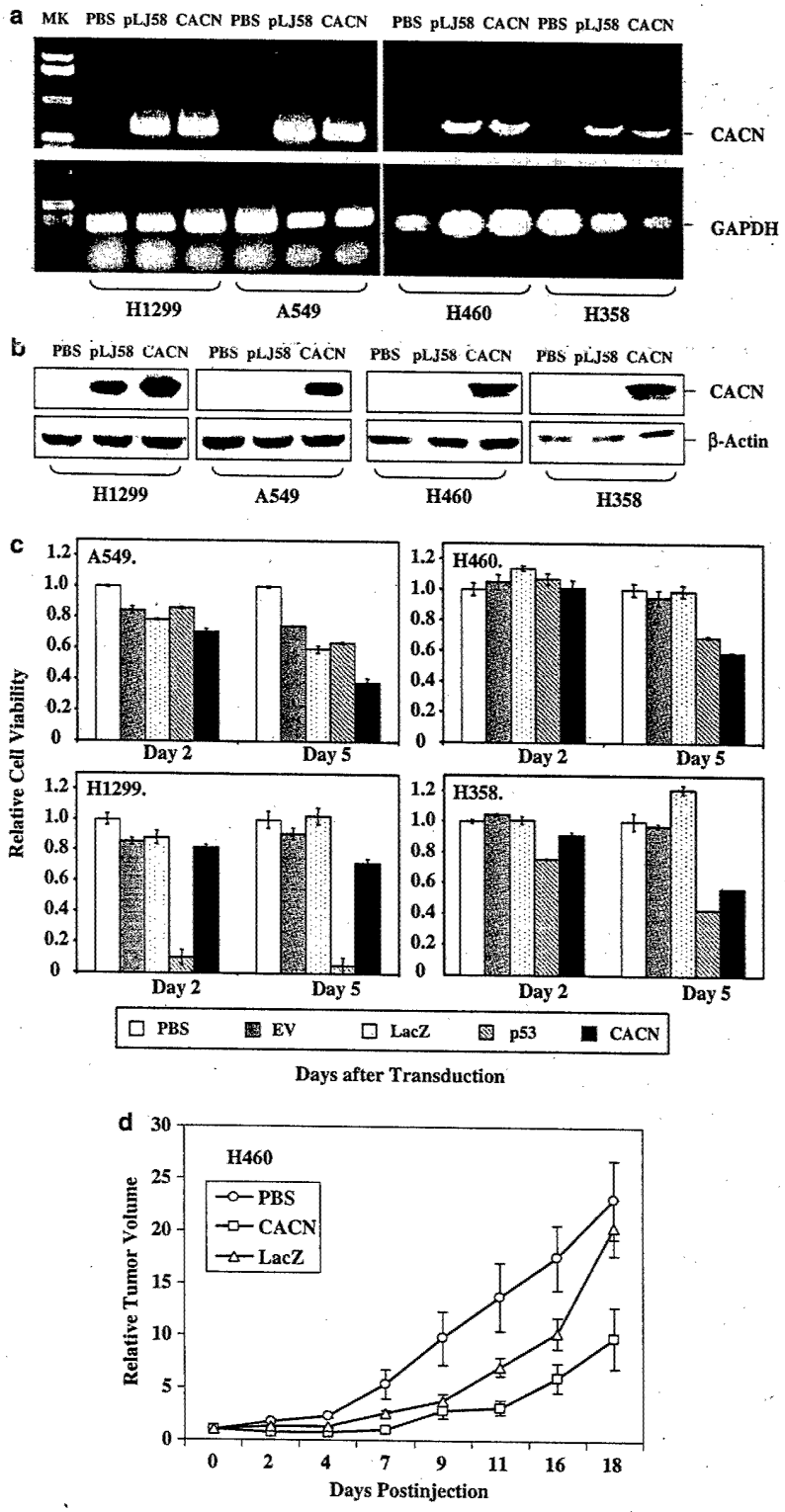

Induction of apoptosis by exogenous expression of CACNA2D2

One of the physiological functions associated with calcium channel proteins is their ability to induce apoptosis by regulating intracellular Ca^{+2} signaling and several downstream pathways (Lam *et al.*, 1994; Walker and De Waard, 1998; Felix, 1999; Wang *et al.*, 1999a; Zhu *et al.*, 1999, 2000). To test whether the growth inhibition by the ectopic expression of CACNA2D2 was caused by induction of apoptosis, we performed FACS analysis with TUNEL reaction and PI staining to examine DNA fragmentation and cell cycle kinetics in Ad-CACNA2D2-transduced cells (Figure 2). Significant induction of apoptosis was observed in Ad-CACNA2D2-transduced A549 (50.1%) (Figure 2a), H460 (22.3%) (Figure 2b), and H358 (18.7%) (Figure 2d) cells at 5 days after transduction compared with cells treated with what was seen with the Ad-EV or Ad-LacZ (from 2 to 10%) control vectors at the same time (Figure 2). However, no significant induction of apoptosis was detected in Ad-CACNA2D2-transduced H1299 cells (Figure 2c) at the same MOIs. The magnitude of and trend toward the induction of apoptosis in these Ad-CACNA2D2-treated cells paralleled the degree and trend towards growth inhibition (Figure 1c). The correlation coefficients between the relative cell viability and the relative apoptotic cell populations in Ad-CACNA2D2-treated cells versus PBS-treated controls/PBS are significant ($P<0.05$) in all four NSCLC cell lines A549, H1299, H460, and H358 cells ($r=-0.96198$, -0.79416, -0.99436, and -0.95744, respectively), but with a less degree of correlation in H1299 cells which are less sensitive to exogenous expression of CACNA2D2, suggesting that the growth inhibition by the ectopic expression of CACNA2D2 might be mediated by the induction of apoptosis. We saw no significant alteration in cell cycle kinetics, such as G1 arrest or G2/M arrest, in these Ad-CACNA2D2-transduced cells (data not shown).

Upregulation of intracellular free cytosolic Ca^{2+}

CACNA2D2 is structurally related to the $\alpha 2\delta 2$ subunit of the VACC protein complex, which has been suggested to regulate Ca^{+2} trafficking through the channel and the retention of VACC at the plasma membrane without significant change in such properties as channel gating or permeation (Wang *et al.*, 1999b; Marais *et al.*, 2001). To examine whether the ectopic overexpression of this CACNA2D2 subunit would increase free cytosolic Ca^{2+} influx, we measured changes in the levels of intracellular Ca^{2+} in Ad-CACNA2D2-transduced cells by a sensitive FACS and fluorescence image analysis with fluorescent Fluo3-AM staining (Kao *et al.*, 1989). Fluo3-AM dye binds specifically to free Ca^{2+} and shows an increase of emission fluorescence at 530 nm upon excitation at 488 nm. The fluorescence intensity depends on how much free Ca^{2+} is bound. We detected a significant increase of fluorescence emission in Ad-CACNA2D2-transduced H460 ($P=0.015$ and 0.03) (Figure 3a (panel c) and b) and A549 ($P=0.001$ and 0.002) (Figure 3a (panel g) and b)

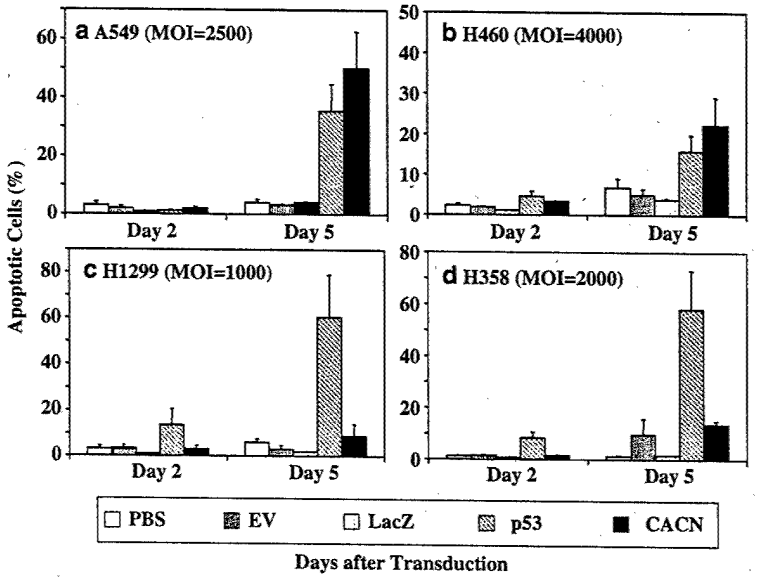

Figure 2 Apoptosis is induced by adenoviral vector-mediated expression of CACNA2D2 *in vitro*. NSCLC cell lines A549 (**a**), H460 (**b**), H1299 (**c**), and H358 (**d**) were tranduced with Ad-CACNA2D2 vectors (CACN) at varied MOIs for each line as shown in Figure 1. Untreated (PBS), Ad-EV (EV)-treated, and Ad-LacZ (LacZ)-treated cells were used as negative controls and Ad-p53(p53)-treated as a positive control. The percentage of apoptosis (TUNEL-positive) in cells transduced for 2 or 5 days, respectively, was determined by FACS analysis. Induction of apoptosis was significant in CACN-treated A549, H460, and H358 cells compared to those in PBS-treated ($P=0.0004$, 0.0321, and 0.0003, respectively) and to those in Ad-LacZ-treated ($P=0.021$, 0.048, and 0.027, respectively) controls 5 days after transduction. Differences in induction of apoptosis were not significant ($P>0.05$) between CACN-treated cells and controls in A549, H460, and H358 cell lines at 48 h post-transduction and in H1299 at both 48 and 120 h post-transduction

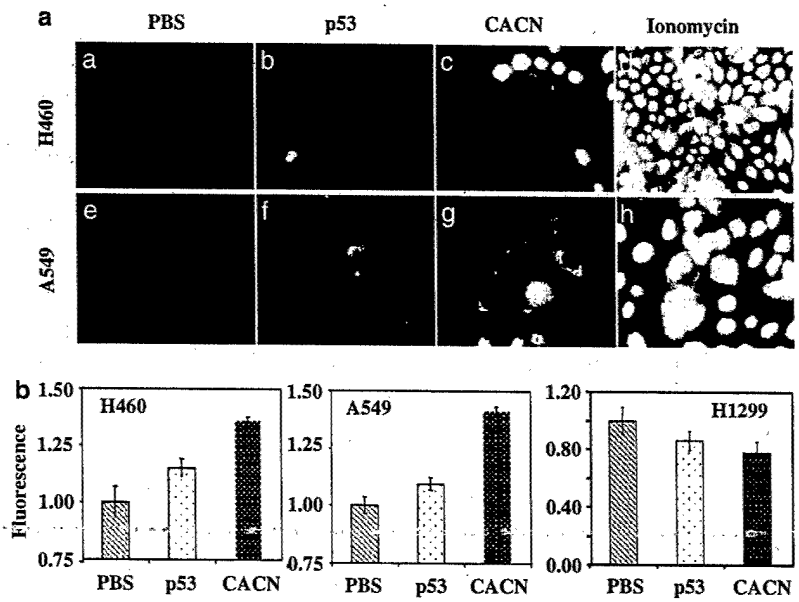

Figure 3 Ectopic expression of CACNA2D2 increased the level of the intracellular free calcium. (**a**) Fluorescence image analysis of free cytosolic Ca^{2+} in Ad-CACNA2D2 (CACN)-transduced H460 and A549 cells by Fluo 3-AM staining. Images of the CACN-treated H460 cells at an MOI of 4000 vp/c (c) and A549 cells (g) at an MOI of 2500 vp/c, untreated (PBS) (a and e) and Adp53 (p53)-treated cells (b and f), and ionomycin-treated control cells (d and h) at 48 h post-treatment are shown. (**b**) Free Ca^{2+}-specific fluorescence emission was quantified by FACS analysis with Fluo 3-AM staining. Cells were treated as described in panel. (**a**) The differences of free intracellular Ca^{2+} are expressed semiquantitatively through the differences in relative fluorescence . The increase in free cytosolic Ca^{2+} was significant in the CACN-treated H460 ($P=0.015$ and 0.032) and A549 cells ($P=0.001$ and 0.002), but not significant in H1299 cells ($P=0.785$ and 0.865) compared with the increase seen with untreated (PBS) and p53-treated controls

48 h after treatment, but this was not seen in the untreated cells and the p53-transduced cells (Figures 2a (panels a and e) and 3b), but not a significant increase in Ad-CACNA2D2-transduced H1299 cells (Figure 3b). An increase in the level of fluorescence emission in Adp53-treated cells (Figure 3a (panels b and f) and b) was also detected, but exhibited a lower magnitude and a slower manifestation (the peak emission was registered 72–96 h post-treatment) than that in Ad-CACNA2D2-transduced cells (the peak emission was registered 48 h post-treatment). The increase of free cytosolic Ca^{2+} occurred shortly prior to apoptosis in these Ad-CACNA2D2-treated cells, suggesting a possible association of the induction of apoptosis by CACNA2D2 activity and the regulation of intracellular Ca^{2+} signaling, homeostasis, or both. However, this experimental setting does not allow to link mechanistically the Ca^{2+} increase to the apoptotic induction. The Fluo3-AM loading and staining conditions were optimized and confirmed by treating cell samples with 2 μg of ionomycin (a ionophore) (Kochegarov *et al.*, 2001) as a positive control, which showed uniform fluorescence emission increase in all treated cells (Figure 3a, panels d and e).

Interruption of mitochondria membrane potential

Depolarization of mitochondria and loss of mitochondria membrane potential can be a rate-limiting step in apoptosis as well as in necrotic cell death (Kroemer and Reed, 2000; Vieira *et al.*, 2000). The emerging evidence suggests that an excessive influx of Ca^{2+} represents a prototypical example of a cell death stimulus where mitochondria membrane depolarization precedes cyt *c* release (Reed and Kroemer, 2000; Vieira *et al.*, 2000). To investigate further the impact of the observed increase in intracellular free Ca^{2+} influx by ectopic expression of CACNA2D2 on mitochondria membrane integrity, we analysed the changes of mitochondria membrane potential in Ad-CACNA2D2-transduced NSCLC cells by FACS with mitochondria membrane potential-specific fluorescent JC-1 staining (Figure 4). Mitochondria depolarization, as demonstrated by a significant fluorescent shift with an increase in green (540 nm) emission (Figure 4a), was observed in Ad-CACNA2D2-transduced H460 and A549, cells between 24 and 48 h after transduction (Figure 4b), but not in untreated or Ad-LacZ-transduced cells. After 72 h of transduction by the Ad-CACNA2D2 vector, more than 84% of the A549 cells (Figure 4b, A549) and 80% of H460 (Figure 4b, H460) cells revealed mitochondria membrane depolarization; however, no significant changes were observed in the H1299 cells (Figure 4b, H1299). Adp53 induced similar changes in H460, A549 and H1299 cells (Figure 4). Mitochondria membrane depolarization preceding induction of apoptosis in cells transduced by Ad-CACNA2D2 at the same MOIs (Figure 2) suggests that the mitochondria depolarization mediated by an elevated level of Ca^{2+} influx is an earlier event in CACNA2D2-induced apoptosis.

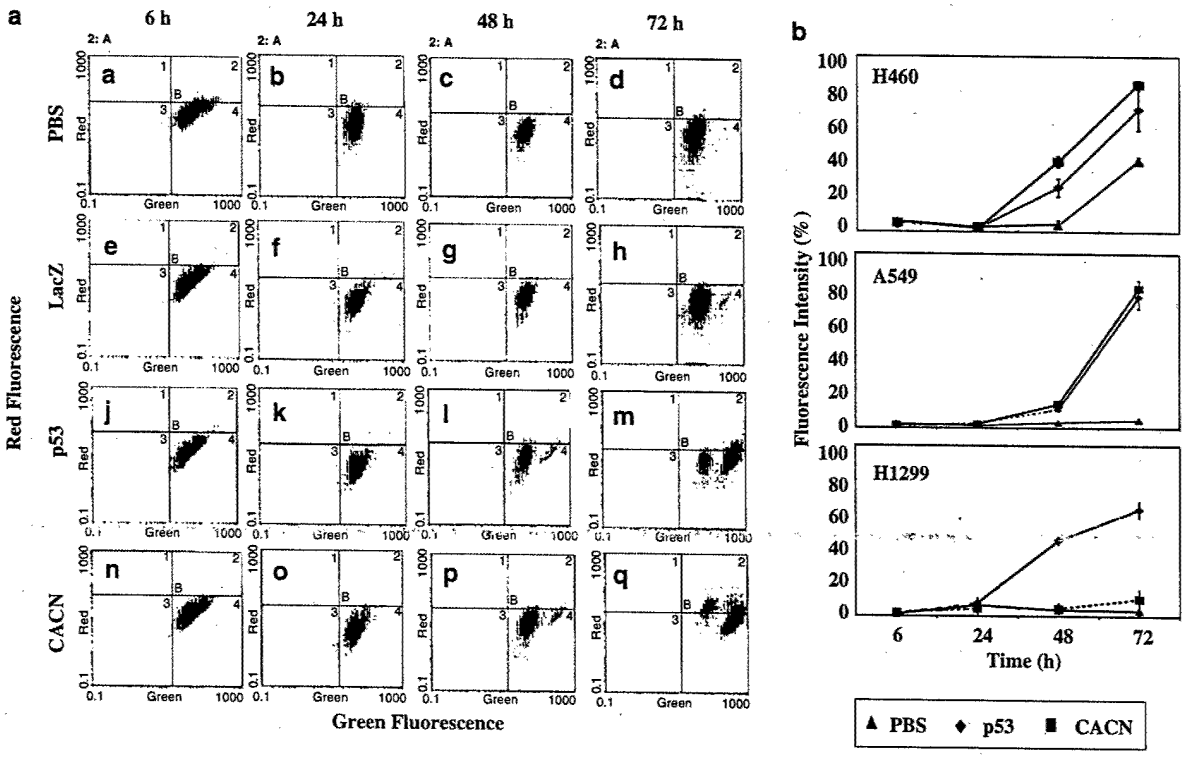

Figure 4 Ectopic expression of CACNA2D2 reduced the mitochondria membrane potential. (**a**) Changes in the mitochondria membrane potential in Ad-CACNA2D2-transduced A549 cells are revealed by FACS analysis with JC-1 staining. A549 cells were transduced with adenoviral vectors for 6, 24, 48, and 72 h at an MOI of 2500 vp/c. Fluorescence emission of red at 590 nm (indicating high membrane potential and aggregation of JC-1 dye) and green at 530 nm (indicating the collapse of membrane potential and the monomer of JC-1 dye) were measured by FACS. CACN (n, o, p, q)- and p53 (j, k, l, m)-transduced cells showed mitochondria membrane depolarization as evidenced by the fluorescence emission shift to the longer wavelength of green. PBS (a, b, c, d)- and LacZ (e, f, g, h)-transduced cells did not show a marked shift to the right. (**b**) Relative green fluorescence was higher in CACN-transduced A549, H460, and H1299 cells than in untreated (PBS) control cell. The decrease of the mitochondria membrane potential or depolarization is significant in the CACN-transduced A549 cells ($P = 0.002$) and H460 ($P = 0.005$) but not in H1299 cells after 48 h of transduction or in the untreated (PBS) control cells

Cyt c *release from mitochondria*

Release of cyt *c* from the mitochondria plays an integral role in apoptosis. To evaluate whether cyt *c* release might be an integral part of CACNA2D2-mediated apoptosis in a process involving regulation of Ca^{2+} influx and interruption of the mitochondria membrane integrity, we performed Western blot analysis of cyt *c* in the fractionated mitochondria and cytosolic lysates in Ad-CACNA2D2-treated A549 cells (Figure 5). The release of cyt *c* from mitochondria to cytosol was detected in both the Ad-CACNA2D2-transduced A549 cells at an MOI of 2500 (viral particles/cell) vp/c (Figure 5a, lanes 3 and 9) and H460 cells at an MOI of 4000 vp/c (Figure 5a, lanes 6 and 12), but no significant changes in cyt *c* in the cytosol fraction were detected in untreated (PBS) (Figure 5a, lanes 1, 4, 7, and 10) and Ad-LacZ-transduced (Figure 5a, lanes 2, 5, 8, and 11) cells. No significant change in levels of the cyt *c* in both the mitochondria and cytosol fractions was observed in Ad-CACNA2D2-transduced H1299 cells (data not shown). Cyt *c* release began at 48 h after transduction and increased over time as demonstrated in Ad-CACNA2D2-transduced A549 cells (Figure 5b). The changes in cell morphology and subcellular localization of cyt *c* (probed with an anti-human cyt *c* monoclonal antibody) were demonstrated in fluorescence images of A549 cells transduced with Ad-CACNA2D2 (Figure 5c). The characteristic pattern of the mitochondria distribution of cyt *c* still remained 24 h after transduction (Figure 5c, panel a) but was lost 48 h after transduction at this MOI (Figure 5c, panel b). The release of cyt *c* from mitochondria into the cytosol and the typical nuclear changes because of apoptosis were evident 48 h after (Figure 5c, panel b) and 72 h after (Figure 5c, panel c) transduction. The accumulation of apoptotic cell populations was also detected 48 h after transduction and increased in time as shown by FACS with PI staining (Figure 5d). The timing of the CACNA2D2-induced cyt *c* release was sequential and matched the timing of CACNA2D2-induced changes in intracellular Ca^{2+} influx (Figure 3) and mitochondria membrane potential (Figures 4 and 5d).

Activation of caspase 3 and PARP

Activation of caspases and PARP by translocation of cyt *c* from mitochondria to the cytosol is one of the

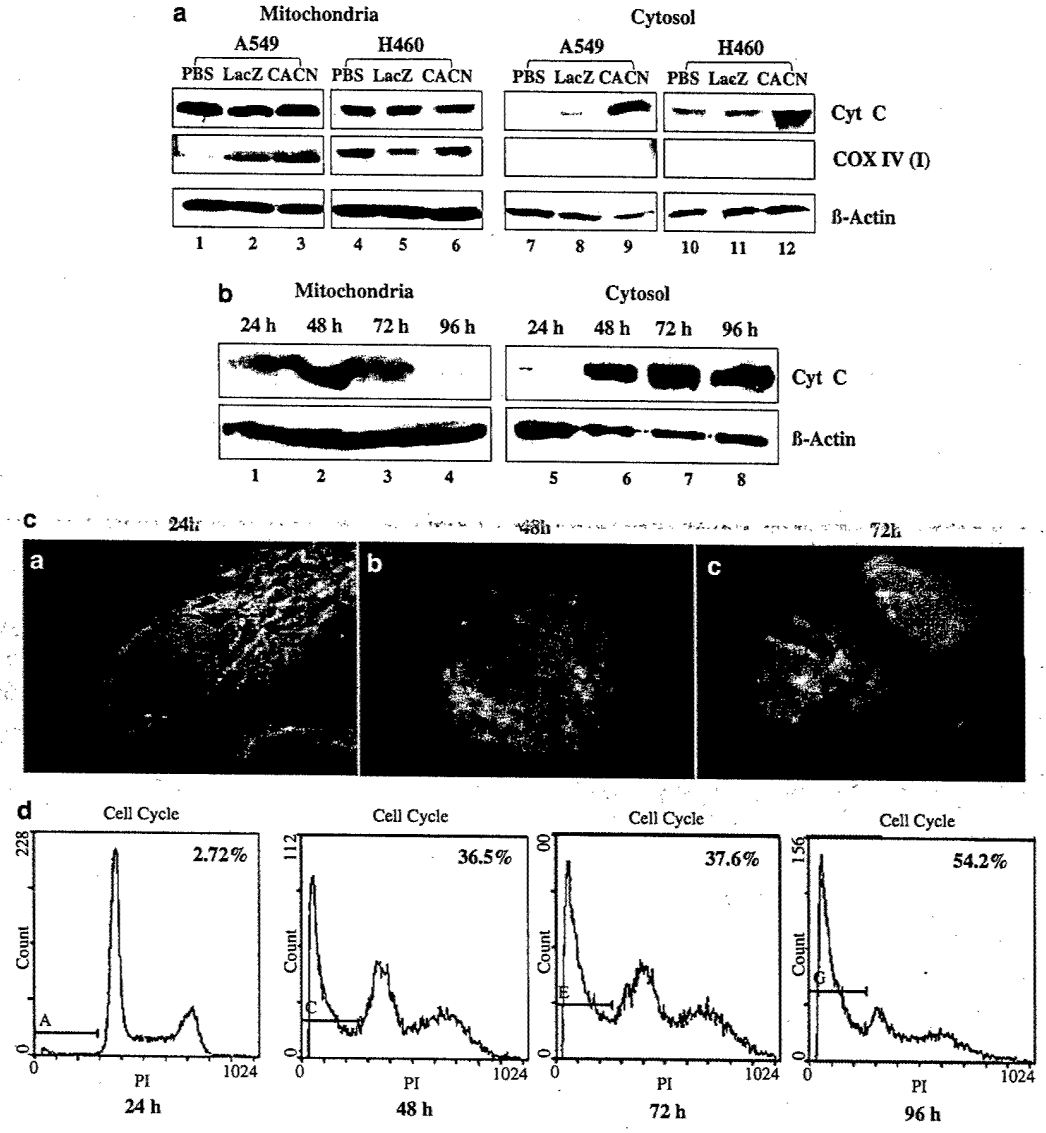

Figure 5 Western blotting was used to analyse cyt *c* release from mitochondria to cytosol in Ad-CACNA2D2-transduced cells. (**a**) Western blot of cyt *c* in CACN-transduced A549 and H460 cells. Cells were transduced with adenoviral vectors at an MOI of 2500 vp/c for A549 and MOI of 4000 vp/c for H460 for 48 h, and untreated (PBS) (lanes 1 and 4) and Ad-LacZ (LacZ)-transduced (lanes 2 and 5) cells were used as controls. Immunoblotting for cyt *c* was performed in fractionated lysates of mitochondria (lanes 1–6) and cytosol (lanes 7–12). Immunoblots of COX IV (I) were used as a mitochondria enzyme marker and *β*-actin as an internal loading control. (**b**) Time course of cyt *c* release in Ad-CACNA2D2-transduced A549 cells. (**c**) Immunofluorescence image analysis of the subcellular rearrangement of mitochondria and translocation of cyt *c* in Ad-CACNA2D2-transduced A549 cells. Mitochondria were probed with an FITC-labeled cyt *c* antibody (green) and the nucleus was counterstained with PI (red). (**d**) Timetable of induction of apoptosis in Ad-CACNA2D2-transduced A459 cells by FACS analysis with PI staining for DNA content. The percentage of induction of apoptosis was indicated by the increase of the $SubG_0$-G_1 cell populations (shown by a bar in each plot)

events that establishes the mitochondrion as an important regulator of cell life and death (von Ahsen *et al.*, 2000; Martinou and Green, 2001). Western blot analysis was performed to evaluate the activation of caspase 3 and PARP downstream of the mitochondria-mediated apoptotic pathway (Figure 6). The activation of both apoptotic executioners, caspase 3 (Figure 6a) and PARP (Figure 6b), was detected in Ad-CACNA2D2-transduced H460 and A549 cells, as demonstrated by the cleaved fragments of the procaspase3 and pro-PARP on the Western blot (Figure 6). These results provide further evidence that CACNA2D2-mediated apoptosis occurs via the mitochondrion.

Discussion

The protein product of the recently cloned CACNA2D2 gene is structurally related to the $\alpha 2\delta 2$ auxiliary subunit of the voltage-activated calcium channel (VACC)

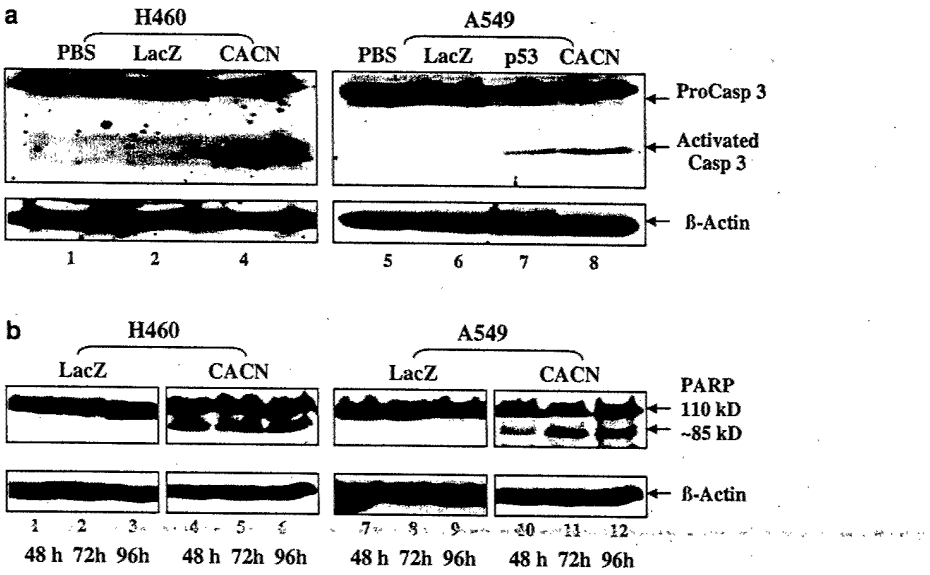

Figure 6 Downstream caspase 3 and PARP are activated by ectopic expression of the CACNA2D2 gene. (**a**) Western blot analysis of caspase 3. The whole cell lysate was prepared from Ad-CACNA2D2 (CACN)-transduced H460 cells (lanes 1–3) at an MOI of 4000 vp/c and A549 (lanes 5 and 6) cells at an MOI of 2500 vp/c after 72 h of transduction, and untreated (PBS) and Ad-LacZ (LacZ)- or Ad-p53 (p53)-transduced cells were used as controls. The cleaved procaspase 3 was indicated by an arrow. (**b**) Western blot analysis of PARP. Cells were transduced by Ad-CACNA2D2 (CACN) at the same MOI as described in **a** for each cell line. The cleaved PARP is indicated by the immunoblotting complexes of about 85 kDa. β-actin was used as an internal loading control

protein complex (Angeloni *et al*., 2000; Gao *et al*., 2000). Various VACC protein subunits such as the pore-forming $\alpha 1$ unit and the auxiliary β, γ, and $\alpha 2\delta$ subunits have been identified and partially characterized (Singer *et al*., 1991; Castellano *et al*., 1993; Brown and Gee, 1998; Burgess *et al*., 1999; Felix, 1999, Hofmann *et al*., 1999; Varadi *et al*., 1999; Catterall, 2000; Lacinova *et al*., 2000). The $\alpha 2\delta 2$ subunit (CACNA2D2) of VACC is a regulatory subunit (Gao *et al*., 2000). Mutation of this gene has been found to lead to a phenotype characterized by epilepsy, ataxia, and alterations of calcium currents in cerebellar cells in mice, which is ultimately fatal (Barclay *et al*., 2001). Although the exact physiological function of CACNA2D2 in nonexcitable cells remains unknown, functional studies of CACNA2D2 have revealed that the activity of CACNA2D2 protein may alter the conductance properties of the pore-forming $\alpha 1$ unit as well as their membrane trafficking and, therefore dynamically regulates Ca^{2+} current through the VACC (Gao *et al*., 2000; Hobom *et al*., 2000; Hurley *et al*., 2000; Klugbauer *et al*., 1999). The very frequent and early loss of expression of CACNA2D2 together with a subset of genes in the 3p21.3 homozygous deletion region of human chromosome 3 in human lung and breast cancers suggest a link between the CACNA2D2 and the regulation of proliferation and cell death in lung cancer pathogenesis, possibly through the regulation of the VACC-mediated Ca^{2+} influx (Angeloni *et al*., 2000; Gao *et al*., 2000; Lerman and Minna, 2000). However, no direct evidence has been presented for this link. In this study, we focused on CACNA2D2-mediated apoptosis by adenoviral vector-mediated ectopic expression of the wt-CACNA2D2 gene in the CACNA2D2-deficient NSCLC cells. We presented indirect evidence to link the CACNA2D2-mediated apoptosis with the regulation of the intracellular calcium content, interruption of mitochondria membrane integrity, and activation of downstream caspases.

Inhibition of tumor cell growth by ectopic expression of CACNA2D2 is concomitant with induction of apoptosis in these Ad-CACNA2D2-transduced NSCLC cells. A significant induction of apoptosis was observed 48 h after transduction. The cell lines most sensitive to CACNA2D2-induced apoptosis were A549 and H460, which contain a wt-p53 gene and are generally resistant to either the transduction of adenoviral vectors or to wt-p53-mediated cell death. Ad-CACNA2D2-transduced H358 cells, which carry a mutated p53 gene, showed remarkable inhibition of cell growth but no significant induction of apoptosis. H1299 cells, which are p53-null, were the most resistant to CACNA2D2-induced growth inhibition and apoptosis *in vitro* and *in vivo*. These results suggest a possible association of the CACNA2D2-mediated apoptosis with the activities of wt-p53, which is very interesting and needs to be explored further.

Based on the evidence that the activity of CACNA2D2 dynamically regulates Ca^{2+} currents in L- and T-type calcium channels (Klugbauer *et al*., 1999; Gao *et al*., 2000; Hobom *et al*., 2000; Hurley *et al*., 2000), we expected that overexpression of CACNA2D2 might result in an increase in the level of cytosolic Ca^{2+} influx. A significant increase in the basal level of the intracellular free Ca^{2+} was indeed detected in Ad-CACNA2D2-transduced H460 and A549 cells using

sensitive free-Ca^{2+}-specific Fluo3-AM staining in a semiquantitative manner. Several factors, however, hinder the accurate determination of the kinetic events of the modulation of Ca^{2+} influx influenced by the adenoviral vector-mediated transient expression of CACNA2D2 protein. Gradual expression of the CACNA2D2 subunit after 24 h of transduction would cause the modulation of intracellular Ca^{2+} influx with time. Since Ca^{2+} is a multivalent messenger, several cytosolic Ca^{2+} binding proteins, such as calmodulin, can bind to the free Ca^{2+} to execute downstream effects on cellular processes, which would significantly reduce the availability of free Ca^{2+}; other Ca^{2+} effectors or mediators, such as calbindin-D, parvalbumin, and calretinin, can buffer the cytosolic increases of Ca^{2+} (Berridge *et al.*, 1998, 2000). Furthermore, Ca^{2+} signals have a wide range of spatial and temporal distribution and so are capable of conveying signals in a very complex way (Lemasters *et al.*, 1998; Berridge *et al.*, 2000; Zhu *et al.*, 2000). Together, these factors make it difficult to detect even the global Ca^{2+} oscillations in our experimental setting; therefore, our data may not represent the accurate dynamic changes of intracellular Ca^{2+} contents and influx.

Mitochondria play a major role in apoptosis triggered by many stimuli. Disruption and permeation of the mitochondria membrane are general phenomena associated with the processes of apoptosis and necrotic cell death (Kroemer and Reed, 2000, Vieira *et al.*, 2000). An excessive mitochondria Ca^{2+} influx has been suggested to be a potent cell death stimulus leading to mitochondria membrane depolarization and cyt *c* release (Reed and Kroemer, 2000; Vieira *et al.*, 2000). Activation of caspases by translocation of cyt *c* from mitochondria to the cytosol is a downstream event through which the mitochondrion's role as a regulator of cell life and death has become unquestioned (Chen *et al.*, 2000; von Ahsen *et al.*, 2000; Martinou and Green, 2001). We demonstrated that ectopic expression of CACNA2D2 was associated with the accumulation of intracellular free Ca^{2+} and the collapse of the mitochondria membrane potential prior to cyt *c* release and nuclear apoptotic changes, suggesting a physiological effect of CACNA2D2 activity in regulating cell survival by indirectly altering the mitochondria membrane integrity in concomitance with cytosolic Ca^{2+} increase. Rupture of the outer membrane results in the release of many proteins such as cyt *c* and some caspases (Desagher and Martinou, 2000). However, whether this is the result of a direct effect of the CACNA2D2-mediated Ca^{2+} oscillations on mitochondria permeability needs to be further investigated. It would also be interesting to explore the CACNA2D2-mediated Ca^{2+}-signaling pathways involved in activation of the proapoptotic mediators such as Bad and Bax and inactivation of the antiapoptotic factors such as Bcl-2 and Bclx that convey the apoptotic signal to the mitochondrion (Gross *et al.*, 1999; Vieira *et al.*, 2000; von Ahsen *et al.*, 2000).

Together, our results suggest that ectopic expression of CACNA2D2 is capable of inducing apoptosis in several NSCLC cell lines. The induction of apoptosis by CACNA2D2 activity is associated with the regulation of cytosolic Ca^{2+} contents and the activation of the mitochondria pathway. Further identification of the physiological functions of CACNA2D2 in unexcitable cells such as normal bronchial epithelial cells, the evaluation of the cellular modulation of endogenous and exogenous expression of CACNA2D2 in response to environmental stimuli such as DNA-damaging agents and oncogene activities in normal and tumor cells, and the characterization of the effects of CACNA2D2 activity on both L- and T-type calcium channels in the presence and absence of selective inhibitors of the various VACC subtypes will provide us insight into the molecular mechanisms in the CACNA2D2-mediated regulation of cell proliferation and cell death in the pathogenesis of lung cancers and other human cancers.

Materials and methods

Cell lines and cell culture

Four human NSCLC cell lines, A549 (homozygous for multiple 3p21.3 markers and wt-*p53*), NCI-H1299 (homozygous for multiple 3p21.3 markers and homozygous deletion of *p53*), NCI-H358 (retained heterozygosity of multiple 3p21.3 markers and homozygous deletion of *p53*), and NCI-H460 (homozygous for multiple 3p21.3 markers and wt-*p53*), with varied 3p21.3 and *p53* gene status, and a normal human bronchial epithelial cell line (HBEC) or fibroblast cells were used for *in vitro* experiments. The multiple 3p21.3 markers located in the 630 kb region used for this analysis were described previously (Fondon *et al.*, 1998). The A549 line was maintained in Ham's F12 medium supplemented with 10% fetal calf serum. The H1299, H358, and H460 lines were maintained in RPMI-1640 medium supplemented with 10% fetal calf serum and 5% glutamine.

Recombinant adenoviral vectors

The recombinant Ad-CACNA2D2 was constructed using our recently developed ligation-mediated plasmid adenovirus vector construction system, named herein pAd-RAP and pAd-RAP-Shuttle. The CACNA2D2 was assembled as a mammalian gene expression cassette that is driven by a CMV promoter and tailed with a bovine growth hormone (BGH) poly (A) signal sequence. Sequences of the CACNA2D2 gene in the viral vectors were confirmed by automated DNA sequencing. A vector expressing the GFP (green fluorescence protein) gene (Ad-GFP) and a vector carrying the β-galactosidase gene *LacZ* (Ad-LacZ) were used to monitor the efficiency of transduction by the viral vectors and as nonspecific transgene expression controls. Ad-EV, an empty E1-deleted vector, was used as a negative control; Ad-p53, a vector containing the wt-*p53* gene, was used as a positive control for tumor suppression. Viral titers were determined by both optical density measurement (i.e. vp/ml) and plaque assay (i.e. plaque-forming units (PFU)/ml).

Animal experiments

All animals were maintained and animal experiments were performed under NIH and institutional guidelines established for the Animal Core Facility at the University of Texas MD Anderson Cancer Center. Procedures for H460 subcutaneous tumor inoculations in *nu/nu* mice were described previously

(Ji *et al*., 1999). When the average tumor size reaches about 0.5 cm in diameter, mice were injected intratumorally three times within a week with Ad-CACNA2D2 and control vectors at a dose of 3×10^{10} PFU (3×10^{12} vp)/tumor in a volume of 0.2 ml. Differences in tumor volumes between treatment groups were analysed with a mixed model ANOVA using the Statistica software (StatSoft Inc., Tulsa, OK, USA). A difference was considered to be statistically significant when $P = 0.05$.

Analysis of CACNA2D2 gene Expression by RT–PCR

Total RNA samples were isolated from Ad-CACNA2D2-transduced tumor cells using TRIZOL reagent (Life Technologies, Grand Island, NY, USA) as instructed by the manufacturer. The RT reaction was performed using a reverse transcription kit with the oligo-d$(T)_{16}$ as a primer under the conditions recommended by the manufacturer (Perkin-Elmer Applied Biosystems, Foster City, CA, USA). The RT–PCR products amplified with human total RNA as a template and glyceraldehyde-3-phosphate dehydrogenase (GAPDH) primers were used as an internal control. The primers for CACNA2D2 were 5′GACTGACCAACACCACTCTTCTC (sense, within CACNA2D2 cDNA) and 5′CTCATCGTACCTCAGCTCCTTCC (antisense, within the BGH poly (A) signaling region). The PCR was performed using an AmpliTaq PCR Kit and a 9600 PCR instrument according to the manufacturer's instructions (Perkin-Elmer Applied Biosystems).

Cell viability assay

Inhibition of tumor cell growth by treatment with Ad-CACNA2D2 and control vectors was analysed by quantitatively determining cell viability using an improved XTT assay (Roche Molecular Biochemicals, Indianapolis, IN, USA). Briefly, cells were plated in 96-well microtiter plates at 1×10^3 cells/well in 100 μl of medium. One day after the cells were plated, a 100-μl aliquot of medium containing individual adenoviral vectors at various multiplicities of infection MOI in units of vp/cell (vp/c) was placed into each sample well, and phosphate-buffered saline (PBS), Ad-EV, Ad-LacZ, and Adp53 were added as controls. On designated sampling days after transduction, cell growth and viability were quantified by XTT assay as described previously (Nishizaki *et al*., 2001). The percentage of cell viability was calculated in terms of the absorbency of treated cells relative to the absorbency of untreated control cells. Experiments were repeated at least three times with quadruplicate samples for each treatment in each individual experiment.

Analysis of apoptosis and cell cycle kinetics

Induction of apoptosis in tumor cells treated with various adenoviral vectors was analysed by flow cytometry (FACS) using terminal deoxynucleotidyl transferase-mediated dUTP nickend labeling (TUNEL) reaction with fluorescein (FITC)-labeled dUTP (Roche Molecular Biochemicals, Mannheim, Germany). Briefly, cells were plated in six-well plates (1×10^6 cells/well) and treated by various Ad-CACNA2D2 vectors; PBS, Ad-EV, Ad-LacZ, and Adp53 were used as controls. At designated times after transduction, cells were harvested and washed in PBS. Cells were processed for FACS analysis to determine apoptosis and cell cycle kinetics as described previously (Ji *et al*., 1999).

Measurement of cytosolic free calcium

The intracellular free Ca^{2+} was measured by FACS and fluorescence image analysis with free-Ca^{2+}-sensitive Fluo3-AM green fluorescent staining (Molecular Probes, Eugene, OR, USA) in Ad-CACNA2D2-transduced A549 and H460 cells. Cells were cultured in 100 mm dishes at about 5×10^6 cells/dish and transduced with adenoviral vectors at varied MOIs. After 24 and 48 h of transduction, cells were collected and washed once with 1 × HBSS supplemented with 1 mM Ca^{2+}, 1 mM Mg^{2+}, and 1% fetal bovine serum (FBS). The Fluo3-AM stock solution was prepared by first dissolving 50 μg of Fluo3-AM dye in 20 μl of DMSO containing 20% of the detergent Fluronic F-127 (Molecular Probes) and then mixing it with 117 μl of FBS. The cells were resuspended in 1 ml of HBSS containing the Fluo3-AM dye in a final concentration of 2.5–5.0 μg/ml, depending on the cell type. The anion carrier inhibitor probenecid was added at a final concentration of 4 mM to minimize the dye leakage. The cells were incubated for 45 min at room temperature on an orbital shaker in the dark. Cells were spun down by centrifugation for 5 min at 1500 r.p.m. and washed once with HBSS. Cells were gently resuspended in HBSS containing 4 mM of probenecid and then incubated for 20 min in the dark to allow cellular esterases to cleave the acetoxymethyl group of Fluo3-AM. Fluorescence intensity in the stained cells was measured by FACS analysis at an excitation wavelength of 488 nm and an emission wavelength of 530 nm. Experiments were performed three times independently. To evaluate the conditions of dye loading, 2 μg of ionomycin, an ionophoric antibiotic synthesized by *Streptomyces conglobatus* sp. (Calbiochem, Fremont, CA, USA), was added to each of the cell samples in a separate tube, and the dynamic fluorescence emission was measured by FACS after baseline fluorescence was assessed. For fluorescence imaging analysis of Fluo3-AM stained cells, the cells were cultured in chamber slides (Falcon), and then treated and stained with Fluo3-AM with the same procedure as was described for FACS analysis. The stained cells were examined under a microscope (Nikon Labophot 2) equipped with a digital camera (Nikon DMX1200, Tokyo, Japan) and the analysis software (Nikon ACT-1 V2.0).

Analysis of mitochondria membrane potential by FACS with JC-1 staining

Changes in mitochondria membrane potential in adenoviral vector-transduced cells were measured by flow cytometry with JC-1 (5,5′,6,6′-tetrachloro-1,1′3,3′-tetraethylbenzimidazolyl-carbocyanine iodide) staining (Molecular Probes, Eugene, OR, USA). JC-1 exists as a monomer at low concentrations or at low membrane potential and emits green fluorescence at 527 nm. However, at higher concentrations or higher membrane potentials, JC-1 forms J-aggregates and emits maximum red fluorescence at ~590 nm. The measurement of the ratio of the red to green JC-1 fluorescence in cells by flow cytometry is a sensitive and specific method for monitoring changes in mitochondria potential in living cells during induction of apoptosis by various agents (Ankarcrona *et al*., 1995; Cossarizza *et al*., 1995). Cells were cultured in six-well plates and, after reaching ~70% confluence, transduced with various adenoviral vectors at varied MOIs. Cells were collected by centrifugation for 5 min at 2000 r.p.m. at 4°C and resuspended in complete medium containing 10 mg/ml JC-1 at a density of 5×10^5 cells/ml. The cells were incubated for 10 min at room temperature in the dark, washed twice with cold PBS, resuspended in 400 ml of PBS, and analysed immediately by flow cytometry.

For *in situ* fluorescent staining with JC-1, cells were cultured in chamber slides. At designated time points, the medium was removed and the cells incubated in reduced serum Opti-MEM-I medium (GIBCO BRL, Grand Island, NY, USA) containing 10 μg/ml of JC-1 for 10 min in the dark. After washing and air-drying, stained cells were immediately examined by fluorescence microscopy.

Western blot analysis

Western blot analysis was performed to evaluate the expression of CACNA2D2 protein, the release of cyt *c*, activation of caspase 3 and PARP, and other protein expression in Ad-CACNA2D2 and control vector-transduced cells. For the preparation of crude cell lysates, cells were suspended in SDS–PAGE running buffer containing a complete set of proteinase inhibitors (Roche Molecular Biochemials, Mannheim, Germany) and lysed for 20 min at 4°C. Cell lysates were passed through a 25-gauge needle and briefly sonicated twice for 30 s. For cyt *c* analysis, cell fractionation was performed to separate mitochondria-enriched fractions from cytosol fractions using an Apo-Alert Cell Fractionation Kit (ClonTech, Palo Alto, CA, USA) according to the manufacturer's instructions. Fractionated cell lysates were kept in equal volume in 2 × lysis buffer supplemented with 62.5 mM urea. Protein concentrations were assayed using the Bio-Rad protein assay reagent (Bio-Rad Laboratories, Hercules, CA, USA). The crude cell lysates (about 50 μg) were used in standard SDS–PAGE and Western blot analysis.

Immunofluorescence staining

Immunofluorescence staining was performed in cells cultured in chamber slides. At designated time points, the cells were washed twice with cold PBS fixed in 4% paraformaldehyde for 15 min at 4°C and made permeable by incubation for 5 min in a solution containing 0.1% Triton X-100 and 0.1% sodium citrate. The cells were incubated with the primary monoclonal mouse anti-cyt C antibody for 60 min at 37°C, and after washing were incubated with the FITC-labeled secondary rabbit anti-mouse IgG antibodies for 60 min. After three washing steps in 0.1% Tween 20–PBS solution and air-drying, the slides were mounted with aqueous mounting medium containing 50 μg/ml of PI for nuclear staining and immediately examined under a fluorescence microscope.

Statistics

All the experiments were repeated at least two times with duplicates or triplicates of samples. The results were expressed as mean $\pm$ s.d. Student's two-sided *t*-test was used to compare the values of the test and control samples. A value of $P<0.05$ was taken as significant.

Abbreviation:
ADP, adenosinediphosphate; CACNA2D2, calcium-channel alfa-2-delta-2 subunit; COX IV (I), cytochrome oxidase IV subunit I; cyt C, cytochrome C; DAPK, death-associated protein kinase; DMSO, dimethylsulfoxide; FBS, fetal bovine serum; HBSS, Hanks balanced saline solution; MOI, multiplicity of infection; NSCLC, non-small cell lung cancer; PARP, poly ADP-ribose polymerase; PI, propidiumiodide; TUNEL, terminal deoxynucleotidyl transferase-mediated dUTP nick-end labeling; VACC, voltage-activated calcium channel; XTT, sodium 3,3′-{1-[(phenylamino)carbonyl]-3,4-tetrazolium}-bis(4-methoxy-6-nitro)-benzene sulfonic acid hydrate; wt, wild-type.

Acknowledgments
The authors would like to thank Karen Ramirez and Wendy Schober-Ditmore for their assistance in FACS analysis, and David McConkey, Leta Nutt, and Abujiang Pataer for discussions on the methodology. This work was partially supported by grants from the National Cancer Institute, the National Institutes of Health SPORE (2P50-CA70907-04); (P01 CA78778-01A1) (JAR); (CA71618) (JDM), a WM Keck Gene Therapy Career Development Grant (LJ), by a grant from the Department of the Army BESCT Lung Cancer Program (DAMD17011068902); by the Swiss National Science Foundation (GLC) and Bernische Krebsliga (GLC); by gifts to the Division of Surgery MD Anderson Cancer Center, from Tenneco and Exxon for the Core Laboratory Facility; by the M. D. Anderson Cancer Center Support Core Grant (CA16672); by a grant from the Tobacco Settlement Funds as appropriated by the Texas State Legislature (Project 8), and by a sponsored research agreement with Introgen Therapeutics, Inc. (SR93-004-1).

References

Angeloni D, Wei MH, Duh FM, Johnson BE and Lerman MI. (2000). *Mol. Cell Probes*, **14,** 53–54.

Ankarcrona M, Dypbukt JM, Bonfoco E, Zhivotovsky B, Orrenius S, Lipton SA and Nicotera P. (1995). *Neuron.*, **15,** 961–973.

Barclay J, Balaguero N, Mione M, Ackerman SL, Letts VA, Brodbeck J, Canti C, Meir A, Page KM, Kusumi K, Perez-Reyes E, Lander ES, Frankel WN, Gardiner RM, Dolphin AC and Rees M. (2001). *J. Neurosci.*, **21,** 6095–6104.

Berridge MJ, Bootman MD and Lipp P. (1998). *Nature*, **395,** 645–648.

Berridge MJ, Lipp P and Bootman MD. (2000). *Nat. Rev. Mol. Cell. Biol.*, **1,** 11–21.

Brown JP and Gee NS. (1998). *J. Biol. Chem.*, **273,** 25458–25465.

Burgess DL, Davis CF, Gefrides LA and Noebels JL. (1999). *Genome Res.*, **9,** 1204–1213.

Castellano A, Wei X, Birnbaumer L and Perez-Reyes E. (1993). *J. Biol. Chem.*, **268,** 3450–3455.

Catterall WA. (2000). *Annu. Rev. Cell Dev. Biol.*, **16,** 521–555.

Chen Q, Gong B and Almasan A. (2000). *Cell Death Differ.*, **7,** 227–233.

Cossarizza A, Cooper EL, Quaglino D, Salvioli S, Kalachnikova G and Franceschi C. (1995). *Biochem. Biophys. Res. Commun.*, **214,** 503–510.

Desagher S and Martinou JC. (2000). *Trends Cell Biol.*, **10,** 369–377.

Felix R. (1999). *Receptors Channels*, **6,** 351–362.

Fondon JW, Mele GM, Brezinschek RI, Cummings D, Pande A, Wren J, O'Brien KM, Kupfer KC, Wei MH, Lerman M, Minna JD and Garner HR. (1998). *Proc. Natl. Acad. Sci. USA*, **95,** 7514–7519.

Gao B, Sekido Y, Maximov A, Saad M, Forgacs E, Latif F, Wei MH, Lerman M, Lee JH, Perez-Reyes E, Bezprozvanny I and Minna JD. (2000). *J. Biol. Chem.*, **275,** 12237–12242.

Gross A, McDonnell JM and Korsmeyer SJ. (1999). *Genes Dev.*, **13,** 1899–1911.
Hobom M, Dai S, Marais E, Lacinova L, Hofmann F and Klugbauer N. (2000). *Eur. J. Neurosci.*, **12,** 1217–1226.
Hofmann F, Lacinova L and Klugbauer N. (1999). *Rev. Physiol. Biochem. Pharmacol.*, **139,** 33–87.
Hurley JH, Cahill AL, Currie KP and Fox AP. (2000). *Proc. Natl. Acad. Sci. USA*, **97,** 9293–9298.
Ji L, Fang B, Yen N, Fong K, Minna JD and Roth JA. (1999). *Cancer Res.*, **59,** 3333–3339.
Kao JP, Harootunian AT and Tsien RY. (1989). *J. Biol. Chem.*, **264,** 8179–8184.
Klugbauer N, Lacinova L, Marais E, Hobom M and Hofmann F. (1999). *J. Neurosci.*, **19,** 684–691.
Kochegarov AA, Beylina SI, Matveeva NB, Leontieva GA and Zinchenko VP. (2001). *Comparative Biochem. Physiol.* **128**(Part A), 279–288.
Kroemer G and Reed JC. (2000). *Nat. Med.*, **6,** 513–519.
Lacinova L, Klugbauer N and Hofmann F. (2000). *Gen. Physiol. Biophys.*, **19,** 121–136.
Lam M, Dubyak G, Chen L, Nunez G, Miesfeld RL and Distelhorst CW. (1994). *Proc. Natl. Acad. Sci. USA*, **91,** 6569–6573.
Lemasters JJ, Nieminen AL, Qian T, Trost LC, Elmore SP, Nishimura Y, Crowe RA, Cascio WE, Bradham CA, Brenner DA and Herman B. (1998). *Biochim. Biophys. Acta.*, **1366,** 177–196.
Lerman MI and Minna JD. (2000). *Cancer Res.*, **60,** 6116–6133.
Marais E, Klugbauer N and Hofmann F. (2001). *Mol. Pharmacol.*, **59,** 1243–1248.
Martinou JC and Green DR. (2001). *Nat. Rev. Mol. Cell Biol.*, **2,** 63–67.
Nishizaki M, Meyn RE, Levy LB, Atkinson EN, White RA, Roth JA and Ji L. (2001). *Clin. Cancer Res.*, **7,** 2887–2897.
Raveh T and Kimchi A. (2001). *Exp. Cell Res.*, **264,** 185–192.
Reed JC and Kroemer G. (2000). *Cell Death Differ.*, **7,** 1145.
Rutter GA and Rizzuto R. (2000). *Trends Biochem. Sci.*, **25,** 215–221.
Singer D, Biel M, Lotan I, Flockerzi V, Hofmann F and Dascal N. (1991). *Science*, **253,** 1553–1557.
Toyota M, Ho C, Ohe-Toyota M, Baylin SB and Issa JP. (1999). *Cancer Res.*, **59,** 4535–4541.
Ueki T, Toyota M, Sohn T, Yeo CJ, Issa JP, Hruban RH and Goggins M. (2000). *Cancer Res.*, **60,** 1835–1839.
Varadi G, Strobeck M, Koch S, Caglioti L, Zucchi C and Palyi G. (1999). *Crit. Rev. Biochem. Mol. Biol.*, **34,** 181–214.
Vieira HL, Haouzi D, El Hamel C, Jacotot E, Belzacq AS, Brenner C and Kroemer G. (2000). *Cell Death Differ.*, **7,** 1146–1154.
von Ahsen O, Waterhouse NJ, Kuwana T, Newmeyer DD and Green DR. (2000). *Cell Death Differ.*, **7,** 1192–1199.
Walker D and De Waard M. (1998). *Trends Neurosci.*, **21,** 148–154.
Wang HG, Pathan N, Ethell IM, Krajewski S, Yamaguchi Y, Shibasaki F, McKeon F, Bobo T, Franke TF and Reed JC. (1999a). *Science*, **284,** 339–343.
Wang M, Offord J, Oxender DL and Su TZ. (1999b). *Biochem. J.*, **342,** 313–320.
Zhu L, Ling S, Yu XD, Venkatesh LK, Subramanian T, Chinnadurai G and Kuo TH. (1999). *J. Biol. Chem.*, **274,** 33267–33273.
Zhu LP, Yu XD, Ling S, Brown RA and Kuo TH. (2000). *Cell Calcium*, **28,** 107–117.
Zochbauer-Muller S, Fong KM, Virmani AK, Geradts J, Gazdar AF and Minna JD. (2001). *Cancer Res.*, **61,** 249–255.